UNIVERSITEIT VAN PRETORIA
UNIVERSITY OF PRETORIA
YUNIBESITHI YA PRETORIA

CONTRIBUTION OF MATRIC SUCTION TO THE SLOPE STABILITY OF TAILINGS DAMS

JACK ADRIAAN BASSON

A dissertation submitted in partial fulfilment of the requirements for the degree of

MASTER OF ENGINEERING (GEOTECHNICAL ENGINEERING)

In the

FACULTY OF ENGINEERING, BUILT ENVIRONMENT AND INFORMATION TECHNOLOGY

UNIVERSITY OF PRETORIA

June 2023

ABSTRACT

Title: Contribution of matric suction to the slope stability of tailings dams

Author: J.A. Basson

Supervisor: Professor S.W. Jacobsz

Co-Supervisor: Doctor Luis Alberto Torres Cruz

Department: Civil Engineering

University: University of Pretoria

Degree: Master of Engineering (Geotechnical Engineering)

The strengthening effect of matric suctions is typically ignored in slope stability analyses. This is due to the uncertainty in the magnitude and reliability of in-situ matric suctions and the effect thereof on the shear strength of the material under consideration. Recent developments in field measurement probes allow for the long-term monitoring of in-situ matric suctions and volumetric water contents. The UP tensiometer was installed alongside volumetric water content sensors at various locations on a platinum and a gold tailings dam and monitored for a number of months.

The inclusion of matric suctions in slope stability analyses required the identification of a suitable model from the literature that can realistically predict the relationship between suction and shear strength. Shear strength vs suction data were generated by shearing various platinum tailings samples using a direct simple shear device. Matric suction was varied between tests by varying the sample water content to observe the effect of suction on shear strength. Limit equilibrium slope stability analyses of the monitored tailings dams allowed the effect of matric suctions on slope stability to be considered once a suitable unsaturated shear strength model was identified that best modelled the shear strength test results. The effect of matric suctions on slope stability was illustrated by comparing safety factors determined using the classical approach, which only relies on saturated soil mechanics and the Mohr-Coulomb (MC) strength model, and an approach which replaced the MC strength model with a suitable unsaturated shear strength model.

The results of unsaturated direct simple shear testing of platinum tailings showed that the model by Vanapalli et al. (1996) best predicts the relationship between matric suction and shear strength. This model, together with the observed unsaturated pore pressure regime observed in the tailings dams

monitored, were used in limit equilibrium analyses to assess the contribution of suctions to the factor of safety against slope failure. It was found that the contribution of matric suction to the factor of safety against slope failure ranged between 1.6% and 3.8% for the platinum tailings dam and between 5.6% and 13% for the finer grained gold tailings dam considered in this study. It was thus concluded that the contribution of matric suction to the stability of the platinum and gold tailings dams investigated was small and that it would be both conservative and realistic to disregard.

DECLARATION

I, the undersigned hereby declare that:

- I understand what plagiarism is and I am aware of the University's policy in this regard;
- The work contained in this thesis is my own original work;
- I did not refer to work of current or previous students, lecture notes, handbooks or any other study material without proper referencing;
- Where other people's work has been used this has been properly acknowledged and referenced;
- I have not allowed anyone to copy any part of my thesis;
- I have not previously in its entirety or in part submitted this thesis at any university for a degree.

Signature of student: 

Student number: **u17029016**

Date: **14 June 2023**

ACKNOWLEDGEMENTS

I wish to express my appreciation to the following organisations and persons who made this dissertation possible:

- Prof S.W. Jacobsz for successfully carrying over his passion for Geotechnical Engineering.
- Doctor Luis Alberto Torres Cruz por su orientación e interés en esta disertación.
- SRK Consulting for their contributions towards this dissertation.
- The academic and technical staff of the University of Pretoria for setting a high-quality standard in the field of Civil Engineering.
- The University of the Witwatersrand and Dr L.A. Torres Cruz for providing the direct simple shear device used for materials testing.
- My family, friends and colleagues for their support.

TABLE OF CONTENTS

1 INTRODUCTION 1-1

1.1 Background 1-1
1.2 Objectives of the study 1-2
1.3 Scope of the study 1-2
1.4 Methodology 1-2
1.5 Organisation of the report 1-3

2 LITERATURE REVIEW 2-1

2.1 Introduction 2-1
2.2 Tailings dams 2-1
2.2.1 General operation 2-2
2.2.2 Failures, causes and aftermath 2-4
2.3 Unsaturated aspects of soils 2-5
2.3.1 Phases of soils, capillarity and matric suctions 2-5
2.3.2 The shrinkage curve 2-8
2.3.3 The soil-water retention curve 2-9
2.4 Unsaturated shear strength of soils 2-11
2.4.1 Shear strength of unsaturated soils 2-12
2.4.2 Measuring the shear strength of unsaturated soils 2-24
2.5 The Direct Simple Shear apparatus (DSS) 2-27
2.5.1 The stress state in a DSS apparatus 2-30
2.5.2 Interpretation of results 2-31
2.5.3 Testing at low stresses 2-32
2.6 Behaviour of tailings under deposition 2-34
2.6.1 The dewatering behaviour of deposited tailings 2-34
2.6.2 The shear behaviour of deposited tailings 2-36
2.7 Slope stability considering unsaturated shear strengths 2-39
2.8 Summary 2-43

3 METHODOLOGY 3-1

3.1 Introduction 3-1
3.2 Material parameters 3-1
3.2.1 Particle size distribution (PSD) and specific gravities (G_s) 3-3
3.2.2 Soil water retention curve 3-4

3.3 Measuring the unsaturated shear strength of tailings 3-7
3.3.1 Sampling from a drying box 3-8
3.3.2 Dense, moist tamped samples 3-12
3.3.3 Loose, moist tamped sample 3-14
3.3.4 Slurry deposited samples 3-15
3.4 Monitoring the unsaturated regime in a tailings dam 3-18
3.4.1 Platinum tailings dam 3-21
3.4.2 Gold tailings dam 3-23
3.5 Consideration of unsaturated soil mechanics principles in slope stability assessments 3-25

4 EXPERIMENTAL RESULTS AND DISCUSSION 4-1

4.1 Introduction 4-1
4.2 Monotonic direct simple shear testing results 4-2
4.2.1 Sampling from a drying box 4-2
4.2.2 Dense, moist tamped samples 4-6
4.2.3 Loose, moist tamped samples 4-9
4.2.4 Slurry deposited samples 4-12
4.2.5 The effect of matric suction on the mobilised shear stress at the phase transfer point 4-19
4.3 Field measurements 4-23
4.3.1 Platinum tailings (Spigotted operation) 4-23
4.3.2 Gold tailings (Daywall-Paddock operation) 4-34
4.3.3 In-situ, unsaturated shear strength behaviour of platinum and gold tailings 4-42
4.4 Considering matric suction in slope stability assessments of tailings dams 4-47
4.5 Discussion 4-54

5 CONCLUSIONS AND RECOMMENDATIONS 5-1

5.1 Conclusions 5-1
5.2 Recommendations 5-3
5.2.1 Consideration of additional materials 5-3
5.2.2 Practical considerations regarding logger installations 5-3
5.2.3 Measurement of unsaturated shear strength with a DSS apparatus 5-4
5.2.4 Confirmation of the pore pressure profile above the phreatic surface 5-5

6 REFERENCES 6-1

LIST OF TABLES

Table 2.1: The seven reviewed unsaturated shear strength equations (Garven, 2009). 2-12

Table 3.1: In-situ void ratios and dry densities at the installation locations of the platinum and gold tailings dams (TD). 3-2

Table 3.2: Minimum and maximum void ratios of platinum and gold tailings samples from the tailings dams in Figure 3.1 and Figure 3.2. 3-3

Table 3.3: Material parameters relevant to the slope stability assessments. 3-28

Table 3.4: Fitted parameters for the Fredlund and Xing (1994) model. 3-29

Table 4.1: Statistical performance of the considered unsaturated shear strength models. 4-22

LIST OF FIGURES

Figure 2.1: Tailings dams owned and operated by Anglo American as of 2019 (Anglo American Tailings factsheet, 2019). 2-1

Figure 2.2: Cross-section of an idealised upstream tailings dam. 2-2

Figure 2.3: Satellite image of the tailings dams West of Johannesburg (Google Earth Pro, 2022). 2-3

Figure 2.4: Satellite image of the complex of tailings dams next to the FNB soccer stadium in Johannesburg (Google Earth Pro, 2022). 2-4

Figure 2.5: Categorized cause of failure over the last 100 years (adapted from Azam & Li, 2010). 2-5

Figure 2.6: Schematic representation of the unbalanced cohesion between water molecules at the air-water interface, adapted from Likos and Lu (2004). 2-6

Figure 2.7: Schematic representation of capillarity. 2-7

Figure 2.8: Typical volume-mass relationship of slurried specimens (Fredlund et al., 2002). 2-8

Figure 2.9: Schematic representation of the reduction in meniscus radius between two soil particles with reducing water content. 2-9

Figure 2.10: Desiccation process of soil and its relationship with the soil-water retention curve. 2-10

Figure 2.11: Comparison of the unsaturated shear strength due to matric suction and the saturated shear strength in a Direct Shear test adapted from Garven, 2009. 2-14

Figure 2.12: Percentage of soils with an acceptable fit when compared with unsaturated shear strength equations, after Garven (2009). 2-15

Figure 2.13: Percentage of tailings samples proportional to the total amount of tailings samples which were successfully predicted, adapted from Garven (2009). 2-15

Figure 2.14: Typical relationship between matric suction and unsaturated shear strength, after Khalili and Khabbaz (1998). 2-17

Figure 2.15: The effective stress parameter plotted against matric suctions, adapted from Khalili and Khabbaz (1998). 2-18

Figure 2.16: The effective stress parameter plotted versus normalised matric suction, from Khalili and Khabbaz (1998). 2-19

Figure 2.17: Relationship between the proportion of pore space filled with water and degree of saturation for an ideal soil, after Öberg (1995). 2-20

Figure 2.18: a) Typical SWRC, b) Typical shear strength behaviour relating to the SWRC. Adapted from Vanapalli et al. (1996).....2-21

Figure 2.19: Shear strength results of unsaturated tests compared to the soil's corresponding SWRC, after Donald (1957).....2-25

Figure 2.20: Unsaturated loading stages and shear strength results of a silty sand (SM) after Nam et al. (2011).....2-26

Figure 2.21: Shearing differences between the DS and DSS.....2-28

Figure 2.22: The effect of principal stress orientation on undrained shear strength (Yoshimine et al., 1998).....2-29

Figure 2.23: Shear modes in a slip surface (Sadrekarimi, 2014).....2-29

Figure 2.24: The stress state in a DSS sample estimated with DEM by (Asadzadeh and Soroush, 2016) 2-31

Figure 2.25: Failure plane assumptions for interpretation of DSS results.....2-32

Figure 2.26: The effect of confining stress on the critical state friction angle of sand (Al Tarhouni and Hawlader, 2021).....2-33

Figure 2.27: Cross sectional view of the drying box (Daliri et al., 2016).....2-34

Figure 2.28: Average gravimetric water content of all the layers after deposition (Daliri et al. (2016)). 2-35

Figure 2.29: Matric suctions after of each newly deposited layer, after Daliri et al. (2016).....2-36

Figure 2.30: Results of gold tailings samples allowed to desiccate to varying water contents, re-wetted and sheared, after Daliri et al. (2014).....2-37

Figure 2.31: Shear results of buried tube samples obtained from a drying box, after Daliri et al. (2016). 2-38

Figure 2.32: SWRC's of the four modelled materials, after Zhang et al. (2014) 2-40

Figure 2.33: Shear strength of a soil with an AEV of 5 kPa plotted over matric suction for the different shear strength models, after Zhang et al. (2014).....2-40

Figure 2.34: Representation of the analysed infinite slope (Zhang et al., 2014).....2-41

Figure 2.35: Safety factors on an infinite slope plotted over slip surface depth of a silty sand with an AEV of 5 kPa, after Zhang et al. (2014).....2-41

Figure 2.36: Flat slope considered with limit equilibrium analysis and unsaturated shear strength equations, after Zhang et al. (2014).....2-42

Figure 2.37: Plot of the critical safety factors plotted against air entry value for the considered shear strength models, after Zhang et al. (2014). 2-43

Figure 3.1: Sampling locations on the platinum tailings dam (Google Earth Pro, 2022). 3-2

Figure 3.2: Sampling location on the gold tailings dam (Google Earth Pro, 2022). 3-3

Figure 3.3: Platinum tailings particle size distribution and Gs. 3-4

Figure 3.4: Gold tailings particle size distribution and G_s. 3-4

Figure 3.5: SWRC measurement apparatus. 3-5

Figure 3.6: Determination of the air entry value on a soil water retention curve of a hypothetical curve. 3-5

Figure 3.7: SWRCs at installations of DAQ1, DAQ2 and DAQ3 on a platinum tailings dam. 3-6

Figure 3.8: The SWRC of a surface sample taken from the daywall on a gold tailings dam. 3-6

Figure 3.9: A Geocomp direct simple shear apparatus based on the NGI DSS (Geocomp, 2022)..... 3-7

Figure 3.10: A 300mm x 600mm drying box filled with slurried platinum tailings instrumented with two tensiometers and one Teros 12 volumetric water content probe. 3-8

Figure 3.11: Tailings sample extruded onto the DSS pedestal. 3-9

Figure 3.12: Schematic of a complete DSS pedestal and sample without the surrounding DSS rings, membrane and O-rings. 3-10

Figure 3.13: Barrelling of low-strength samples due to self-weight and top cap loading. 3-10

Figure 3.14: Placement of tensiometers on the sheared sample (top), example of pore pressure measurements after shearing (bottom). 3-11

Figure 3.15: Matric suctions of the dense moist tamped samples measured with a tensiometer before and after shearing. 3-13

Figure 3.16: Void ratios achieved during formation, consolidation and shearing. 3-15

Figure 3.17: Tensiometers placed on top of a sample slurried into a membrane stretched over the DSS rings to monitor the generation of matric suctions during drying. 3-17

Figure 3.18: Schematic of the University of Pretoria high capacity tensiometer. 3-18

Figure 3.19: TDR volumetric water content sensors, 5TM (left), Teros 12 (right). 3-19

Figure 3.20: Calibration curve of the Teros 12 probe to gold and platinum tailings for volumetric water content. 3-20

Figure 3.21: Variation in void ratio during calibration of the Teros 12 probe. 3-20

Figure 3.22: Measured increase of tailings depth at DAQ1. 3-21

Figure 3.23: Data acquisitioning systems (DAQ) layout on a platinum tailings dam (Google Earth Pro, 2022). 3-22

Figure 3.24: Sensor configuration at DAQ1 (not to scale). 3-22

Figure 3.25: Sensor configuration at DAQ2 and DAQ3 (not to scale). 3-23

Figure 3.26: Data acquisitioning system position on a gold tailings dam (Google Earth Pro, 2022). ... 3-24

Figure 3.27: Sensor configuration (not to scale). 3-24

Figure 3.28: Extrapolation of the pore pressure build-up into the unsaturated region of a tailings dam slope. 3-26

Figure 3.29: Cross-section of the analysed platinum tailings dam slope showing the slip surfaces considered. 3-27

Figure 3.30: Cross-section of the analysed gold tailings dam slope showing the slip surfaces considered. 3-28

Figure 3.31: Soil water retention curves of gold and platinum tailings used in the GeoStudio analyses. 3-29

Figure 3.32: Increases in shear strength due to suction calculated from the SWRC. 3-29

Figure 4.1: Pore pressure measurements from the drying box. 4-2

Figure 4.2: Monotonic DSS results on three samples taken from the dying box. 4-3

Figure 4.3: Pore pressures (top) and temperature (bottom) measurements from the drying box. 4-4

Figure 4.4: The effect of sub-zero pore water temperature on water content. 4-5

Figure 4.5: Monotonic DSS results of the second sampling attempt from the drying box. 4-6

Figure 4.6: Monotonic DSS results of the second approach (Mobilised shear stress vs shear strain). 4-7

Figure 4.7: Monotonic DSS results of the second approach (Mobilised shear stress vs void ratio). ... 4-8

Figure 4.8: One-dimensional consolidation. 4-9

Figure 4.9: Comparison between overconsolidated and normally consolidated samples a) consolidation, b) shearing. 4-10

Figure 4.10: Consolidation of nominally moist tamped samples to 50 kPa vertical stress. 4-11

Figure 4.11: Matric suctions in the nominally compacted samples measured with a tensiometer before and after shearing. 4-11

Figure 4.12: Drained, mobilised shear stresses of saturated and unsaturated, nominally moist tamped samples. 4-12

Figure 4.13: Pore pressure measurements from the samples slurried into the assembled DSS rings. ... 4-13

Figure 4.14: Matric suctions measured before consolidation and after shearing versus gravimetric water content. 4-13

Figure 4.15: SWRC fitted to datapoints relating to matric suctions and degrees of saturations measured from the sheared samples. 4-14

Figure 4.16: Comparison between the SWRC measured in the lab at in-situ densities and the SWRC fitted to data presented in Figure 4.15. 4-15

Figure 4.17: Shear stress measurements from drained, monotonic DSS testing on undisturbed slurry deposited tailings samples. 4-15

Figure 4.18: Mobilised shear stress plotted against void ratio of drained, monotonic DSS tests on undisturbed slurry deposited samples. 4-16

Figure 4.19: Plot of the dilation angle used to find the phase transfer point. 4-17

Figure 4.20: Shear stress results plotted against void ratio for dense platinum tailings samples. 4-18

Figure 4.21: Mobilised shear stress at phase transfer for unsaturated slurried tailings at varying matric suctions, measured after shearing. 4-18

Figure 4.22: Mobilised shear stress at phase transfer of unsaturated moist tamped tailings at varying matric suctions measured after shearing. 4-19

Figure 4.23: Mobilised shear stress at phase transfer of dense, unsaturated tailings plotted versus matric suction. 4-20

Figure 4.24: Increase in shear strength at the phase transfer point of dense, unsaturated tailings samples plotted over matric suction. 4-21

Figure 4.25: Degree of saturation, pore pressure and temperature monitored at varying depths near the wall of a platinum tailings dam. 4-24

Figure 4.26: Two different cases of water infiltration behaviour after tailings deposition measured from the same installation. 4-26

Figure 4.27: Comparison between laboratory and in-situ soil water retention behaviour. 4-27

Figure 4.28: Matric suction profile for suctions measured between depths of 0.25 m and 1.7 m at DAQ1. 4-28

Figure 4.29: Matric suction profile for suctions measured between depths of 1.4 m and 2.9 m at DAQ1. 4-29

Figure 4.30: Matric suction profile for suctions measured between depths of 2.8 m and 4.3 m at DAQ1. 4-29

Figure 4.31: Calculated coefficients of variations in matric suction plotted versus measurement depth at DAQ1. 4-30

Figure 4.32: Surface measurements of water content, pore pressure and temperature halfway along the beach of a platinum tailings dam (DAQ2). 4-31

Figure 4.33: Matric suction profile for suctions measured between depths of 0.25 m to 1.75 m at DAQ2. 4-33

Figure 4.34: Surface measurements of water content, pore pressure and temperature on the pool edge of a platinum tailings dam (DAQ3). 4-34

Figure 4.35: Sensor configuration of the probes in the daywall of a gold tailings dam, repeated from Figure 3.25. 4-35

Figure 4.36: Matric suctions measured at varying depths on the inside of the daywall. 4-35

Figure 4.37: Matric suctions measured on the outer and inner edge of a gold tailings dam daywall. ... 4-37

Figure 4.38: Pore pressure and degree of saturation measured in a daywall closest to the pool. 4-38

Figure 4.39: Pore pressure and degree of saturation measured in a daywall closest to the outer slope. 4-38

Figure 4.40: Comparison between in situ soil water retention behaviour and a drying curve measured on moist tamped material in the laboratory. 4-39

Figure 4.41: Cristal growth on a gold tailings sample. 4-40

Figure 4.42: Matric suction profile for suctions measured between depths of 0.25 m to 5.90 m on the gold tailings dam. 4-41

Figure 4.43: Calculated coefficients of variations in matric suction plotted versus measurement depth on the gold tailings dam. 4-41

Figure 4.44: Comparison in the variability of matric suction measurements in gold tailings and platinum tailings. 4-42

Figure 4.45: Shear strength gained from matric suctions at varying depths near the wall of a platinum tailings dam. 4-43

Figure 4.46: Increase in shear strength from matric suction calculated from the SWRC of platinum tailings. 4-44

Figure 4.47: Shear strength gained from near-surface matric suctions measured on the beach of a platinum tailings dam. 4-44

Figure 4.48: Comparison between matric suction induced shear strength gains, both estimated from matric suctions but with water contents measured with the Teros12 probe and inferred from the SWRC. 4-45

Figure 4.49: Increase in shear strength from matric suction calculated from the SWRC of gold tailings. 4-46

Figure 4.50: Analysed profile of the platinum tailings dam with the considered slip surfaces. 4-48

Figure 4.51: Analysed profile of the gold tailings dam with the considered slip surfaces. 4-48

Figure 4.52: Calculated porewater pressure at the bottom of each slice of each slip surface on the platinum tailings dam. 4-49

Figure 4.53: Calculated porewater pressure at the bottom of each slice of each slip surface on the gold tailings dam. 4-49

Figure 4.54: Safety factors of the platinum tailings dam. 4-51

Figure 4.55: Safety factors of the gold tailings dam. 4-52

Figure 4.56: Increases in shear strength due to matric suctions at the typical minimum, average and maximum values measured on the platinum tailings dam. 4-53

Figure 4.57: Increases in shear strength due to matric suctions at the typical minimum, average and maximum values measured on the gold tailings dam. 4-54

SYMBOLS

τ_{us}	Unsaturated shear strength
U_a	Pore air pressure
U_w	Porewater pressure
θ	Volumetric water content
ϕ'	Drained friction angle
$(U_a - U_w)_b$	Air entry pressure
χ	Effective stress parameter
c'	Drained cohesion
Sr	Degree of saturation
Θ	Normalised volumetric water content
τ	Shear stress
$\sigma - U_a$	Net effective stress
$U_a - U_w$	Matric suction
ψ	Matric suction
A_w	Porewater area
A_{tot}	Total pore area
θ_s	Saturated volumetric water content
θ_r	Residual volumetric water content
ϕ^b	Unsaturated friction angle
σ_N	Total normal stress
Ko	Coefficient of earth pressure at rest
ϕ'_{cs}	Drained critical state friction angle
γ	Density (kN/m^3)

1 INTRODUCTION

1.1 BACKGROUND

The ore extraction process of mining creates large volumes of solid and liquid waste stored in tailings dams which are also known as tailings storage facilities (TSF). The stability of these large, self-confining structures is critical as failure has the potential to cause vast damage and loss of life in the case of a brittle failure. Due to the high risk involved, tailings dam owners are often required to spend large sums of money to ensure the stability of these structures.

Conventional limit equilibrium slope stability assessment methods often only consider the saturated, strength of tailings. However, a majority of the critical slip surface in a well operated tailings dam often passes through unsaturated material. The strength advantages that could be drawn from the unsaturated portion of a slope is typically disregarded due to the uncertainty about the matric suction behaviour in the slopes of active tailings dams.

It is well known that matric suctions are generated in unsaturated soils and contribute to strength in the form of apparent cohesion resulting from matric suction. However, the strength gained from matric suctions is generally unknown for mainly two reasons, the first, being due to the scarcity of sufficient in-situ matric suction and water content data on tailings dam slopes, leading to questions about reliability of suctions over time. The second reason is that the exact contribution of matric suctions to shear strength is unknown.

This project aimed to measure the temporal trends of matric suctions and water contents in a tailings dam and to find an unsaturated shear strength equation applicable to tailings. A comment is then made on the effect of matric suction on the slope stability of tailings dams once the objectives have been met. Data was gathered over sufficient time such that comment can be made about the trends of matric suctions in an operating facility. An unsaturated shear strength model, focussing on the strength gained from matric suctions, was identified from the literature from which values could be predicted following calibration against shear strengths measured from tests. This model was then used to estimate the expected gain in shear strength of unsaturated, in-situ tailings as deposition occurred. Finally, the identified strength model was applied into limit equilibrium slope stability analyses to determine the contribution of matric suctions to the safety factor of tailings dam slopes.

1.2 OBJECTIVES OF THE STUDY

The study had the following objectives:

The first objective of this study is to find an unsaturated shear strength model that can predict the expected gain in shear strength due to matric suctions.

The second objective is to observe the behaviour of pore pressures and water contents in the unsaturated regime of active tailings dams to provide insight on the suction and water content variation prevalent in these dams.

Results from the first and second objectives will be used to comment on the third and main objective which is to consider matric suctions in a limit equilibrium, slope stability assessment and compute its effects on the calculated safety factor against slope failures.

1.3 SCOPE OF THE STUDY

Unsaturated shear strength models, applicable to silty sands, were identified from literature. The models were evaluated by comparing predicted values with measured, unsaturated shear strength data to identify a single model which provides the best fit.

In-situ pore pressure and water content measurements were performed in the unsaturated region in active platinum and gold tailings dams over a period of 13 and 8 months respectively. These measurements were used in conjunction with a verified unsaturated shear strength model to find the effect of deposition and evaporation cycles had on the estimated shear strength of tailings in the unsaturated region of a tailings dam.

The effect of matric suction on the calculated safety factor of slopes was considered in both the cases of the platinum and the gold tailings dam. The safety factor was calculated for the cross-sections of the slopes nearest to the location where the probes were installed.

1.4 METHODOLOGY

A direct simple shear device was used to measure the shear strength of unsaturated tailings at varying degrees of matric suctions. The matric suction component was controlled by changing the formation water content of moist tamped samples and changing the drying time of slurried samples. The method used to find the relationship between matric suction and unsaturated shear strength was an iterative process which evolved as problems in the methodology were encountered and solved.

High capacity tensiometers and volumetric water content sensors were installed next to each other at various locations on a platinum and a gold tailings dam to monitor the behaviour of matric suctions and water contents over time. The platinum tailings dam was a spigotted operation and sensors were installed near the outer wall, halfway across the beach and next to the pond. The gold tailings dam is a daywall-paddock operation in which the sensors were installed in the daywall at varying depths.

The contribution of matric suction to the calculated slope safety factor was determined by running a series of limit equilibrium analyses. SLOPE/W, the slope stability component of the GeoStudio software package, was used to calculate the slope safety factor values. Safety factors obtained from calculations which considered the effect of matric suction on shear strength, were compared to values derived from classical limit equilibrium analyses which only consider the Mohr-Coulomb strength model and do not take matric suctions into account. The critical slip surface of each berm in both slopes were considered.

1.5 ORGANISATION OF THE REPORT

The report consists of the following chapters and appendices:

- Chapter 1 serves as introduction to the report containing the introduction, objectives, scope and methodology.
- Chapter 2 contains a literature study which focusses on the types and general operation procedure of tailings dams, soils as a three-phase material, the strength of tailings in an unsaturated state, the behaviour of matric suctions and water contents in active tailings dams and the effect of suction on slope stability.
- Chapter 3 describes the methodology undertaken during the study. This includes the methodology undertaken to determine soil properties such as the soil water retention curve, grading curves, calibrations, to make in-situ measurements and methods and results related to perform DSS testing.
- Chapter 4 contains the results and analysis of the gathered data.
- Chapter 5 contains the conclusions and recommendations of the study.

2 LITERATURE REVIEW

2.1 INTRODUCTION

The literature study focusses on the types and general operation procedure of tailings dams, soils as a three-phase material, the strength of tailings in an unsaturated state, strength measurement methods for unsaturated soils and the effect of matric suction on slope stability.

2.2 TAILINGS DAMS

The mining industry has played an integral role in the development of South Africa's economy for over a century. The extraction of minerals generates large volumes of solid and liquid waste of which more than half a ton of waste is generated to obtain approximately 1 g of gold (Ripley et al., 1982). Figure 2.1 contains data from Anglo American, a well-known international mining company, which summarizes the total number of tailings dams owned by them, of which 55 (64%) are in South Africa. This illustrates the responsibility that large mining houses accept regarding the environmental and socio-economic risks pertaining to tailings dams.

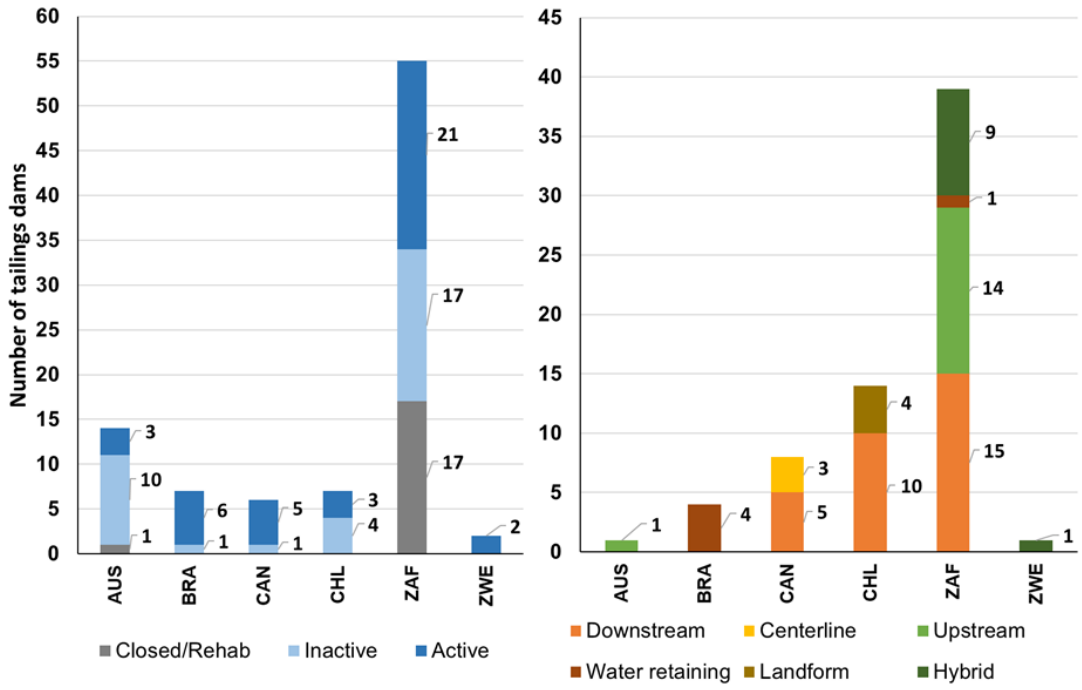

Figure 2.1: Tailings dams owned and operated by Anglo American as of 2019 (Anglo American Tailings factsheet, 2019).

Note: AUS = Australia, BRA = Brazil, CAN = Canada, CHL = Chile, ZAF = South Africa, ZWE = Zimbabwe.

A tailings dam failure can have widespread effects on communities and the environment downstream of the failure such as the frequently mentioned Feijão tailings dam failure in Brazil (2019) which released 9.7 million cubic meters of tailings within less than 5 minutes resulting in extensive social, economic and environmental damage.

The report on the technical causes of the abovementioned tailings dam failure listed the following unfavourable conditions upon failure of the slope (Robertson et al., 2019):

- A **steep design** on an upstream operation.

- **Water management** occasionally allowed the pond to advance closer to the wall such that finely graded and weak tailings were deposited near the crest.

-The crest was set back which resulted in the **construction of the containment berm on weaker, underlying tailings**.

- **Insufficient drainage** caused **high phreatic surface** levels, especially towards the toe.

-A **high rainfall season** may have resulted in a **loss of matric suction** and subsequently a **small strength loss in the unsaturated region** of the slope.

2.2.1 General operation

The downstream method, centreline method and the upstream method are commonly used for tailings dam construction. Upstream construction (Figure 2.2) is the most common and affordable method in South Africa. Other methods include combination of different construction methods and water retaining structures which are built with more competent material capable of storing both water and tailings in direct contact. More detail on the construction, operation and management can be read in Vick (1983).

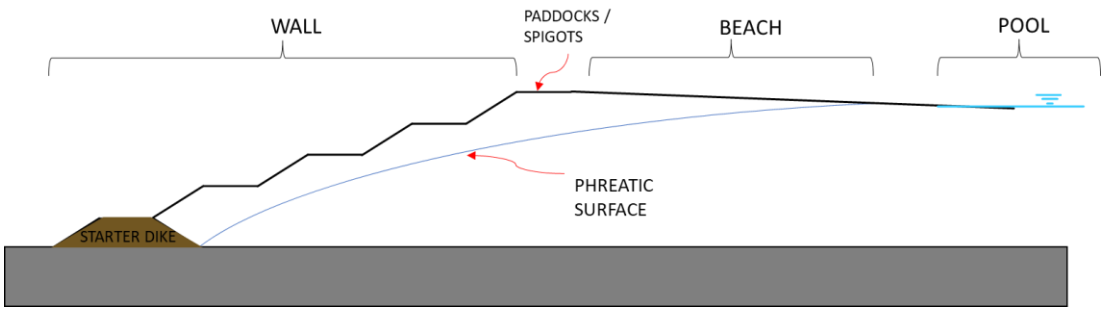

Figure 2.2: Cross-section of an idealised upstream tailings dam.

Typical tailings discharge methods include spigotting and single-point discharge methods. Spigotting occurs when valves are selectively opened along a peripheral pipe transporting

tailings on the outer wall. Single point discharge can be found in day-wall operations. Day-wall tailings dams have paddocks on top of the crest which are constantly being rebuilt as they are filled with tailings. Paddocks are separate dam-like compartments on top of the outer wall which are either packed by hand or built with machinery. Each paddock has a discharge pipe that is opened or closed as needed. At night tailings are deposited on the beach and allowed to flow towards the pond or night pan.

Figure 2.3 puts the common occurrence of tailings dams in South Africa into perspective as the light-coloured patches on the image shows the high degree of spatial integration of tailings dams into densely populated areas. The coordinates and eye altitude for the figure is listed in the references. Therefore, the quality of design, construction and proper operation of these facilities are exceptionally important. Another example of the integration of tailings dams with society is the tailings dam complex near the FNB soccer stadium, approximately 20 km from Soweto, (Figure 2.4) which hosted various FIFA world cup matches during 2010 including the opening and final games.

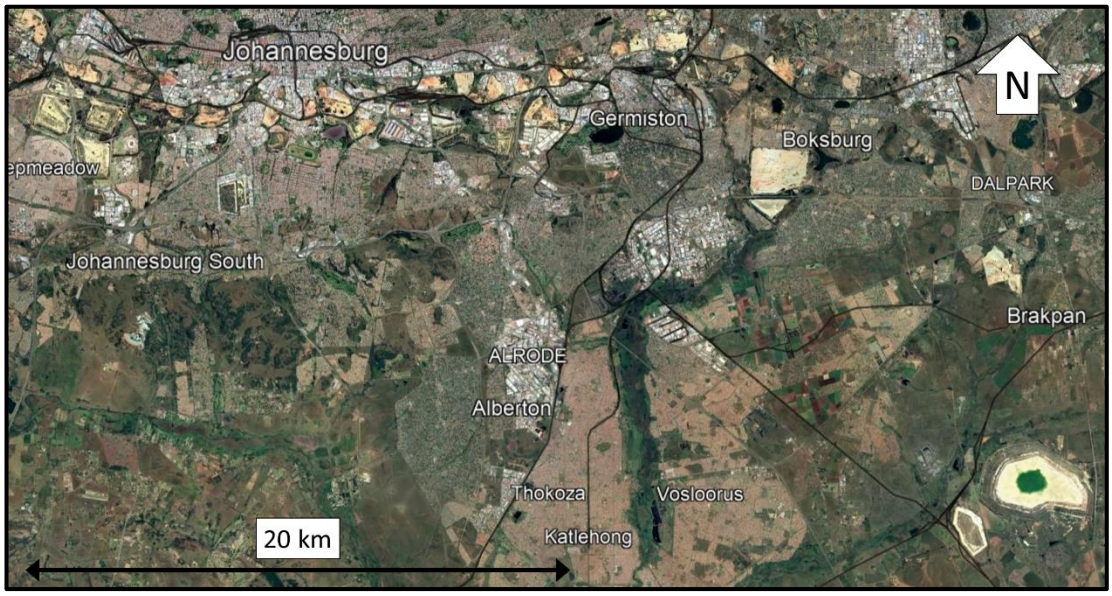

Figure 2.3: Satellite image of the tailings dams West of Johannesburg (Google Earth Pro, 2022).

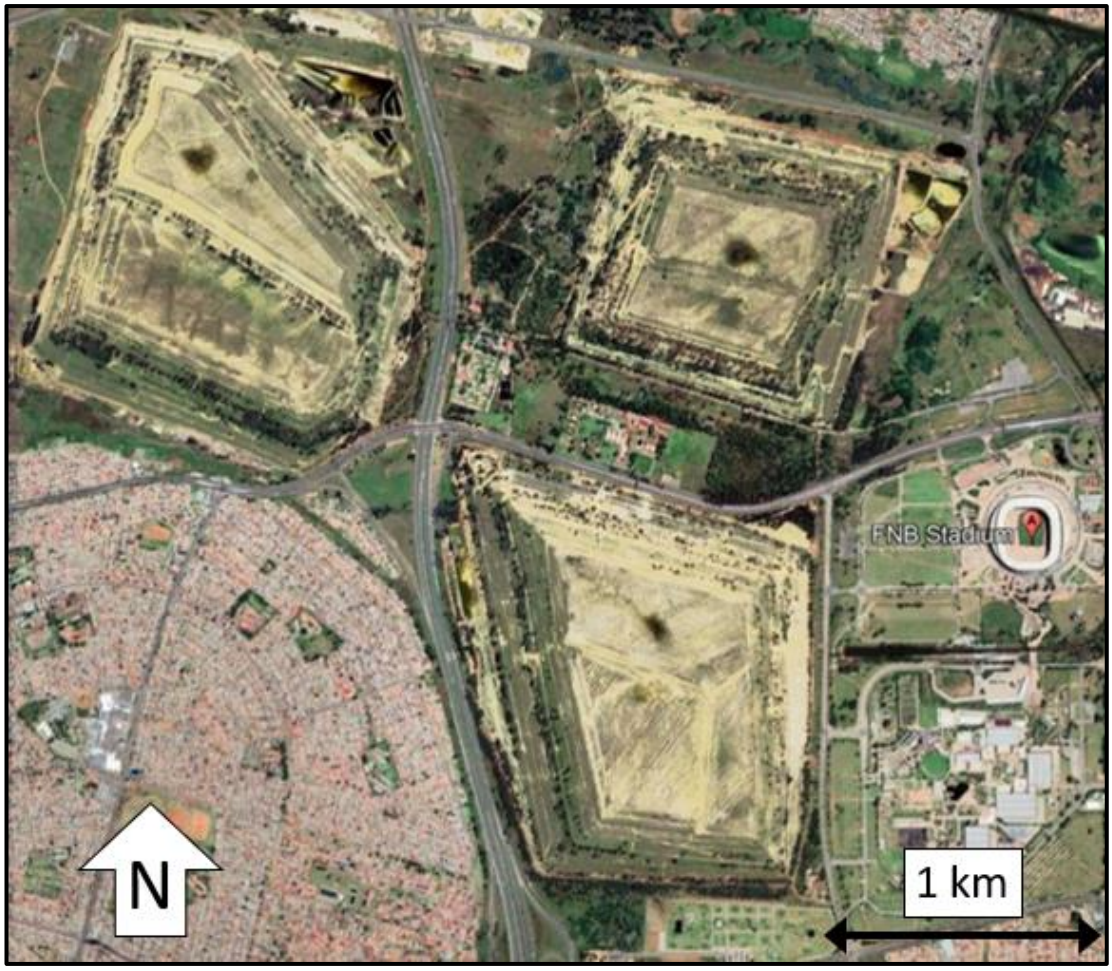

Figure 2.4: Satellite image of the complex of tailings dams next to the FNB soccer stadium in Johannesburg (Google Earth Pro, 2022).

2.2.2 Failures, causes and aftermath

Santamarina et al. (2019) identified the main failure mechanisms for tailings dam failures as:

- Overtopping of ponded water eroding the slopes (e.g., Merriespruit, South Africa, 1994).
- Shear of foundation soils (e.g., Mount Polley, Canada, 2014).
- Shear of underconsolidated material of low permeability deposited on or close to the retaining wall (e.g., Samarco, Brazil, 2015).

Azam and Li (2010) concluded the two main reasons for failures of tailings dams are unusual rainfall events and poor management. Figure 2.5 shows how the causes of failure differ from the periods of 1910 to 1999 and 2000 to 2009 (Azam and Li, 2010).

The most recent tailings dam failure occurred in September 2022 when a kimberlite tailings dam at Jagersfontein diamond mine breached in South Africa for reasons unknown at the time of drafting this report.

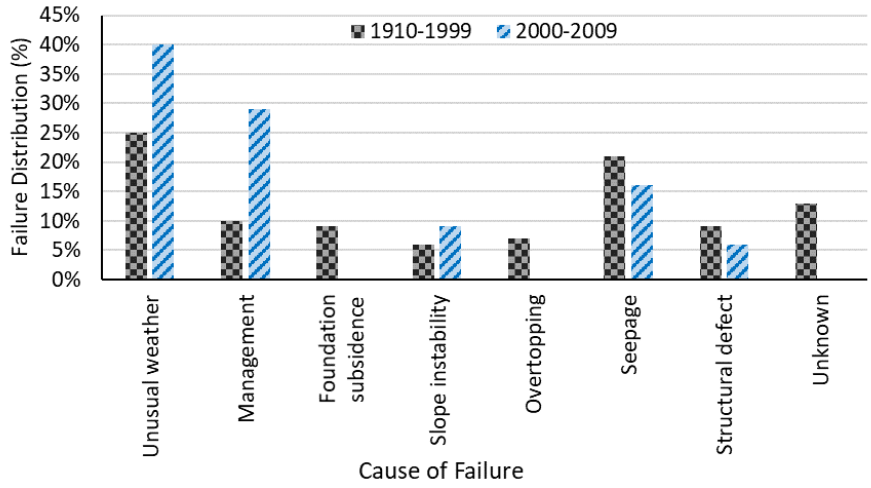

Figure 2.5: Categorized cause of failure over the last 100 years (adapted from Azam & Li, 2010).

Failure due to unusual weather has increased by almost a factor of two from 25% to 40 % and, according to Azam & Li, could be ascribed to the recent climate changes and increased unusually high rainfall events.

Failures due to mismanagement increased almost threefold showing the effect of malpractice in recent times. The other remaining categories may all fall under the topic of theoretical and technological advancement. Events of foundation subsidence virtually disappeared from 2000 to 2009. Neither did overtopping occur again, providing the condition that the main reason for overtopping was not malpractice (Azam and Li, 2010). Seepage related failures also decreased as did failures related to structural events. Slope stability failures from 2000 to 2009 showed a proportional increase compared to the slope stability failures that occurred between 1910 and 1999. The stability of slopes is highly dependent on the shear strength of the involved soils. This dissertation therefore aims to research the effect of matric suctions on the unsaturated shear strength of tailings.

2.3 UNSATURATED ASPECTS OF SOILS

2.3.1 Phases of soils, capillarity and matric suctions

Unsaturated soils consist of three elements: soil, air, water. The water phase in unsaturated soils can be divided further into two separate groups consisting of free water and adsorbed water.

Free water has a higher mobility than adsorbed water therefore requires less energy to be removed from the soil. Adsorbed water exists at residual states where its properties are influenced by the molecule's proximity to soil particles. Physiochemical interactions between the water molecules and soil particles start to play a role at this stage. The surface charge of

soils can also alter the characteristics of adsorbed water such as density, viscosity, dielectric properties, and freezing temperature (Likos and Lu, 2004).

In a liquid-gas system, the geometry of the interface between the air and water phases is governed by maintaining a pressure equilibrium across the interface. Unlike water, the surface tension of air is negligible. The measurement unit for surface tension is N/m and can thus be conceptualised as the maximum amount of tension that a thin water skin can resist per unit length. The surface tension of water is inversely correlated to temperature and is 71.29 mN/m at 25°C (Likos and Lu, 2004). Daily fluctuations in temperature can have an effect on matric suction.

Surface tension in a liquid at a gas-liquid interface is created by the unequilibrated cohesion forces experienced by the fluid molecules a finite distance away from the interface. Figure 2.6 schematically represents how water molecules on the surface are subjected to increased forces in the direction of the fluid. Polarized liquids, such as water, tend to have high surface tensions.

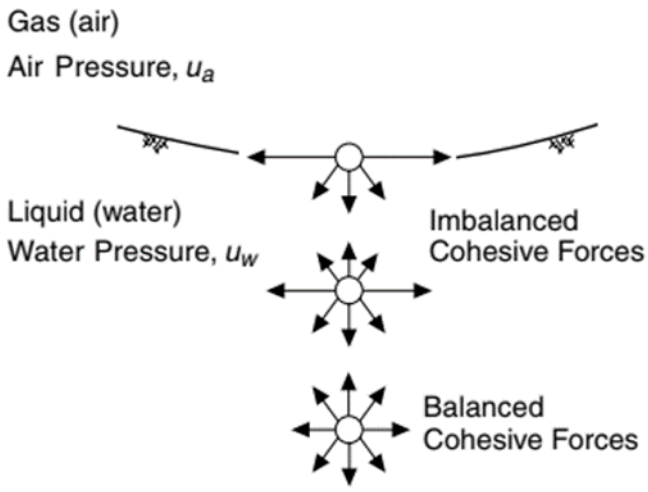

Figure 2.6: Schematic representation of the unbalanced cohesion between water molecules at the air-water interface, adapted from Likos and Lu (2004).

The pressure difference across an air-water interface is not created by surface tension, rather the tension in the water is generated due to a difference in pressure between the two phases (Likos and Lu, 2004). Generally, the phase experiencing the higher pressure will tend to expand. For example, the pressure in a balloon is higher than the pressure surrounding it, resulting in a concave surface towards the high-pressure side. The air pressure in an unsaturated soil is typically equal to atmospheric pressure and larger than the pore water pressure. Resulting in a concave surface towards the air phase. Equilibrium of forces shall therefore be reached by the maximum allowed surface tension of water.

Matric suctions in soils can conceptualised by using the analogy of a capillary tube (Figure 2.7). Say the tube radius is R, containing a fluid with a surface tension of T dividing a gas-fluid interface. The pressure in the gas phase is u_a and u_w corresponds to the pressure of the fluid and $u_a > u_w$.

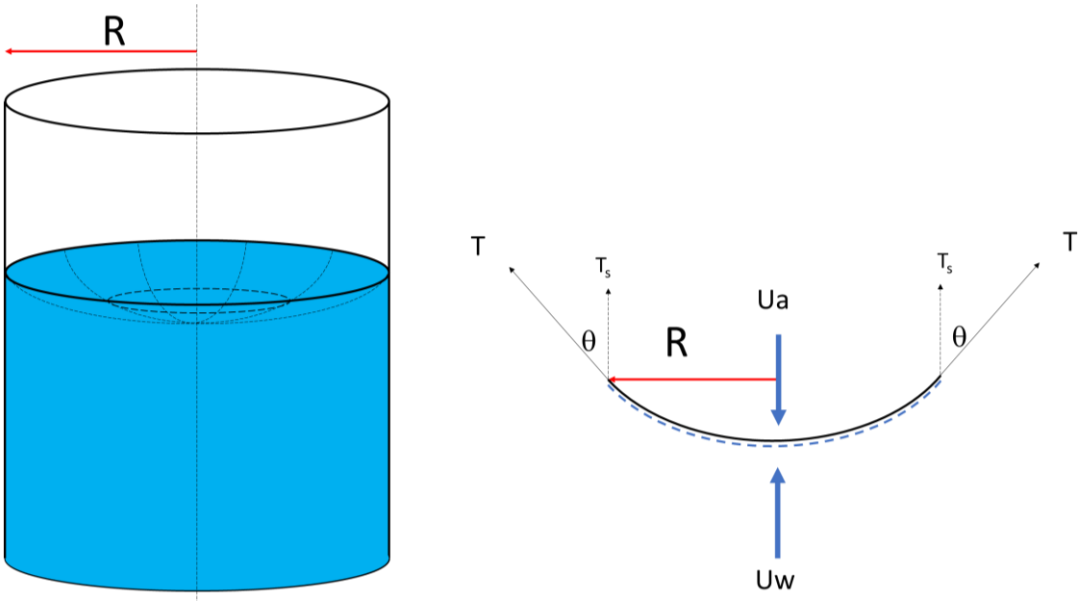

Figure 2.7: Schematic representation of capillarity.

The pressure difference over the interface can be converted to a resultant vertical force by finding the product of the projected area of the interface and the change in pressure over the interface which shall result in Equation 2.1. Force F_1 is negative due to the sign convention used.

$$F_1 = -(u_a - u_w)\pi R^2 \qquad (2.1)$$

Force, F_1, should be counteracted by an equal force in the opposite direction according to Newton's third law which is the tension between the water's contractile skin and the sidewalls of the capillary tube (Force F_2). This can be found by the product of the vertical component of force T and the circumference of the capillary tube.

$$F_2 = Tcos(\theta)2\pi R \qquad (2.2)$$

Letting $F_1 = F_2$ and solving for (u_a - u_w), which is usually termed the matric suction (ψ) component, will result in Equation 2.3:

$$u_a - u_w = \frac{-2TCos(\theta)}{R}$$

$$Let\ TCos(\theta) = T_s$$

$$u_a - u_w = \psi = \frac{-2T_s}{R} \qquad (2.3)$$

This simple equation shows that soil matric suction is inversely correlated to the radius of the interface or in geotechnical terms, highly dependent on the void size distribution.

2.3.2 The shrinkage curve

Matric suctions in soils will change the effective stress thereof and hence, according to the fundamental principles of soil mechanics, cause the element to distort or experience volume change. Therefore, drying of a soil causes an increase in matric suction, changing the effective stress which leads to a reduction in volume.

Fredlund et al. (2002) presented an equation and methods to describe the change in volume associated with drying in a soil water retention curve (SWRC).Typical shrinkage behaviour of slurried samples can be seen in Figure 2.8 where the sample initially follows the saturation line up to the point where matric suctions reach the air entry value. Once residual conditions have been reached there will be no further change in void ratio which can also be considered as the shrinkage limit. The shrinkage limit describes the water content at which no more volume change will occur due to drying.

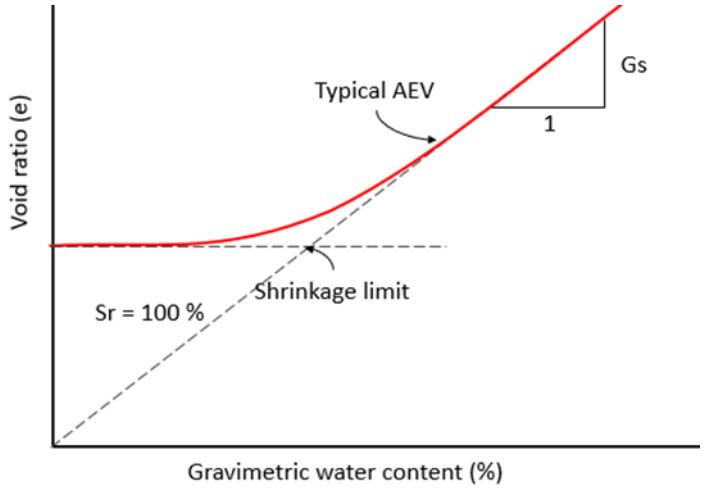

Figure 2.8: Typical volume-mass relationship of slurried specimens (Fredlund et al., 2002).

Fredlund et al. (2002) proposed the following best-fit equation to characterize the shrinkage behaviour of soils:

$$e(w) = a_{sh}\left[\frac{w^{sh}}{b_{sh}^{c_{sh}}} + 1\right]^{1/c_{sh}} \quad (2.4)$$

Where:

$e(w)$ = void ratio as a function of gravimetric water content

a_{sh} = minimum void ratio

b_{sh} = slope of the tangent line

c_{sg} = curvature of the shrinkage curve

The characterization of the shrinkage curve in combination with a model representing the water retention behaviour of a particular soil allows for the evaluation of volume change as a function of matric suction. Determination of the void ratio or degree of saturation of a soil upon drying becomes possible once the relationship between volume change and suctions has been established.

2.3.3 The soil-water retention curve

The blue shaded area in Figure 2.9 represents a soil's water content and shows how the radius of the meniscus reduces upon reduction in water content. Inspection of Equation 2.3 ($\psi = \frac{-2T_s}{R}$) in conjunction with Figure 2.9 shows that a reduction in the water content, reduces the radius of the menisci and should thus increase matric suction. Hence, lower water contents relate to higher suctions.

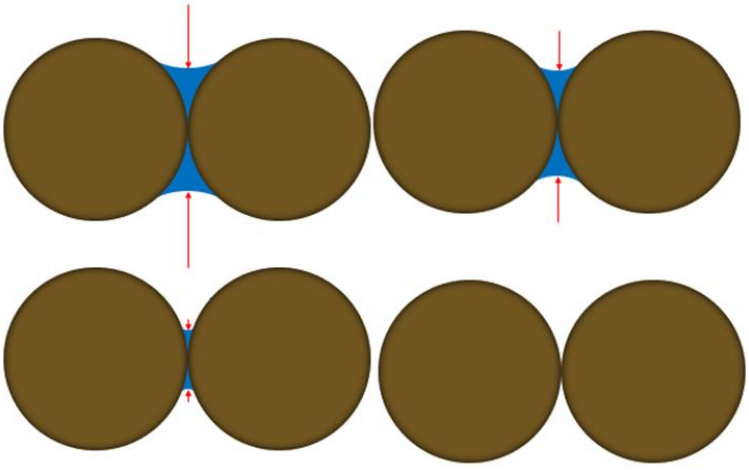

Figure 2.9: Schematic representation of the reduction in meniscus radius between two soil particles with reducing water content.

Figure 2.10 is a plot of gravimetric water content plotted over matric suction and shows the stages that a soil undergoes upon drying. A soil element will start fully saturated with zero matric suction. As matric suctions increase, the degree of saturation shall initially remain close to unity. This is due to drying experienced on the outer edges of the soil element forming menisci on the edges before desaturation of internal pores. It is usually the larger pores, which desaturate first, responsible for the generation of matric suctions at high water contents.

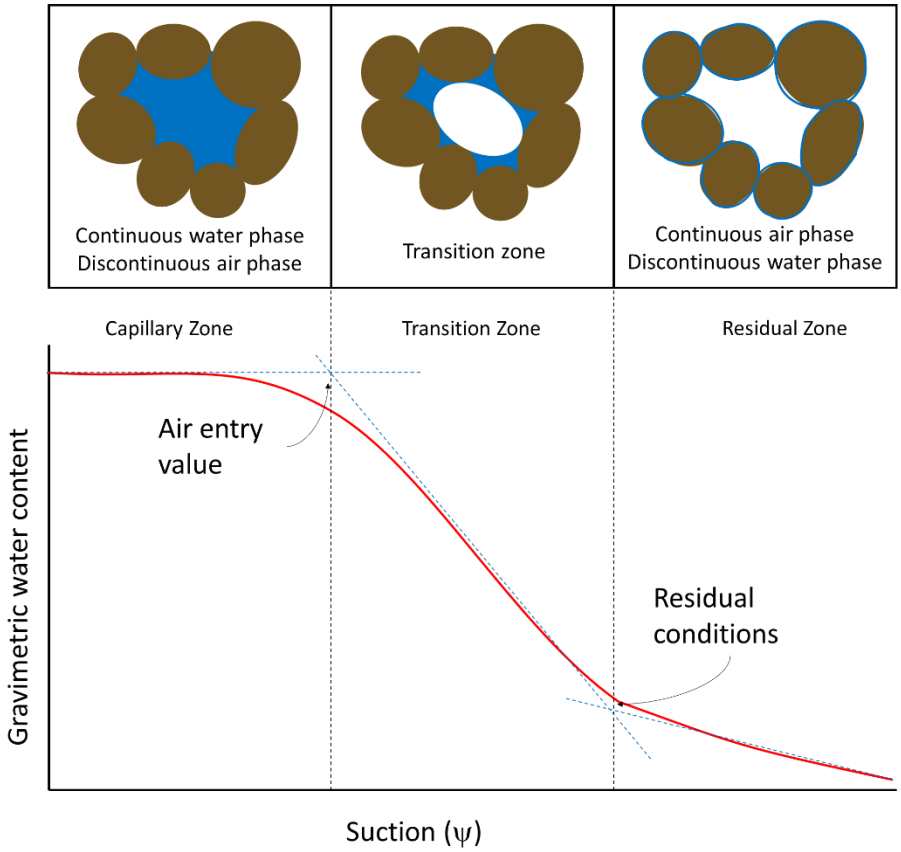

Figure 2.10: Desiccation process of soil and its relationship with the soil-water retention curve.

The soil-water retention curve is helpful in determining the coefficient of permeability for water in unsaturated soils as a function of water content. This is a preferred alternative to direct measurements of coefficients of permeability as direct measurements are laborious and complicated (Fredlund and Rahardjo, 1993).

Sillers and Fredlund (2001) statistically evaluated soil-water retention curve models for geotechnical purposes and found the Fredlund and Xing (1994) model as the most accurate solution. The Fredlund and Xing model tended to converge more rapidly when finding the correct fitting parameters for experimental data even if the initial fitting parameters were far from the correct value.

Fredlund and Xing (1994)

The Fredlund and Xing (1994) model is based on the same methodology as the Van Genuchten model but also considers pore size distribution (Ng and Menzies, 2014).

$$\theta = C(\psi)\theta_s \left[\frac{1}{\ln\left(e+\left(\frac{\psi}{a}\right)^n\right)} \right]^m \quad (2.5)$$

Where:

$$C(\psi) = \left[1 - \frac{\ln\left(1+\frac{\psi}{\psi^r}\right)}{\ln\left(1+\frac{10^6}{\psi^r}\right)} \right]$$

ψ = Matric suction (kPa).

ψ_r = Matric suction at residual conditions (kPa).

θ = Volumetric water content.

θ_s = Saturated water content.

a, n and m = Fitting parameters.

e = Euler's number.

$C(\psi)$ = Correction factor forcing the curve to pass through 1 000 000 kPa at zero water content.

The a-parameter is related to, but generally larger, than the air entry pressure. If "m" is relatively small, then "a" can be set equal to the air entry pressure. The n-parameter is used to set the sharpness of the curve near the air entry value, where the "m" controls the slope of the curve towards the higher end of the matric suction range.

2.4 UNSATURATED SHEAR STRENGTH OF SOILS

Matric suctions contributes to shear strength by increasing the interparticle effective stress. Slope stability assessments generally only consider a saturated or completely dry case and exclude the strengthening effects of partially saturated soils. Shear strengths in the case of a dry or drained, saturated case can be assessed with the Mohr-Coulomb strength model which requires a drained friction angle parameter ϕ' and cohesion c'. Cases where pore pressures do

not have sufficient time to dissipate, which is not applicable to completely dry cases, will be assessed with some sort of undrained shear strength (S_u).

Traditionally, the contribution of matric suctions to shear strength in partially saturated cases is neglected and usually disregarded. This is primarily due to the difficulty of measuring in-situ matric suctions on slopes and the uncertainty in the contribution of suction to strengths. Other factors may include scarcity of data and reliability of matric suctions. Therefore, inclusion of matric suctions into slope stability analyses first requires validation by long term field measurements and verification of shear strength models. Slope stability is governed by geometry, pore pressures, self-weight and shear strength of which the latter three tie in with unsaturated soils.

2.4.1 Shear strength of unsaturated soils

Garven (2009) reviewed 25 empirical equations from the literature for predicting the strength of unsaturated soils of which seven were compared with 130 datasets from 51 soils.

An equation's fit was considered acceptable if the predicted value was within 10% of the measured value. Equations were fitted to the matric suction component's contribution to shear strength rather than the combined strength of both the net stress and matric suction as the effect of suction on the total strength is typically small. Tolerances were changed to a different criterion in cases where the shear strength values fell below 50 kPa, in which case an acceptable fit was declared if the predicted value plotted within 5 kPa from the experimental data.

Seven equations could successfully predict the shear strength of unsaturated soils with a variation in matric suction. Only 8% of the soils could not be predicted with any of the seven functions. Table 2.1 summarizes the seven best equations identified by Garven (2009).

Table 2.1: The seven reviewed unsaturated shear strength equations (Garven, 2009**).**

Author	Equation
Aubeny and Lytton (2003)	$\tau_{us} = f_1(u_a - u_w)\theta tan\phi'$
Khalili and Khabbaz (1998)	$\chi = \left[\frac{(u_a - u_w)}{(u_a - u_w)_b}\right]^{\eta}$
Lytton (1996)	$\tau_{us} = (u_a - u_w)\theta_w tan\phi'$

Öberg and Sällfors (1995)	$\tau = c' + (\sigma - u_a) + S(u_a - u_w)tan\phi'$
Tekinsoy et al. (2004)	$\tau_{us} = tan\phi'[(u_a - u_w)_b + p_{at}]\ln\left(\frac{(u_a - u_w) + p_{at}}{p_{at}}\right)$
Vanapalli et al. (1996)	$\tau_{us} = (u_a - u_w)\Theta^{\kappa} tan\phi'$
Vilar (2006)	$\tau_{us} = \frac{(u_a - u_w)}{\frac{1}{tan\phi'} + \left(\frac{1}{\tau_{us-max}} - \frac{1}{(u_a - u_w)_{max} tan\phi'}\right)}$

The experimental data contained results from both triaxial tests and direct simple shear tests. The basis of the direct simple shear test is discussed in section 2.5. Different total shear strengths were measured from the two test methods at the same matric suction due to the nature of the loading and shearing mode on the sample. This therefore requires the removal of the saturated shear strength component from the total shear strength component before the effect of matric suction on shear strength can be studied.

Unsaturated shear strength relies on the net normal stress between particles and the matric suction stress exerted onto the particles. The net normal stress is the stress related to components such as self-weight and loading which increases effective stress and is not related to matric suction. Suction stress is the increase in effective stress due to matric suction.

In the case of a direct simple shear test, the confining pressure is applied perpendicular to the horizontal plane with a vertical load and is therefore equal to the net normal stress. An increase in matric suction will thus not increase the saturated strength component in a direct simple shear sample as the vertical load is kept constant. This therefore implies that, if the effect of matric suction is to be studied with a direct simple shear apparatus, then a constant load test is preferred as opposed to a constant volume test.

Figure 2.11 shows how matric suction contributes to shear strength by plotting data points above the saturated shear strength. Unsaturated shear strengths are found by removing the saturated strength component.

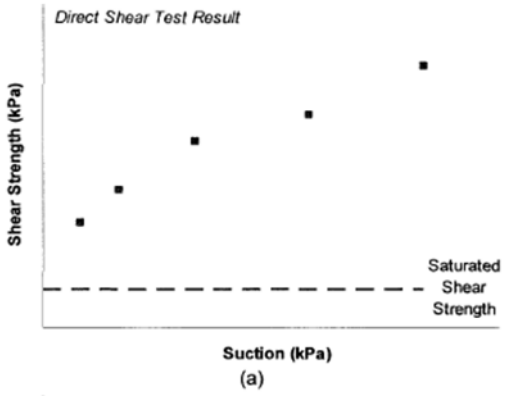

Figure 2.11: Comparison of the unsaturated shear strength due to matric suction and the saturated shear strength in a Direct Shear test adapted from Garven, 2009.

Figure 2.12 presents the performance of the seven unsaturated shear strength equations fitted to all the available soil types. Figure 2.13 presents the performance of the unsaturated shear strength equations fitted to the tailings datasets.

Figure 2.12 shows how the proposed equation by Vilar fitted 93% of all the available soil types when considering its estimation in strength-gain from matric suctions. Its applicability when predicting total shear strength reduced to 62%. However, Vilar's equation requires a measured shear strength point for curve fitting purposes which, in terms of unsaturated soil testing, is often not an option. Equations by Khalili and Khabbaz (55%), Öberg et al. (52%), and Vanapalli et al. (48%) performed well when predicting strength gained from matric suctions.

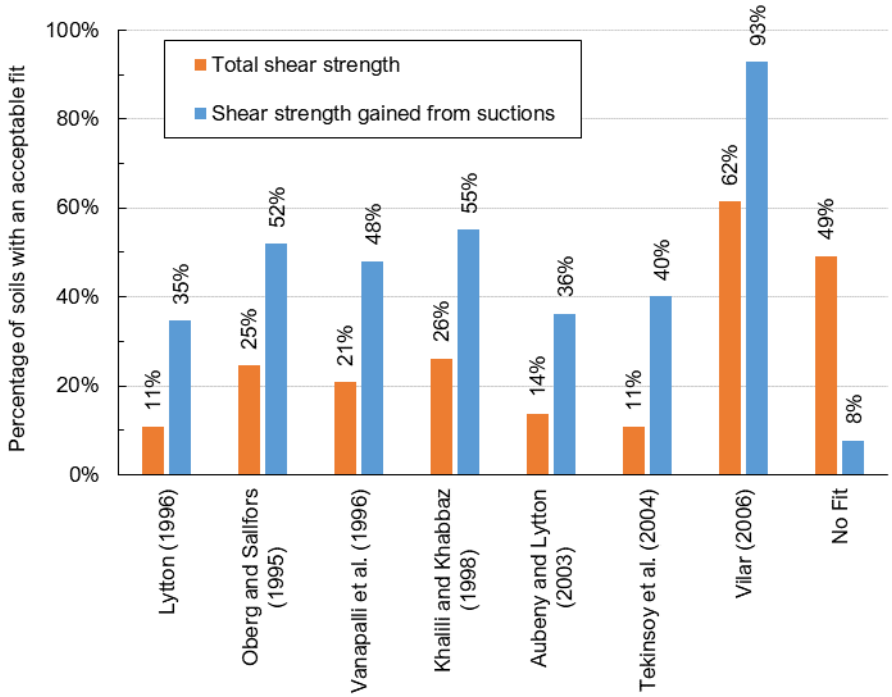

Figure 2.12: Percentage of soils with an acceptable fit when compared with unsaturated shear strength equations, after Garven (2009).

Figure 2.13 shows that the four equations that performed best when estimating the unsaturated shear strength of tailings were, in decreasing order of acceptable fit, Vilar (2006), Khalili and Khabbaz (1998), Öberg and Sällfors (1995), and Vanapalli et al. (1996). The discussion of these equations follow Figure 2.13.

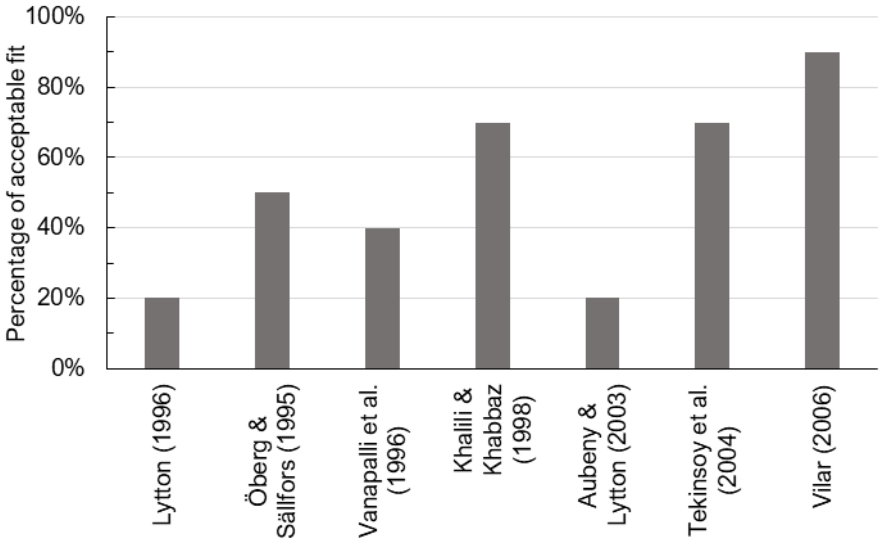

Figure 2.13: Percentage of tailings samples proportional to the total amount of tailings samples which were successfully predicted, adapted from Garven (2009).

Khalili and Khabbaz (1998)

The equation proposed by Khalili and Khabbaz is built upon Bishop's equation:

$$\sigma' = (\sigma - u_a) + \chi(u_a - u_w) \quad (2.6)$$

Where:

σ' = Effective stress

σ = Total stress

u_a = Pore air pressure

u_w = Porewater pressure

$(\sigma - u_a)$ = Net total stress

$(u_a - u_w)$ = The difference between pore air pressure and porewater pressure

χ = Effective stress parameter related to the degree of saturation

χ has a value of 1 for fully saturated soils and 0 for dry soil but for partially saturated soils it is often difficult to quantify and highly variable as it is related to soil structure. Khalili and Khabbaz (1998) therefore attempted to find a relationship between the effective stress parameter and the air entry value of a soil. Determination of χ would typically occur by analysis of shear strength data. Substitution of Equation 2.6 into the Mohr-Coulomb failure envelope will yield the following relationship:

$$\tau = c' + [(\sigma - u_a) + \chi(u_a - u_w)]tan\phi' \quad (2.7)$$

Where:

τ = Unsaturated shear strength

The drained shear strength of a saturated soil is $\tau_0 = c' + (\sigma - u_a)tan\phi'$ with $u_a = u_w$. The contribution of matric suction to shear strength is thus $\tau - \tau_0 = \chi(u_a - u_w)tan\phi'$. Solving for χ equates to:

$$\chi = \frac{\tau - \tau_0}{(u_a - u_w)tan\phi'} = \frac{a}{b} \quad (2.8)$$

Khalili and Khabbaz (1998) analysed 14 datasets to find the relationship between the effective stress parameter (χ) and matric suction. Figure 2.14 is a typical example on how the effective stress parameter was found for any given suction. One may find upon inspection of Equation 2.8 that, parameter "a" is the increase in shear strength due to matric suction ($a = \tau - \tau_0$) and parameter "b" is defined by $(u_a - u_w)tan\phi'$ illustrating what the shear strength would have been due to matric suction if the entire suction component contributed to strength.

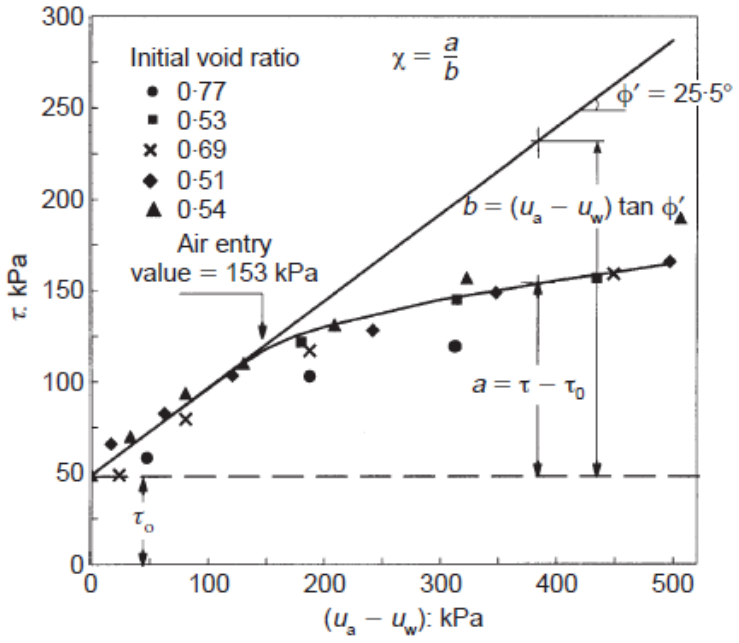

Figure 2.14: Typical relationship between matric suction and unsaturated shear strength, after Khalili and Khabbaz (1998).

The effective stress parameter (χ) was then determined for 14 datasets. Plotting of the effective stress parameter (χ) against matric suctions (u_a-u_w) (Figure 2.15) shows a clear relationship, such that the difference between the datasets occurred mostly due to the different air entry values of the soils.

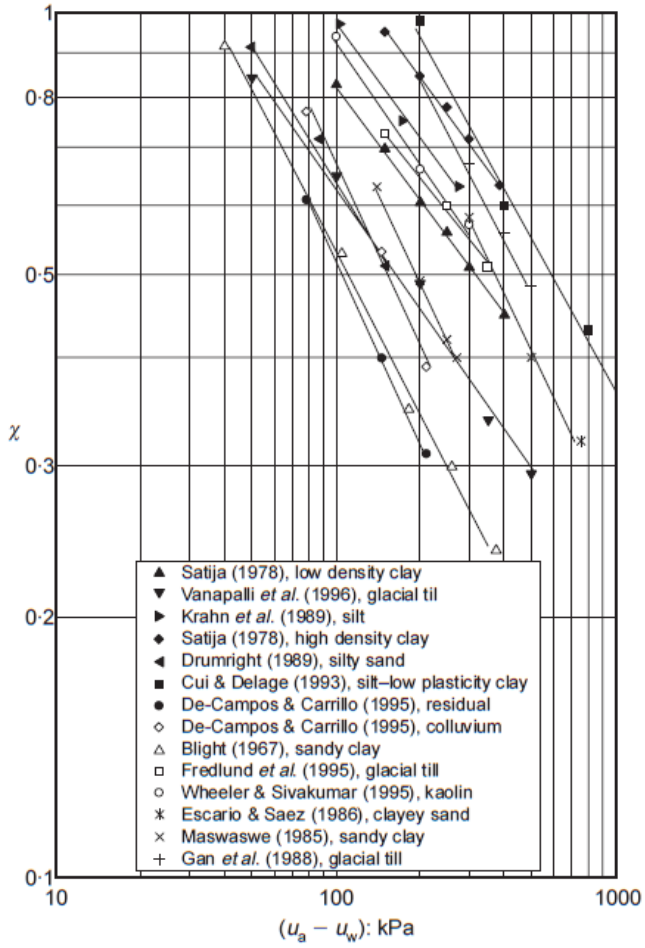

Figure 2.15: The effective stress parameter plotted against matric suctions, adapted from Khalili and Khabbaz (1998).

After normalization of matric suctions in Figure 2.15 with their corresponding air entry values ($(u_a-u_w)_b$) a log-linear relationship is obtained between the effective stress parameter and normalised matric suction as plotted in Figure 2.16. All datasets had coefficients of correlation greater than 0.98. The slopes of the resulting linear relationships ranged between 0.4 and 0.65 for clayey and sandy soils respectively, while a value of 0.55 is advised for soils where this relationship is unknown.

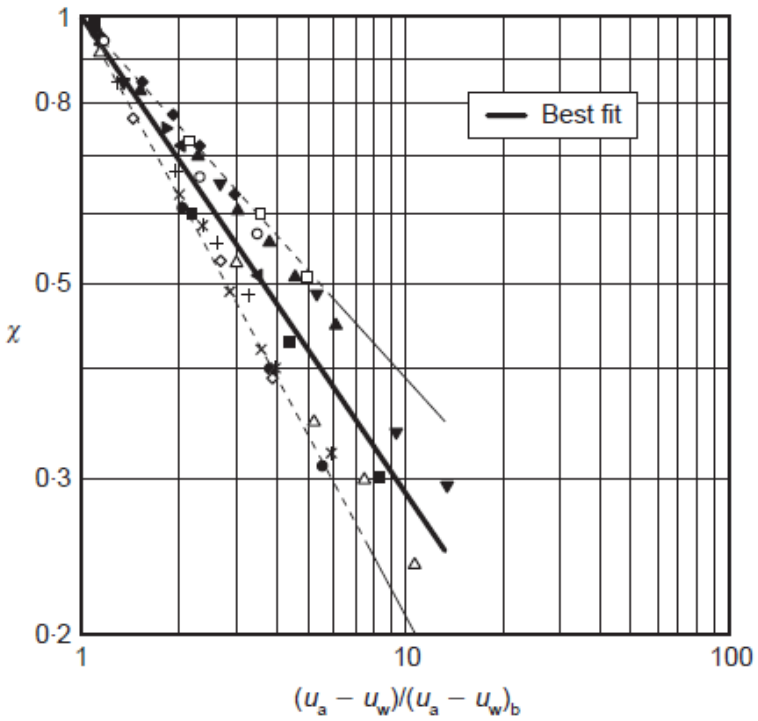

Figure 2.16: The effective stress parameter plotted versus normalised matric suction, from Khalili and Khabbaz (1998).

The produced best-fit relationship between χ and matric suction is:

$$\chi = \left[\frac{(u_a - u_w)}{(u_a - u_w)_b}\right]^{-0.55} \quad (2.9)$$

Where $(u_a - u_w)_b$ is the soil's air entry value or bubbling pressure.

Öberg and Sällfors (1995)

The equation proposed by Öberg and Sällfors is based on Bishop's unsaturated shear strength equation and the hypothesis that the soil-water retention curve is one of the main controlling factors of the shear strength of unsaturated soils.

The function of the χ-factor in Bishop's equation is to express the proportion of matric suction pressures that contribute to shear strength. Therefore, the Öberg and Sällfors equation relies on the idea that the χ-factor reflects the fraction of pore area occupied by water. Assuming the air phase pressure is equal to atmospheric, the shear strength equation may be represented by:

$$\tau_f = c' + \left(\sigma - \frac{A_w}{A_{tot}} u_w\right) tan\phi' \quad (2.10)$$

Where:

A_w = Area of pore space filled with water

A_{tot} = Total pore space area

$\frac{A_w}{A_{tot}}$ = the proportion of pore space filled with water.

Öberg (1995) showed that the change in the proportion of pore space filled by water plotted as a function of the degree of saturation is not linear in the case of an ideal soil consisting of identical spheres (Figure 2.17).

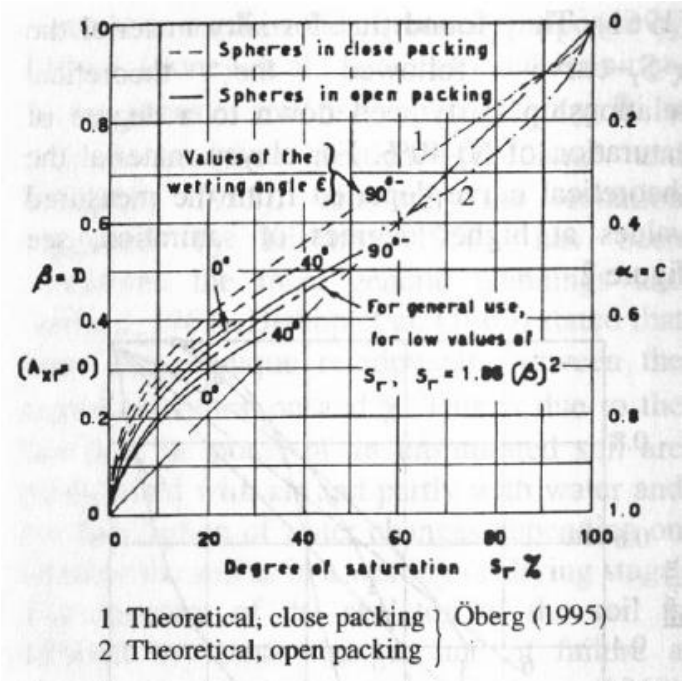

Figure 2.17: Relationship between the proportion of pore space filled with water and degree of saturation for an ideal soil, after Öberg (1995).

$\frac{A_w}{A_{tot}}$ is larger than the degree of saturation at low water contents with the difference between the two values increasing as the packing of a soil increased. At high saturation levels $\frac{A_w}{A_{tot}}$ is smaller than the degree of saturation. Soils with bi-modal pore size distributions, for example a clay, will experience desaturation in the following manner:

Upon the onset of desaturation, the pore water between the larger particles will drain and start generating matric suctions which are coupled to the larger particles. Hence, $\frac{A_w}{A_{tot}}$ will initially reduce faster than the degree of saturation, as the smaller pores have not yet been affected, and will plot slightly below the diagonal line in Figure 2.17. At this stage the soil will remain saturated as most of the voids are still filled with water (Bishop et al., 1960).

This allows for the estimation of the shear strength of non-clayey soils for degrees of saturation above 50% as the χ-parameter is roughly equal to the degree of saturation. The error between χ and the degree of saturation (S_r) for $S_r < 20\%$ is smaller as the effect of matric suction on undrained shear strength diminishes as the degree of saturation approaches zero.

Replacing of χ with S_r in equation 2.7 leads to the following equation:

$$\tau = c' + (\sigma - S_r U_w) tan\phi' \qquad (2.11)$$

Measurement of the soil-water retention curve will allow for the determination of matric suction correlated with the existing degree of saturation.

Vanapalli et al. (1996)

The hypothesis proposed by Vanapalli et al. (1996) also relies on the idea that the change in shear strength of unsaturated soils is related to the ratio of pore-area filled by water if a cross section is to be taken through a soil element. This implies a correlation between the soil-water retention curve and unsaturated shear strength.

This effect was illustrated in Vanapalli et al. (1996) by Figure 2.18 which plots a SWRC on the left and an unsaturated shear strength envelope for varying degrees of matric suction on the right.

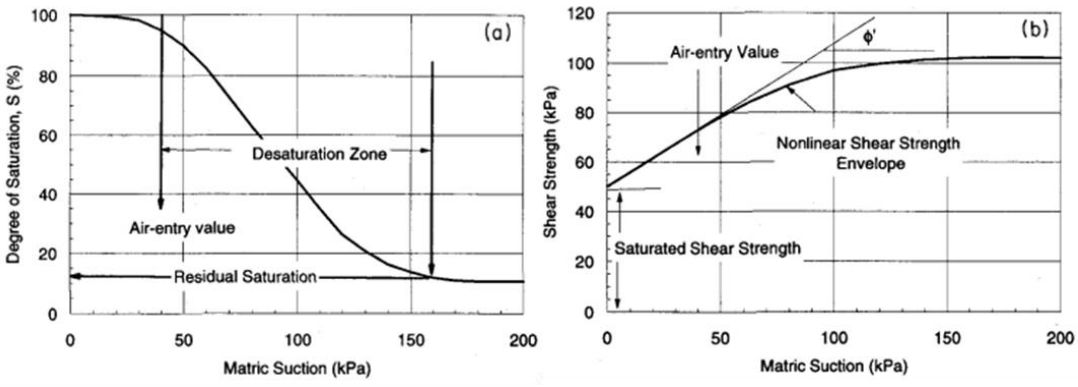

Figure 2.18: a) Typical SWRC, b) Typical shear strength behaviour relating to the SWRC. Adapted from Vanapalli et al. (1996).

Figure 2.18 complements Figure 2.14 showing the reason for the non-linearity of the contribution of matric suction to strength. As long as the soil remains saturated, which coincides with matric suctions below the air entry value, the increase in shear strength is linearly correlated to the increase in matric suction as illustrated in Figure 2.18 (b). However, during the transition phase of the SWRC from saturated to residual conditions the rate of increase in

the shear strength as a function of suction reduces. This can be ascribed to the reduction in continuity of the water phase as previously explained. The shape of the shear strength envelope for matric suctions greater than residual conditions cannot be predicted as it may remain constant, reduce or even increase (Vanapalli et al., 1996).

The analytical SWRC- equation of Fredlund and Xing (1994) and the shear strength equation by Fredlund et al. (1978) form the basis of the Vanapalli et al. (1996) equation. The contribution of matric suction to shear strength is related to the normalised area of pore water ($a_w = {A_w}/{A_{tot}}$) as previously mentioned. The normalised area of pore water ranges between unity and zero, like the degree of saturation. Vanapalli thus proposed the following relationship: $a_w = \Phi^{\kappa}$ where Φ is the normalised water content ($\frac{\theta-\theta_r}{\theta_s-\theta_r}$ in equation 2.13) and κ is a fitting parameter.

Hence, the proposed equation to predict shear strength at any matric suction value is written as:

$$\tau = c' + (\sigma_n - u_a)tan\phi' + (u_a - u_w)\,\Phi^{\kappa}tan\phi' \qquad (2.12)$$

Where:

σ_n = net normal stress

u_a = pressure of the air phase (generally assumed as zero for practical purposes)

The air pressure (u_a) is equal to the water pressure during saturated conditions simplifying Equation 2.12 to the general Mohr-Coulomb shear strength equation. The parameter κ is used to fit the equation to experimental data. Experimental tests were conducted for various values for κ of which 2.2 provided the best fit.

Vanapalli et al. (1996) also provided an alternative solution which relies on the residual conditions obtained from the SWRC allowing for the exclusion of κ:

$$\tau = c' + (\sigma_n - u_a)tan\phi' + (u_a - u_w)\left(\frac{\theta-\theta_r}{\theta_s-\theta_r}\right)tan\phi' \qquad (2.13)$$

Where:

$\left(\frac{\theta-\theta_r}{\theta_s-\theta_r}\right)$ = effective degree of saturation

θ_s = saturated volumetric water content

θ_r = residual volumetric water content

Equation 2.13 can be used in terms of both the volumetric water content and degree of saturation.

Vilar (2006)

Vilar (2006), continuing on the work presented in Vilar (1992), applied the following empirical hyperbolic equation to successfully predict the unsaturated shear strength of Brazilian soils:

$$\tau = c' + \sigma' tan\phi' + \frac{(u_a - u_w)}{a + b(u_a - u_w)} \quad (2.14)$$

Where:

c' = Effective saturated cohesion

$\sigma' tan\phi'$ = Product of effective stress and the tangent of the soil's frictional angle

a, b = Fitting parameters

ψ or ($u_a - u_w$) = Matric suction

Therefore, the matric suction-induced shear strength component from Equation 2.14 is referred to as a type of cohesion by Vilar:

$$\tau_{us} = \frac{(u_a - u_w)}{a + b(u_a - u_w)} \quad (2.15)$$

Parameter "a" aims to include the effect of the air entry value on the shear strength increase in soils. The model assumes that the relationship between c from equation 2.15 and matric suction ($u_a - u_w$) tends to zero as suction decreases.

Hence: $\lim_{(u_a - u_w) \to 0} \frac{dc}{d(u_a - u_w)} = \frac{1}{a} = tan\phi'$

Matric suctions will not significantly contribute to strength at residual conditions, it is even possible to expect a loss in shear strength at very dry conditions (Vilar, 2006). In the case of Equation 2.14, Vilar assumed that shear strength will reach an ultimate value at residual conditions for the sake of simplicity. This therefore requires an ultimate shear strength measurement at residual conditions for the determination of parameter b.

Hence: $b = \frac{1}{\tau_{us-max}} - \frac{1}{(u_a - u_w)_{max} tan\phi'}$

Where:

τ_{us-max} = Ultimate shear strength at residual conditions

$(u_a - u_w)_{max}$ = Matric suction at residual conditions

Substitution of *a* and *b* into Equation 2.15 will result in:

$$\tau_{us} = \frac{(u_a - u_w)}{\frac{1}{tan\phi'} + \left(\frac{1}{\tau_{us-max}} - \frac{1}{(u_a - u_w)_{max} tan\phi'}\right)} \quad (2.16)$$

2.4.2 Measuring the shear strength of unsaturated soils

Donald (1957) was arguably one of the first researchers who attempted to measure the shear strength of unsaturated fine sands and coarse silts with a modified direct shear apparatus. Tests were done over matric suctions ranging from 0 to 30 kPa and presented the relationship between shear strength and the SWRC. Results by Donald (1957), shown in Figure 2.19 prove the dependency of shear strength in the case of unsaturated sands with the SWRC. All the strength results reported a well-defined peak followed by a plateau at a shear strength level higher than the shear strength that corresponds to a matric suction of 0 kPa. The peak in shear strength appears to occur over the same matric suction range as the air entry value of the soil.

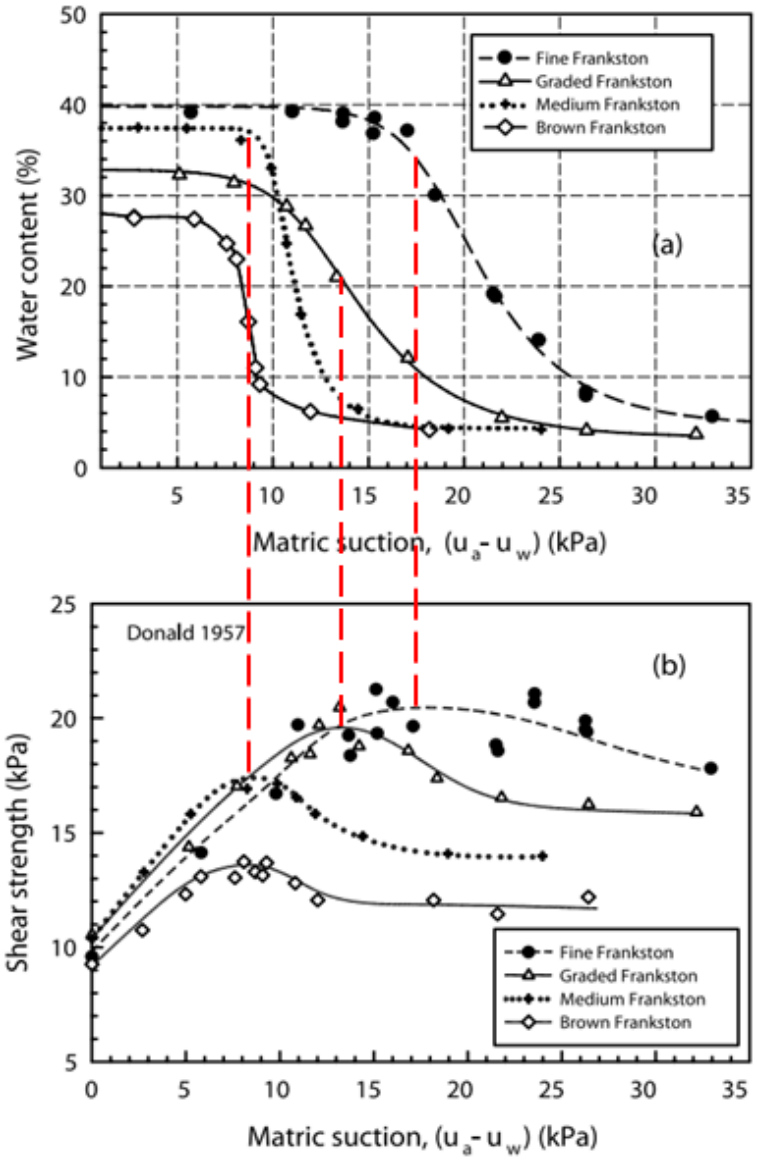

Figure 2.19: Shear strength results of unsaturated tests compared to the soil's corresponding SWRC, after Donald (1957).

The following correlations were found between the SWRC and the shear strength of unsaturated sands:

- The peak in unsaturated shear strength coincides with the air entry value of the soil.
- Strength gained from matric suctions quickly dissipate in soils with SWRCs with narrow transition zones. This typically happens with coarser materials that desaturate rapidly with low AEV's.
- A finer grading in soils tends to not only increase the peak in unsaturated shear strength but also widen the range over which the strength gain exists.

Apart from the results shown in Figure 2.19, the direct shear apparatus may still be conceived as an undesirable test due to the following disadvantages:

- Complex stress distributions within the sample (Matthews, 1988).
- Generation of non-uniform strains upon shearing (Matthews, 1988).
- Uncertainty in the measurement of stresses due to the change in area of the shear plane.
- Stress controlled tests could not observe behaviour beyond peak strength (critical state) (Matthews, 1988).

Nam et al. (2011) used the multistage direct shear device to measure the shear strength of unsaturated soils. This device shears samples in a staged manner where the confining stress is increased with each step. Additionally, the device used by Nam et al. was modified to control matric suctions by means of the axis translation technique capable of reaching a matric suction of 500 kPa.

Intact testing was done on four materials: a silty sand (SM), two low plasticity clays (CL1, CL2) and a high plasticity silt (MH) of which only the silty sand will be discussed (Nam et al., 2011). A single sample was used in both the saturated and unsaturated cases where the response was monitored during each stage. Each step included an increase in normal stress for the saturated sample. The normal stress was kept constant for the unsaturated case and the matric suction was doubled with each step, starting at 25 kPa and ending at 200 kPa with an additional step to 290 kPa. Figure 2.20 shows how the friction angle of the silty sand (SM) changed as the matric suction increased.

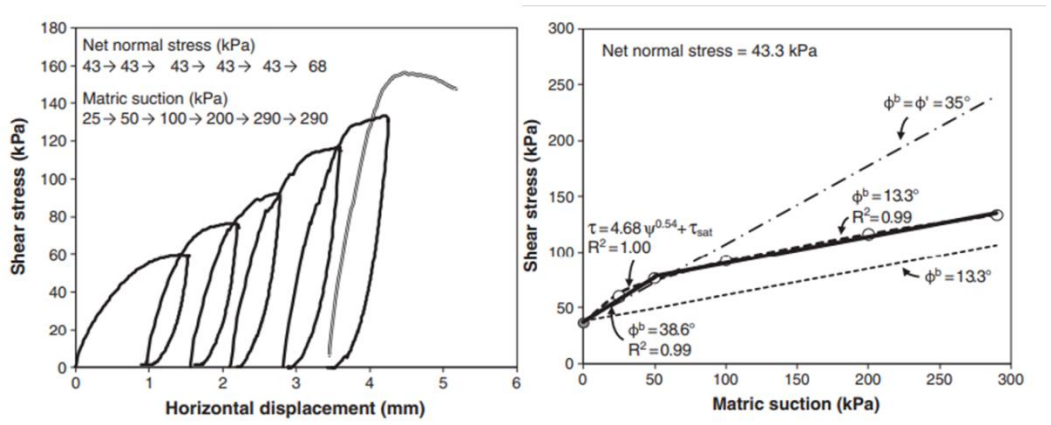

Figure 2.20: Unsaturated loading stages and shear strength results of a silty sand (SM) after Nam et al. (2011).

Initially, the unsaturated friction angle is larger than the saturated friction angle (ϕ^b = 38.6 > ϕ_{cs}' = 35°). Once the soil's air entry value is reached at a matric suction of 60 kPa the friction angle ϕ^b reduces to 13.3°. This is if the relationship between unsaturated shear strength and matric suction is assumed linear, as proposed by Fredlund et al. (1978) ($\tau = c' + \psi \tan\phi^b + \sigma_n \tan\phi'$). An alternative equation with a better fit can be found when considering the relationship proposed by Abramento and Carvalho (1989):

$$\boldsymbol{\tau = a\psi^b + d} \qquad (2.17)$$

Where:

Ψ = matric suction

a, b = fitting parameters

d = saturated shear strength

2.5 THE DIRECT SIMPLE SHEAR APPARATUS (DSS)

The direct simple shear device (DSS) is an improvement on the direct shear apparatus as it can subject the sample to uniform deformations and rotating principal stress axes. In 1936 the Swedish Geotechnical Institute built the first DSS capable of shearing specimens under uniform strain (Ladd and Edgers, 1972). The most used DSS type is the Cambridge University DSS which shears a cubical sample between rigid plates and the Norwegian Geotechnical Institute (NGI-type) DSS which shears a disc-shaped specimen. The sample is confined by end plates and a membrane which is surrounded by thin, stacked Teflon rings. This configuration allowed for vertical displacement while preventing radial deformations. The sample is sheared by horizontally translating either the top or bottom end plate.

Undrained tests, when considered in the same context of triaxial testing, are not possible in the standard NGI direct simple shear apparatus. Instead, constant volume conditions are enforced on the sample. Dyvik et al. (1987) found that truly undrained DSS tests results are equivalent to constant volume tests for all practical purposes for normally consolidated clays. Ultimate strengths and stress-strain curves of both the undrained and constant volume tests were similar. Dyvik et al. (1987) also showed that the change in pore pressure is equal to the change in vertical stress needed to enforce constant volume conditions, that is: $du = -d\sigma_N$. Geometrical inspection of Figure 2.21 shows how constant volume conditions are maintained in the DSS. The top and bottom platens are kept parallel and at equal height during shear whilst only allowing horizontal displacement. Drained tests in the DSS are achieved by maintaining a constant vertical load allowing volume change.

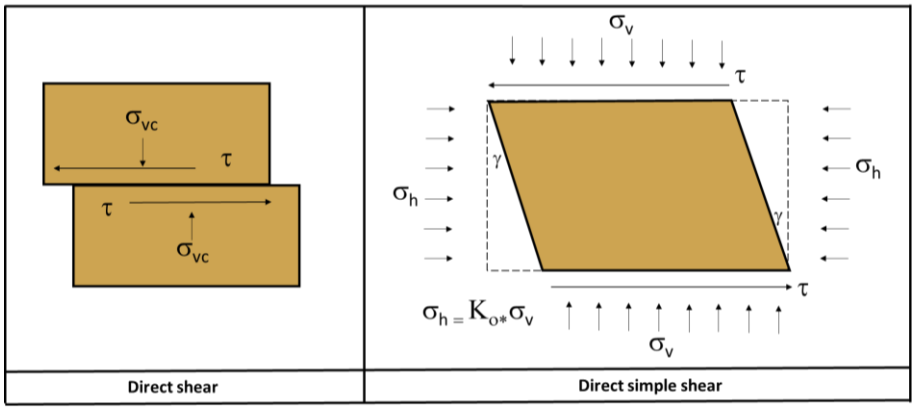

Figure 2.21: Shearing differences between the DS and DSS.

Yoshimine et al. (1998) studied the effect of principal stress orientations on the undrained shear strength of Toyoura sand. The triaxial compression test, with a principal plane inclination of 0°, showed the highest strength with the lowest contraction potential. The opposite was true once the principal stresses were rotated by 90° for the triaxial extension test.

Yoshimine et al. (1998) also considered the strength of undrained direct simple shear tests as simple shear conditions are commonly encountered in slopes. Rotation of the principal stresses in the DSS were observed until phase transformation was reached. Thereafter the inclination of the principal plane tended to vary between 40° and 45°, irrespective to the initial consolidation stress ratio. The undrained strength measured from the DSS proved to vary between the strengths of undrained triaxial compression and extension tests as shown in Figure 2.22. The difference in peak strengths is such that it should be considered to include strengths measured with a DSS in slope stability calculations.

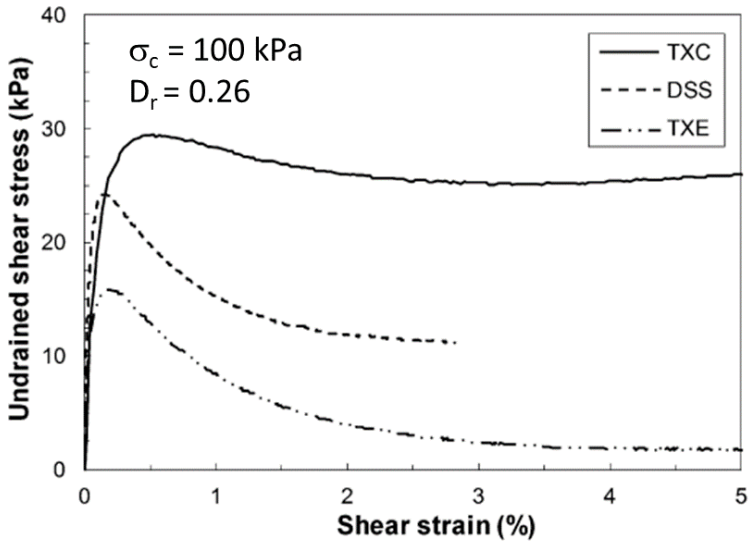

Figure 2.22: The effect of principal stress orientation on undrained shear strength (Yoshimine et al., 1998**), (TXC: Triaxial Compression, DSS: Direct Simple Shear, TXE: Triaxial Extension).**

It is known that varying modes of shear are found along a slip surface. Sadrekarimi (2014) proposed to divide a slip surface, as shown in Figure 2.23, into segments corresponding to the most suitable shear mode. The shear mode in the upper section of a slip surface will experience compression shear up to the point where α, the angle of the failure plane to horizontal measured counterclockwise, is larger than 30°. Simple shear will be experienced in the middle part of the slip surface where α is between -15° and 30°, while extension shear is experienced where α is less than -15°.

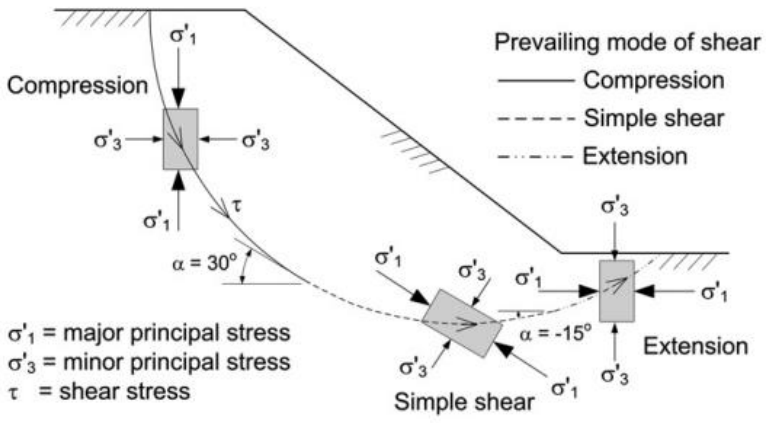

Figure 2.23: Shear modes in a slip surface (Sadrekarimi, 2014**).**

The varying shear modes in a slip surface makes the DSS a desirable device to acquire strength parameters as the failure mode in a DSS represents the shearing mode which shall be experienced by a large section of a slip surface.

Advantages of the DSS as opposed to triaxial tests (Ladd and Edgers, 1972):

- Consolidation tests provide the same results as an oedometer test.
- Decreased probability of reliability issues related to leakage or loss of pressure.
- Larger shear deformations can be reached in the same timeframe compared to triaxial tests.
- Measured shear strengths are more applicable to the stress state found in slip surfaces.
- Shear stresses can be applied to the sample during consolidation to simulate consolidation on a slope.

Disadvantages of the DSS as opposed to triaxial tests (Ladd and Edgers, 1972):

- Uncertainty in the meaning of the measured shear stress as the inclination of the major principal plane is unknown.
- Errors are generally larger due to the small sample size.
- The horizonal stresses in the sample are unknown.

2.5.1 The stress state in a DSS apparatus

The full stress state within a DSS is indeterminate (Dunlop and Duncan, 1966). The stress state on the horizontal plane can only be estimated when considering equilibrium and the average shear and normal stresses applied to the sample.

Ladd and Edgers (1972) summarized important aspects on the analysis in the direct-simple shear device:

- Strains and stresses may be assumed as uniform within the sample. Therefore, the measured normal and shear stress values are representative.
- Stress rotations occur during shear where Yoshimine et al. (1998) found that the inclination of the principal plane tends to vary between 40° and 45°.
- No consistent relationship exists between the applied shear and normal stresses (τ/σ) as the inclination of the principal plane is continuously rotating as the shear stress reaches its maximum value.
- It is likely that $\tau/\sigma < \tan\phi < \sin\phi$ for normally consolidated clays.

- For very large strains $\tan\phi < \tau/\sigma < \sin\phi$.

Asadzadeh and Soroush (2016) used DEM analyses to fundamentally investigate the stress state in a constant stress DSS. Constant stress test are analogous to drained triaxial tests as the load on the sample is kept constant whilst allowing the sample volume to change during shearing. Figure 2.24 plots the simulated major and principal stresses in a DSS over shear strain.

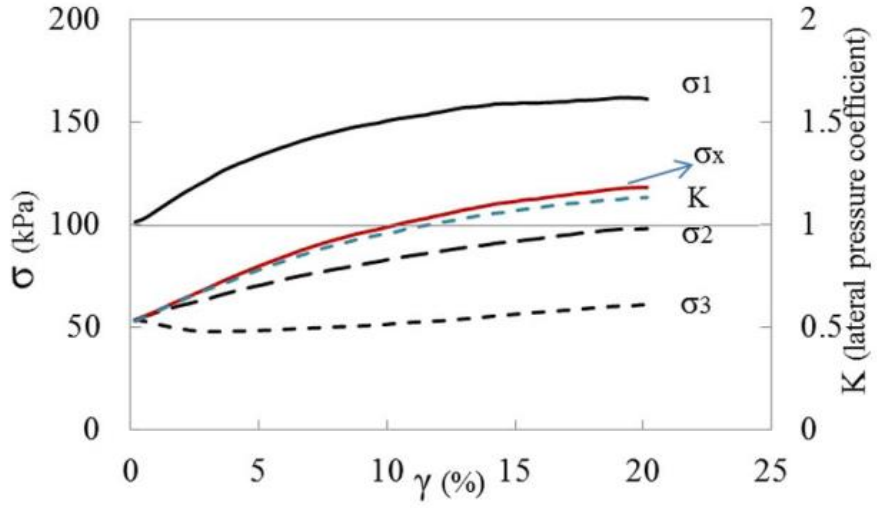

Figure 2.24: The stress state in a DSS sample estimated with DEM by (Asadzadeh and Soroush, 2016**)**

Asadzadeh and Soroush (2016) concluded that during consolidation and before shearing, the normal stress applied to the sample is the major stress. The horizontal stress (σ_x) at this point may therefore be calculated with the coefficient of earth pressure at rest (K_o). During shearing, the horizontal stresses tend to increase and approach the normal stress (K = 1) as the sample reaches peak shear strain whereafter K exceeds unity at larger strains.

2.5.2 Interpretation of results

The friction angle can be calculated based on one of three assumptions. Figure 2.25 shows the three possible failure states on a Mohr circle of stress.

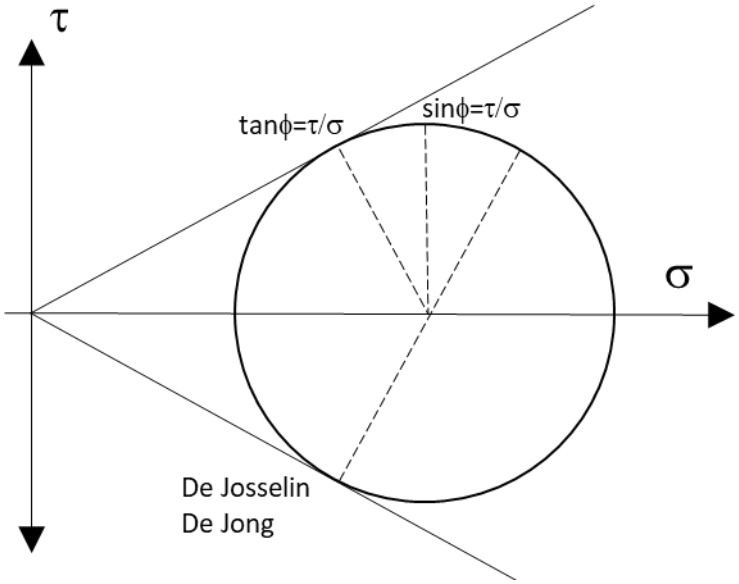

Figure 2.25: Failure plane assumptions for interpretation of DSS results.

The first failure state assumes that the horizontal plane is the plane of maximum obliquity therefore, $\tan\phi = \tau/\sigma$. The second assumption dictates the horizontal plane as the plane of maximum shear stress, therefore, $\sin\phi = \tau/\sigma$. The third assumption was proposed by De Josselin de Jong (1971) where the maximum stress obliquity is found on the vertical plane as opposed to the horizontal plane.

2.5.3 Testing at low stresses

Considering tests at low stresses may be advantageous as matric suctions in silty sands are typically small and should not be masked by high confining stresses. Most soil strength tests are carried out at intermediate (<100 kPa) to high stress levels as the linear Mohr-Coulomb failure criterion deviates from the true failure envelope at low confining stresses (Bishop, 1966).

Fukushima and Tatsuoka (1984), Lings and Dietz (2004) and Rousé (2018) all found an increase in the critical state friction angle of sand at low confining stresses in both the triaxial compression and direct shear tests, with one of the reasons being dilation. Bolton (1986) showed that dilatancy reduces as the confining stress increases due to a reduction in volume change tendency and encouragement of particle breakage. The opposite is true for low confining stresses as the tendency for volume change increases as particles are allowed to roll over each other instead of being crushed. Bolton did not have access to satisfactory low stress data on sand and therefore limited the relative dilatancy index (I_R) to 4, limiting the maximum dilation angle to 20° for plane strain conditions and 12° for triaxial strain. The relative dilatancy index is a parameter related to the relative density of a sand which controls the dilatancy thereof.

The behaviour of sand under monotonic, direct simple shearing at low stresses was considered by Al Tarhouni and Hawlader (2021). Samples were sheared under a constant normal stress ranging between 12.5 and 400 kPa. Their stress-strain behaviour findings concluded that the critical state friction angle could not be measured with the constant stress DSS test as the critical state friction angle (ϕ_{cs}') is overestimated at low stress levels as shown in Figure 2.26. A reason therefore might be due to the increase in horizontal confining stresses caused by the rigid, stacked confining rings. The ratio between horizontal and vertical stresses in a DSS test (K) is required to calculate the stress state of the sample which increases throughout the test as shown in Figure 2.24 and is generally unknown.

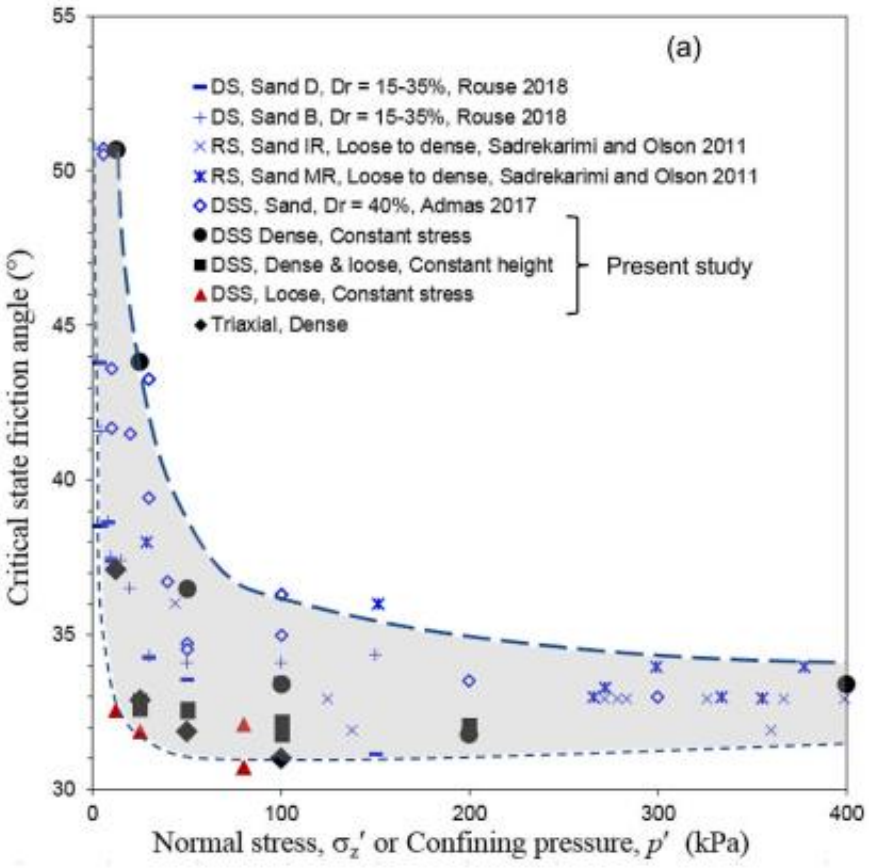

Figure 2.26: The effect of confining stress on the critical state friction angle of sand (Al Tarhouni and Hawlader, 2021**).**

Determination of the critical state friction angle with constant stress tests, at low confining stresses, is challenging as shear strains in the order of 40 to 50% are required to reach constant volume conditions as dilatancy still occurs at high strains. Dense samples in a constant stress DSS test even tended to experience a constant angle of dilation of 2° at high shear strains, at which the uniformity of strains and stresses are questionable. The critical state in the DSS was calculated upon zero dilation which generally occurred at shear strains beyond 16% (Al

Tarhouni and Hawlader, 2021). Figure 2.26 shows how the friction angle tended to increase at a faster rate as the vertical confining stress reduced, especially below values of 50 kPa. It is also clear that the denser the sample the larger the effect of confining pressure on the friction angle as the dense data points often plotted higher than data points corresponding to loose samples.

2.6 BEHAVIOUR OF TAILINGS UNDER DEPOSITION

The inclusion of matric suctions in slope stability analyses of tailings deposits is unconventional due to the uncertainty in the behaviour of suctions with time. Matric suctions in active tailings dams should therefore be monitored to quantify the reliability and typical magnitude thereof.

2.6.1 The dewatering behaviour of deposited tailings

Daliri et al. (2016) considered the dewatering behaviour of densified gold tailings in a drying box, also known as a lysimeter, with plan dimensions of 0.7 m x 1.0 m and depth of 1.0 m as shown in Figure 2.27. Measurements included water contents, matric suctions and mass balance by placement of the drying box on loadcells. Water contents were measured with the 5TE sensor. Matric suctions were measured with UMS T5 tensiometers capable of measuring pore pressures between +100 kPa and -95 kPa. Three pairs of tensiometers and water content sensors were placed in each layer as shown in Figure 2.27.

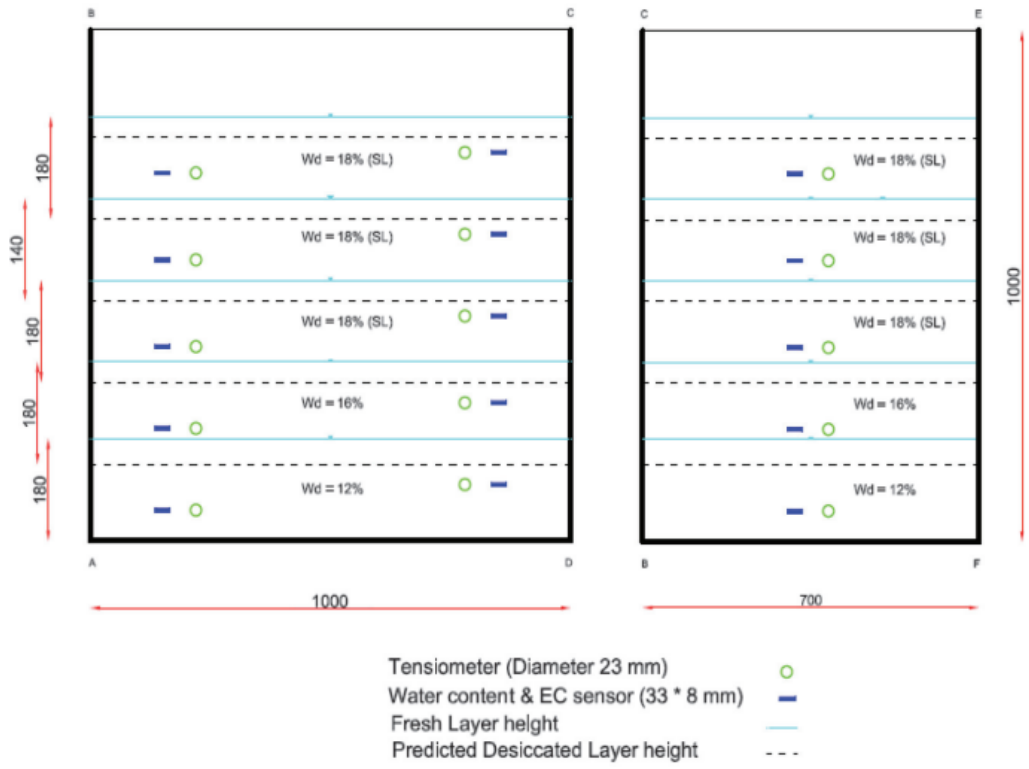

Figure 2.27: Cross sectional view of the drying box (Daliri et al., 2016).

Five layers were deposited in the drying box at gravimetric water contents of 38%. Figure 2.28 plots the gravimetric water content data over time as the layers were deposited and allowed to desaturate. The first two layers dried to water contents of 12% and 16 % respectively. The remaining top three layers were allowed to dry to a water content of 18%. Heavy rainfall was simulated with two re-saturation events between the third and fourth layer (Days 39 and 49 in Figure 2.28).

Dewatering was observed to have two distinguishable phases. The first phase was related to the drainage and settlement of a newly deposited layer and usually lasted for one to two hours for the initial layers. The fifth and last layer, deposited on the rewetted fourth layer, showed an increase in duration of the first phase as the underlying tailings had increased prevailing water contents. Settlement of the fifth layer took approximately one to two days as opposed to a few hours.

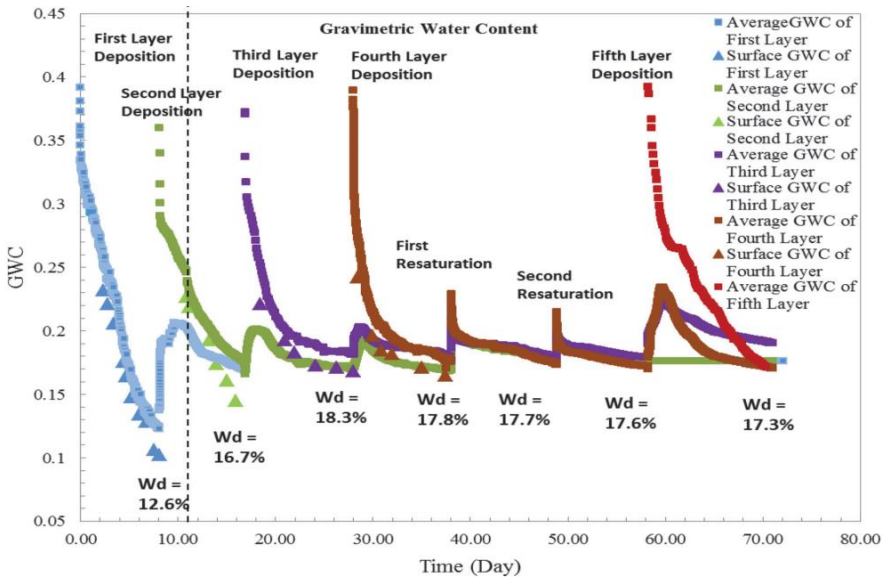

Figure 2.28: Average gravimetric water content of all the layers after deposition (Daliri et al. (2016)).

The second phase was related to a reversal in the pore water drainage direction and lasted longer than the first phase of which its duration increased as the volume of underlying tailings increased. On the ninth day after deposition of the first layer the water content in the first layer increased sharply as it desaturated the freshly deposited second layer. However, on the eleventh day the rate of desaturation decreased in the first layer but stayed constant in the second layer whilst no drainage was observed. This proved that the drainage direction of the first layer reversed from downwards to upwards which characterises the onset of the second phase.

Onset of the second dewatering phase can also be identified in Figure 2.29. Matric suctions within the second layer increased rapidly after deposition. However, a trend reversal is seen in the suctions around day 15 which is correlated to an increase in water content. The second layer is thus being recharged by pore water migrating from the first layer.

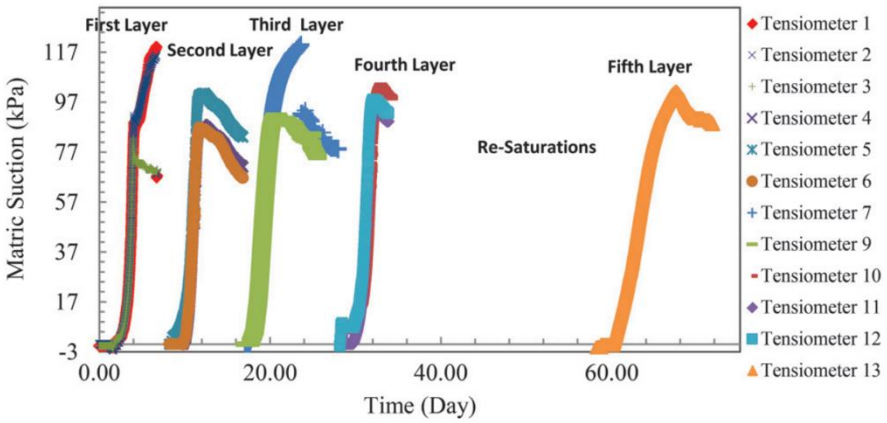

Figure 2.29: Matric suctions after of each newly deposited layer, after Daliri et al. (2016).

The drying box test by Daliri et al. (2016) showed that matric suctions dissipated entirely upon deposition of newer layers. This behaviour might not necessarily be representative of what occurs on active tailings dams. The effect of underlying, unsaturated tailings has been shown to be advantageous to drainage and the generation of negative pore water pressures but may delay the regeneration of matric suctions by recharging of pore water in the upper layers. The quantity of drier, underlying tailings in dams greatly exceeds that of the drying box. This therefore illustrates the need of the measurement of matric suctions and water contents on active tailings dams.

2.6.2 The shear behaviour of deposited tailings

Daliri et al. (2016) considered the shear behaviour of multi-layered tailings by shearing samples in a DSS-device as well as the effect of sample tubes on the shear response in unsaturated tailings. Two different sampling methods were used. One where a sampling tube was buried vertically in the box and filled with tailings as the tailings level rose, while the other involved inserting a thin walled 70 cm sampling tube into the tailings with a hydraulic jack. The buried sample tube was excavated by removal of the box's sidewalls.

Shear behaviour results of samples obtained from the drying-box were compared to small-scale tests by Daliri et al. (2014). The small-scale tests aimed to show the effect of drying on the shear strength of thickened gold tailings in comparison with mechanically consolidated samples. Two layers of tailings were deposited in a cylinder (25 cm diameter) of which both

were deposited at typical pumping water contents of 38% for the small-scale test. Deposited tailings were allowed to settle, and dry to varying water contents below and above the shrinkage limit between 30 and 4%.

Daliri et al. followed the same testing procedure in both the cases of 2014 and 2016. The samples were re-wetted until matric suctions dissipated entirely then, placed in a simple shear device and consolidated to vertical effective stresses of 50, 100, 200 and 400 kPa. Shearing was done after unloading to an effective vertical stress of 50 kPa. Figure 2.30, plotting shear stress against effective normal stress, shows how samples tended to strain-harden as the extent of drying increased. Samples which were only allowed to settle but not desiccate showed contractive, strain-softening behaviour.

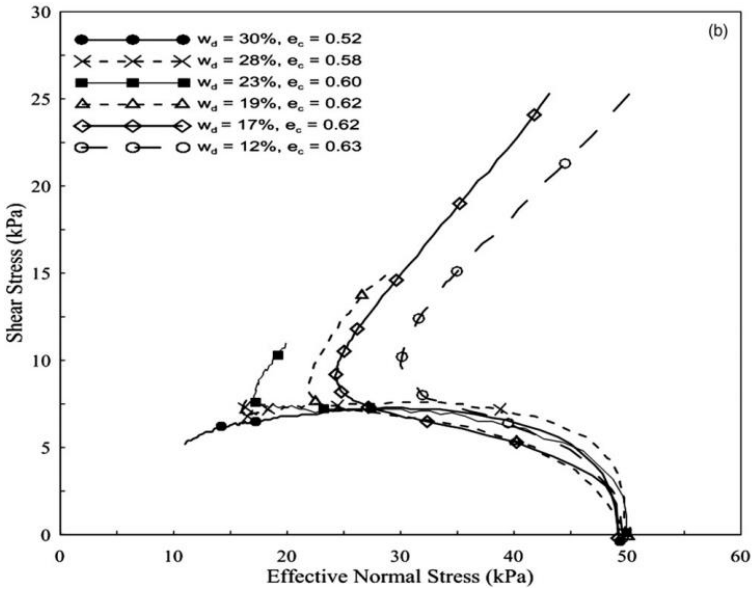

Figure 2.30: Results of gold tailings samples allowed to desiccate to varying water contents, re-wetted and sheared, after Daliri et al. (2014).

The shear behaviour of samples from the drying box was marginally stiffer when compared to the response of the small-scale samples (Daliri et al., 2016). The stiffness of the samples increased with desiccation extent. Figure 2.31 only contains results from the buried tube samples as results of the samples recovered with a thin-wall sampler reported practically identical results once again showing how the sample that was allowed to dry the most mobilised higher shear stresses.

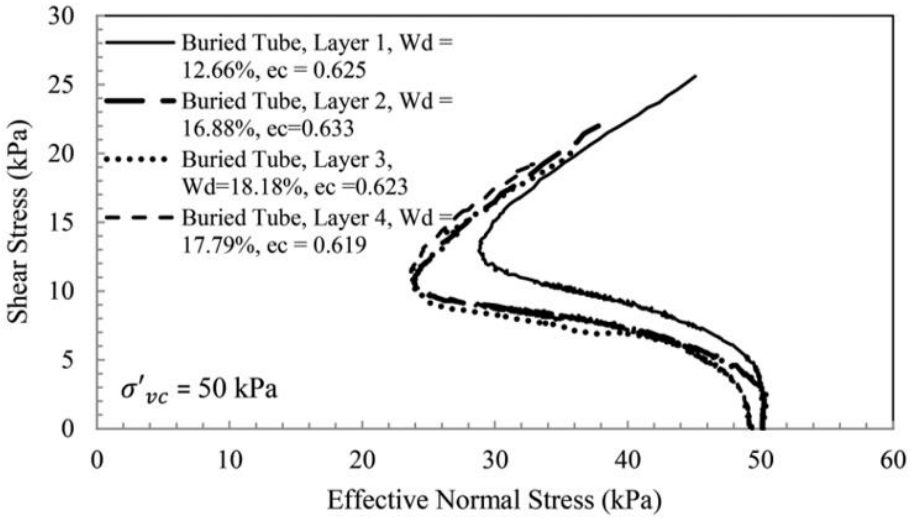

Figure 2.31: Shear results of buried tube samples obtained from a drying box, after Daliri et al. (2016).

The shear behaviour of tailings deposited in layers is thus highly dependent on the extent of desiccation. The increase in shear strengths reduced once matric suctions exceeded the air entry value of the tailings as the proportion of suctions contributing to effective stresses reduces rapidly once matric suctions exceed the air entry value (Daliri et al., 2016). The extent of dilatancy upon shearing is positively correlated to the degree of desiccation. Even a small degree of drying changes the shear behaviour of gold tailings from contractive to dilative under the abovementioned conditions. The increase in strength of the drying box samples may be ascribed to the increased degree of wetting and drying cycles it had undergone.

The results presented by Daliri et al. (2016) lead to the following conclusions:

- The shear response of samples which were obtained by driving a thin-walled sampling tube into desiccated tailings is practically equivalent to the response obtained from sampling tubes buried in the tailings during deposition.
- Even the slightest degree of consolidation and desiccation changed the shearing behaviour from contractive to dilative.
- The extent of dilation is proportional to the degree of desiccation, even at low matric suctions.
- Stiffness is proportional to the degree of desiccation.

2.7 SLOPE STABILITY CONSIDERING UNSATURATED SHEAR STRENGTHS

The unsaturated shear strength equations discussed in Section 2.4 can be applied in both the saturated and unsaturated regime, implying that the shear strength can be better estimated over a whole slope whether the porewater pressures are positive or negative.

Fredlund and Zhang (2013) modelled the effect of both the linear and nonlinear unsaturated shear strength equations on slope stability. The shear strength models included in their study were:

- Fredlund et al. (1996)
- Vanapalli et al. (1996)
- Vilar (2006)
- Khalili and Khabbaz (1998)
- Bao et al. (1998)

Limit equilibrium slope stability analyses were rederived. Fredlund and Zhang (2013) reported that derivations were straight forward as long as a mathematical equation was available to estimate the shear strength of an unsaturated soil.

Unsaturated shear strength envelopes are highly dependable on the SWRC, hence four materials were modelled which were characterized by their different SWRC's (Figure 2.32). The only difference between materials is the air entry value of the soil. AEV's are 0.5 kPa, 5 kPa, 50 kPa and 500 kPa. Only the material with AEV = 5 kPa is discussed in this study as it best approximates the behaviour of platinum and gold tailings studied later in this dissertation.

The unsaturated shear strength envelopes for material No. 2, calculated with the stated models, are plotted in Figure 2.33. Curves corresponding to models by Fredlund et al. (1996), Vanapalli et al. (1996) and Vilar (2006) all overlap with increases in strength up to 10 kPa where $\psi \approx 20$ to 25 kPa before reaching residual conditions at matric suctions in the order of 100 kPa. Strength estimations with the model by Khalili and Khabbaz (1998) do not reduce as matric suctions increase beyond the air entry value. It therefore appears that most of the models except that proposed by Khalili and Khabbaz would be suitable for low plasticity tailings.

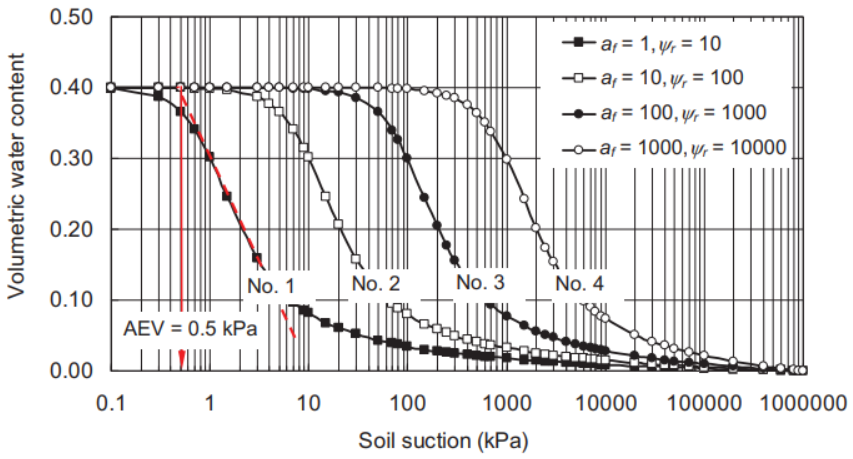

Figure 2.32: SWRC's of the four modelled materials, after Zhang et al. (2014) .

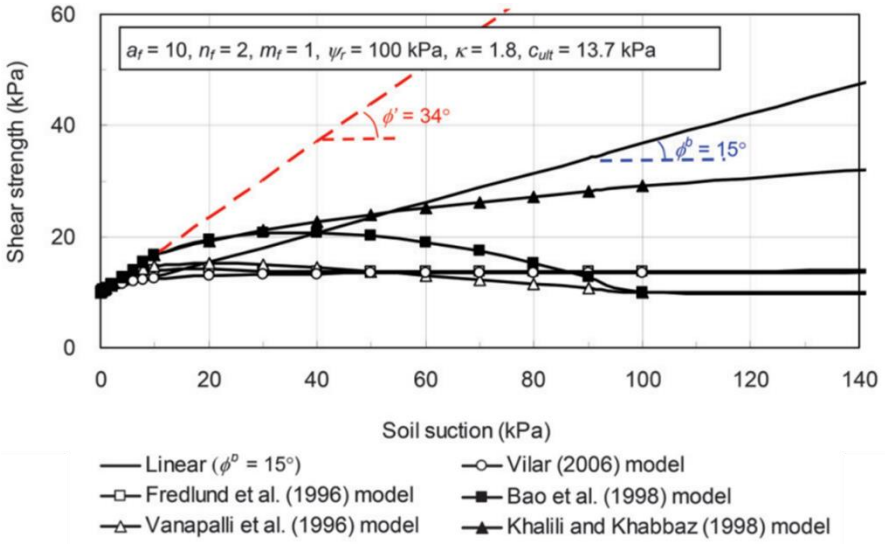

Figure 2.33: Shear strength of a soil with an AEV of 5 kPa plotted over matric suction for the different shear strength models, after Zhang et al. (2014).

The stability of an infinite slope inclined at 40° with the water table at a depth of 10 m parallel to the ground surface was considered with the abovementioned shear strength equations (Figure 2.34).

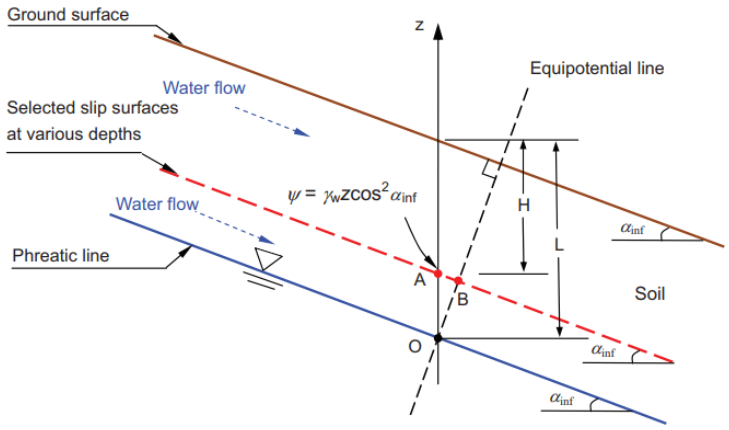

Figure 2.34: Representation of the analysed infinite slope (Zhang et al., 2014**).**

Matric suctions were assumed by extrapolating the hydrostatic pressure above the water table. The matric suction at the surface of the inclined slope was therefore estimated as 57.5 kPa. Results were represented in Figure 2.35 by showing the safety factors plotted over the depth of slip surface. The safety factor is inversely correlated to the depth of the slip surface.

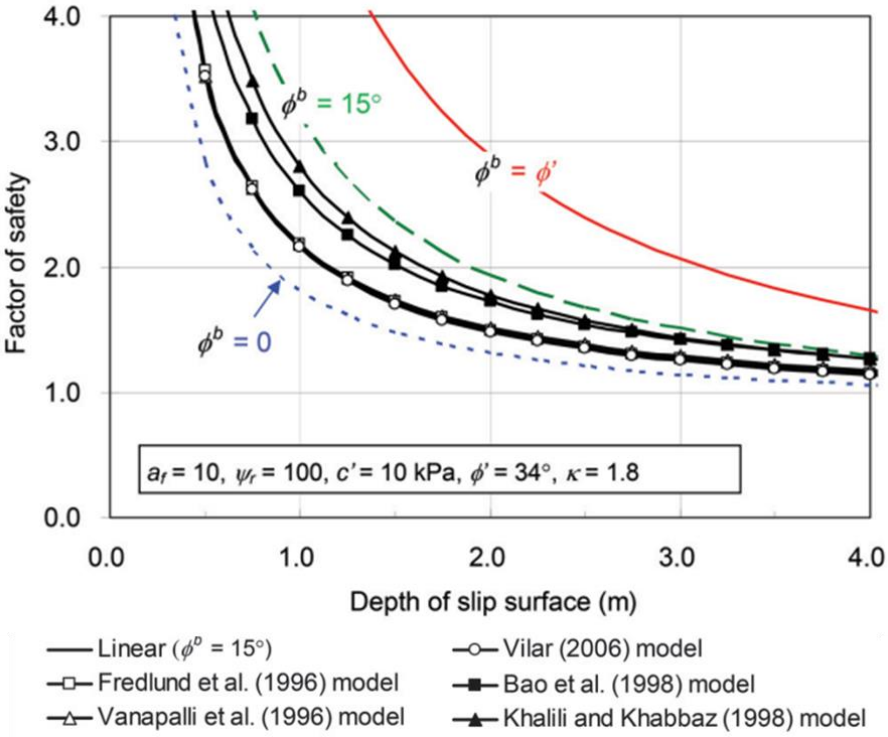

Figure 2.35: Safety factors on an infinite slope plotted over slip surface depth of a silty sand with an AEV of 5 kPa, after Zhang et al. (2014).

Three curves were added to the safety factor plot (blue, green and red) in Figure 2.35 for comparison reasons. Blue represents the classical Mohr-Coulomb, saturated shear strength equation (ϕ^b=0°). Red represents the case where the matric suction component contributes in

its entirety to shear strength ($\phi^b=\phi'=34°$) and green where only a portion of the suction component contributes to shear strength ($\phi^b=15°$).

All the unsaturated strength models showed that it should not be assumed that the total matric suction component contributes to strength which is represented by the case plotted in red. Models by Fredlund (1996), Vanapalli (1996) and Vilar (2006) show good agreement whilst the models by Bao et al. (1998) and Khalili and Khabbaz (1998) show higher stability values.

An additional slope stability problem was considered for a slope inclined at 30° and a high-water table as shown in Figure 2.36.

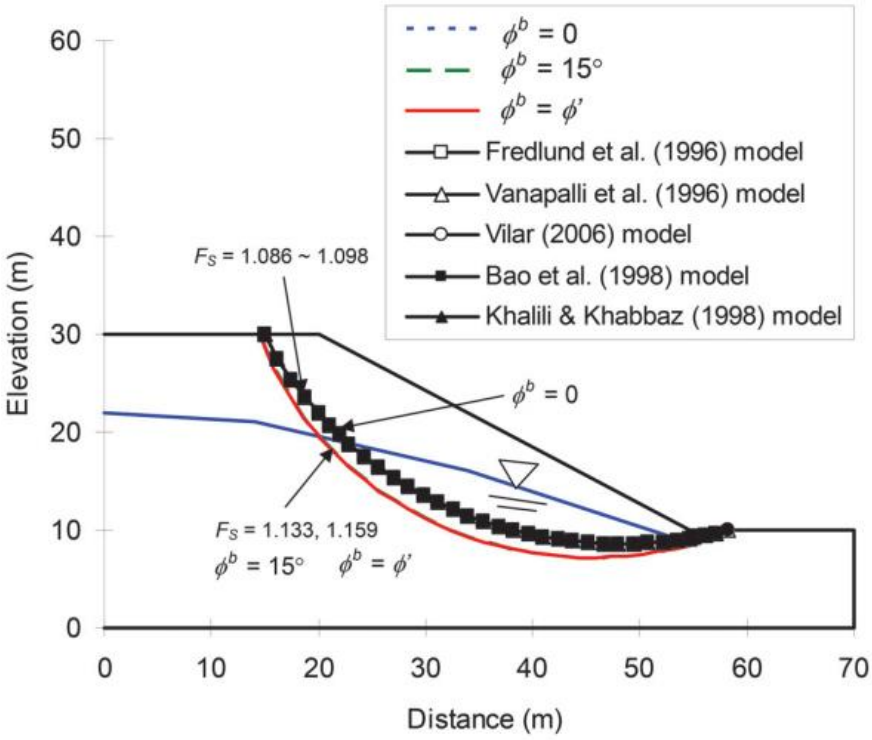

Figure 2.36: Flat slope considered with limit equilibrium analysis and unsaturated shear strength equations, after Zhang et al. (2014).

The analysis showed that all the critical slip surfaces, when considering different unsaturated shear strength models, overlapped with the slip surface corresponding to zero matric suctions. This observation is advantageous to the application of unsaturated shear strength to stability analyses as the mode of failure does not change dramatically. The effect of the air entry value of soils on the slope stability of slopes is shown in Figure 2.37.

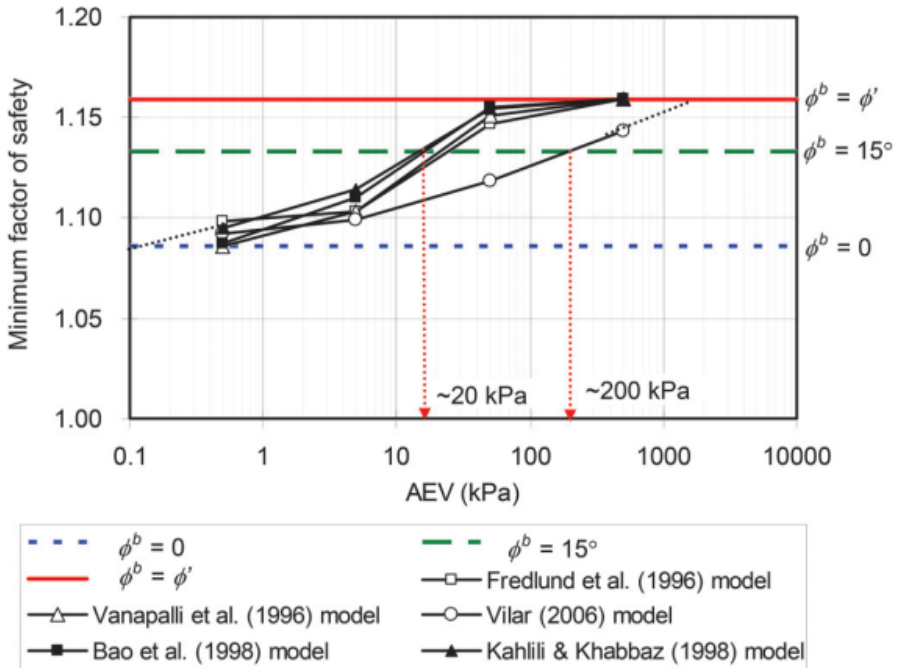

Figure 2.37: Plot of the critical safety factors plotted against air entry value for the considered shear strength models, after Zhang et al. (2014).

The safety factor of the slope shown in Figure 2.36 when ignoring the strengthening effects of matric suctions is 1.086. The safety factor increases between 1.2% and 5.3% upon consideration of suctions using the equations discussed. The contribution of matric suctions to shear strength did not significantly increase the safety factor of the slope in consideration with low air entry values. All models show an increase in stability as the air entry value increases. This is due to the omission of an AEV-related parameter in Vilar's equation.

2.8 SUMMARY

The literature review presents various models relating the shear strength of unsaturated soils and matric suction. The advantages that could be gained from including matric suctions in slope stability analyses are generally not considered in practice due to the uncertainty regarding its effect on shear strength, as well as uncertainty in the behaviour and reliability of matric suction data due to the scarcity thereof.

A study observing only the behaviour of matric suctions in tailings dams without consideration of water content would be insufficient if the goal was to comment on the behaviour of the in-situ, unsaturated, shear strength of tailings and its effect on slope stability. A large proportion of the discussed unsaturated shear strength models generally require a water content related parameter suggesting that measurement of water content is a requirement.

Drying box data (Daliri et al., 2016) showed that matric suctions routinely reached values in the order of 100 kPa and totally dissipated upon tailings deposition, but, are quickly regenerated in a matter of a few days after drainage had occurred. However, the behaviour of suctions exposed to deposition events on tailings dams may differ from that reported by Daliri et al. (2016) as the presence of underlying tailings may influence their behaviour due to its capacity to recharge upper layers with porewater. The behaviour of matric suctions due to rainfall events may also be different in the field as opposed to a laboratory test.

The most suitable model to predict the unsaturated shear strength of tailings should be found before matric suction and water content data could successfully be utilised to refine their effect on strength and hence, slope stability assessments. This could be done by measuring the shear strength of unsaturated soils at varying matric suctions. The measurement of the unsaturated shear strength of soils with a simple shear device, to which a model could successfully be fitted, was achieved by various researchers as discussed in section 2.4.2. However, research verifying unsaturated shear strength models on tailings with a direct simple shear could not readily be found. The direct simple shear device is considered as an improvement on the direct shear device due to the improved shear mode which eliminate stress concentrations(Ladd and Edgers, 1972). Shear strengths measured with a DSS device are more suitable in the case of slope stability analyses as a large proportion of the soil along a slip surface is under simple shear conditions (Sadrekarimi, 2014). Verification of unsaturated shear strength models to tailings was therefore attempted with a DSS and is presented in Chapter 4.

New slope stability equations were re-derived by Fredlund and Zhang (2013) to include the effect of matric suctions with unsaturated shear strength models. It was found that inclusion of suctions in slope stability analyses does not change the mode of shear in flat slopes and can increase the safety factor between 1% to 5% for sandy silts on flat slopes.

The effect of matric suctions on shear strength was studied by shearing unsaturated platinum tailings samples in a DSS-device at varying matric suctions. Thereafter, an unsaturated shear strength model was chosen from the literature that could best model the relationship between matric suction and unsaturated shear strength.

In-situ matric suctions and water contents were monitored from active platinum and gold tailings dams. The measurements were then used to study the behaviour of matric suctions and water contents driven by deposition of new tailings and desiccation. The gathered data was also used to estimate the effect of the measured matric suctions on the in-situ strength of tailings.

The unsaturated shear strength equation chosen from the literature was used in conjunction with the gathered field data as inputs for limit equilibrium slope stability analyses to find the effect of matric suction on the stability of active tailings dam slopes.

3 METHODOLOGY

3.1 INTRODUCTION

The literature review shows that uncertainty in the contribution of matric suctions to shear strength prevents its inclusion in the stability analyses of tailings dams. The lack of knowledge regarding matric suctions arises from the scarcity of data and difficulty in monitoring of suctions over prolonged periods. This also holds for the case of water contents as the fluctuations of the in-situ magnitude thereof is uncertain. However, a tensiometer developed at the University of Pretoria (Jacobsz, 2018) allows for the monitoring of in-situ matric suctions in tailings dams over prolonged periods. Also, volumetric water content sensors, relying on time domain reflectometry (TDR) technology, enabled the monitoring of in-situ water contents in tailings dams.

The high cost of commercially available loggers drove the development of a custom-built data acquisitioning system (DAQ) capable of recording water contents and matric suctions on active tailings dams over time. Two microcontrollers served as the main components of the loggers. The development, operating principle and design of the loggers are discussed by Basson et al. (2021). Three loggers were placed near the wall (DAQ1), halfway across beach (DAQ2) and next to the pond (DAQ3) of a platinum tailings dam. A separate logger was placed on the slope of a gold tailings dam. This monitoring system allowed for the observation of matric suctions and volumetric water content variations in two tailings dams over a period of more than a year.

A DSS apparatus was used to measure the effect of matric suctions on the shear strength of unsaturated tailings. Pore pressures were not controlled during shearing but were measured before consolidation and after shearing using a tensiometer. The goal of the testing regime was to obtain data to which a suitable model could be calibrated to model the increase in mobilised shear strength from known matric suctions. Once a suitable model was found, limit equilibrium slope stability analyses were run to investigate how consideration of matric suction would affects the safety factor against slope failure of a tailings dam slope.

3.2 MATERIAL PARAMETERS

The material parameters applicable to this study were measured on platinum tailings and gold tailings. The platinum tailings dam, which is a spigotted operation, is in Limpopo, South Africa. The gold tailings dam, which is a daywall-paddock operation, is located near Johannesburg, South Africa. Both are upstream and active tailings dams.

Figure 3.1 shows the monitoring locations on the platinum tailings dam and Figure 3.2 shows the sampling location on the gold tailings dam. A cubic surface sample, with side lengths of 150 mm, were taken at each installation which allowed for the determination of the void ratio and moisture contents. The same samples were also used for PSD and G_s tests, SWRC tests and DSS tests. In-situ dry densities are summarised in Table 3.1 and minimum and maximum dry void ratios are summarized in Table 3.2.

Table 3.1: In-situ void ratios and dry densities at the installation locations of the platinum and gold tailings dams (TD).

Installation location	Void ratio	In-situ dry density (ρ_d) [kg/m^3]
DAQ1 (Platinum TD)	1.03	1734
DAQ2 (Platinum TD)	1.14	1635
DAQ3 (Platinum TD)	1.16	1577
DAQ (Gold TD)	0.99	1456

Figure 3.1: Sampling locations on the platinum tailings dam (Google Earth Pro, 2022).

Figure 3.2: Sampling location on the gold tailings dam (Google Earth Pro, 2022).

Table 3.2: Minimum and maximum void ratios of platinum and gold tailings samples from the tailings dams in Figure 3.1 and Figure 3.2.

Material	e_{min}	e_{max}
Platinum tailings	0.59	1.26
Gold tailings	0.47	1.57

3.2.1 Particle size distribution (PSD) and specific gravities (G_s)

Grading curves were determined with an automatic particle size analyser using laser diffraction technology and specific gravities were determined with a pycnometer. Three different PSDs were determined for the platinum tailings (Figure 3.3) as the grading is affected by the flow distance from the discharge point.

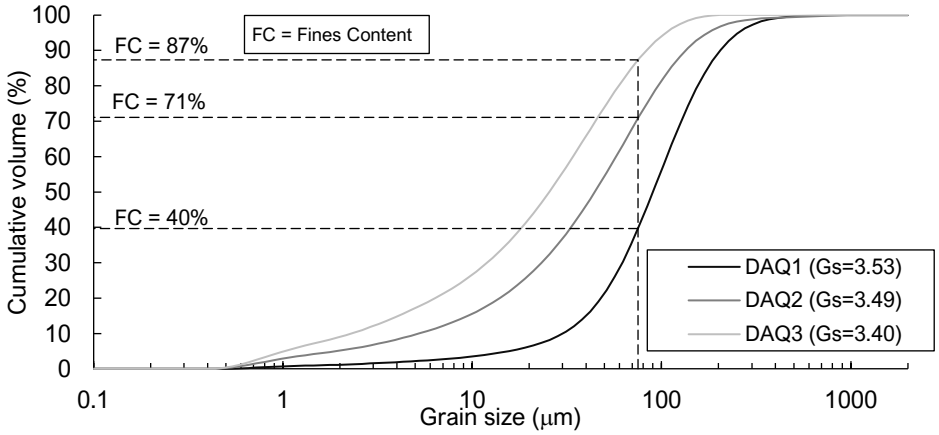

Figure 3.3: Platinum tailings particle size distribution and Gs.

It was assumed that one sample from the gold tailings dam would suffice due to it being a day-wall operation and all measurements were taken in the daywall before any significant changes in the PSD due to sorting associated with flow distance can occur.

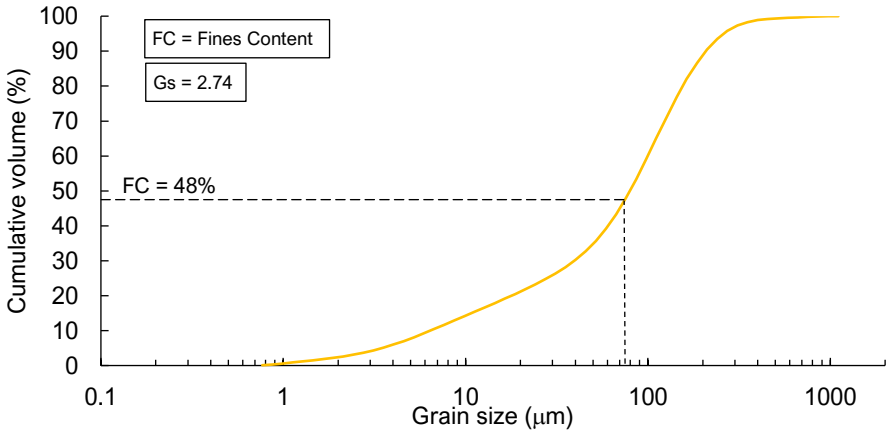

Figure 3.4: Gold tailings particle size distribution and G_s.

3.2.2 Soil water retention curve

The SWRC is highly dependent on the particle size distribution of a soil and is measured in the laboratory by recording matric suctions over a range of water contents. Le Roux and Jacobsz (2021) describes, in detail, the method employed to measure the SWRC which relied on tracking the mass change, matric suction generation and volumetric change of a disc-shaped soil sample as it dried with an automated data acquisitioning system. Figure 3.5: SWRC measurement apparatus.Figure 3.5 shows the SWRC measurement apparatus with annotated components. Changes in the sample mass was measured with a mass balance with a resolution of 0.01g, while volumetric

changes were measured with distance measuring lasers. SWRCs were measured at the in-situ density of each sample

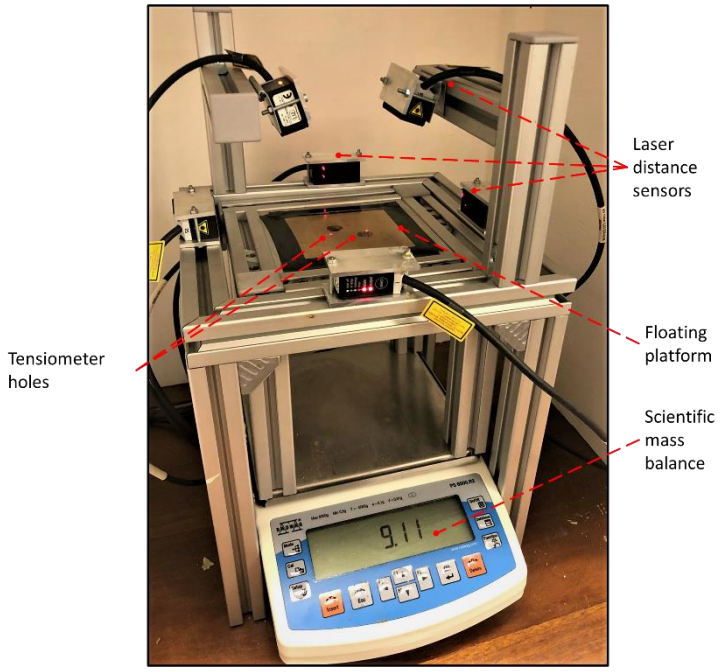

Figure 3.5: SWRC measurement apparatus.

Section 2.4.2 discussed models to predict the unsaturated shear strength of soils, it also showed the importance of the air entry value of a soil in terms of unsaturated shear strength. Figure 3.6 plots a hypothetical SWRC and construction lines used to find the AEV.

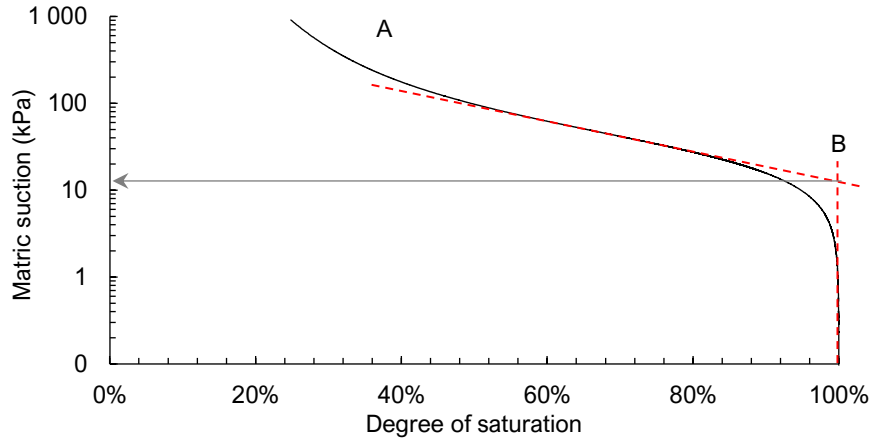

Figure 3.6: Determination of the air entry value on a soil water retention curve of a hypothetical curve.

Line A is fitted through the flat part of the SWRC over the transition zone, line B is fitted through the capillary zone of the curve. The AEV is equal to the matric suction value at the intersection of lines A and B, 10 kPa in this example.

Figure 3.7 plots SWRCs corresponding to samples taken at each installation on the platinum tailings dam.

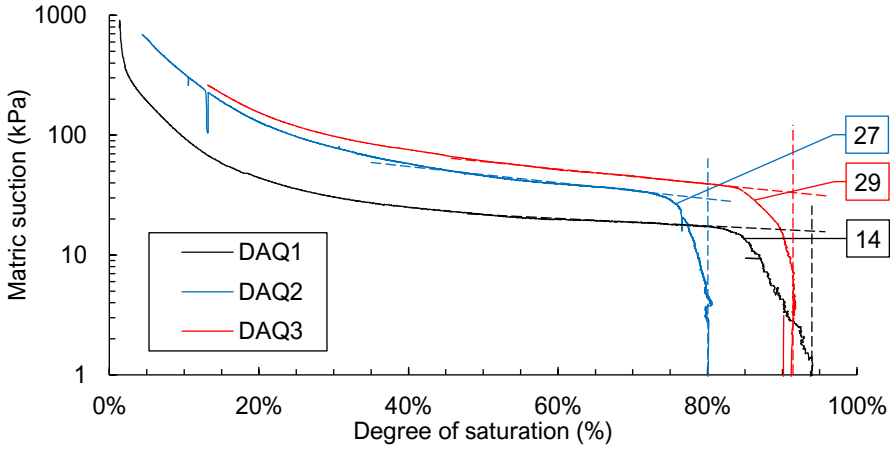

Figure 3.7: SWRCs at installations of DAQ1, DAQ2 and DAQ3 on a platinum tailings dam.

Air entry values at the in-situ density of the platinum tailings were determined as 14 kPa, 24 kPa and 29 kPa for the samples taken near the wall (DAQ1), midway across the beach (DAQ2) and next to the pond (DAQ3) respectively. Figure 3.8 plots a gold tailings SWRC.

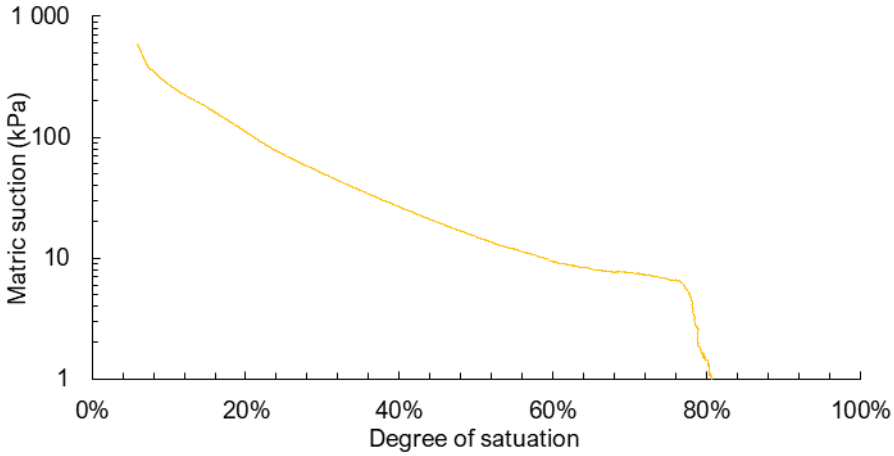

Figure 3.8: The SWRC of a surface sample taken from the daywall on a gold tailings dam.

The AEV of the sample taken from the daywall of the gold tailings dam was determined as 9 kPa.

3.3 MEASURING THE UNSATURATED SHEAR STRENGTH OF TAILINGS

A Geocomp™ ShearTrac-II direct simple shear apparatus, at the University of the Witwatersrand (Figure 3.9), was used to measure the unsaturated shear strength of platinum tailings at varying matric suctions in a temperature-controlled room. The samples tested had a maximum height of 25 mm and a diameter of 63.5 mm. All samples were sheared at a rate of 20% shear strain per hour as the time for 90% consolidation allowed for faster shearing rates according to the ASTM standard (D-17, 2017), due to the low clay contents of the sheared samples.

Figure 3.9: A Geocomp direct simple shear apparatus based on the NGI DSS (Geocomp, 2022**).**

The pore pressures in the samples were measured directly with a tensiometer before consolidation and again immediately after shearing, as the matric suctions may have changed throughout the testing procedure. The aim was to find a correlation between the measured unsaturated shear strength and the matric suction in the sample. The testing strategy (discussed in Sections 3.3.1 to 3.3.4) was developed iteratively until a fourth and final approach was found which delivered acceptable results. A summary of

the recommendations that should be kept in mind when attempting to measure unsaturated shear strengths with a DSS-apparatus is discussed in Section 5.2.3. Selected results are presented in this chapter to illustrate the development of the experimental methodology.

3.3.1 Sampling from a drying box

A drying box (Figure 3.10) was filled with slurried tailings and allowed to dry under outdoor conditions. This included exposure to direct sunlight and wind conditions as would typically be encountered on a tailings dam and encouraged desiccation to occur within a week. The expectation was that samples taken from a drying box, exposed to similar drying conditions that a tailings dam would experience, would show strengths closest to reality. Tailings was placed in the drying box and sufficient tap water was added for full saturation. After mixing, free water had accumulated above the tailings surface after the tailings had settled. The excess water was then decanted from the box to speed up the desiccation process. The pore pressures and water contents of the platinum tailings in the drying box were continuously monitored as drying occurred. Samples were then taken as soon as a targeted matric suction value was reached. The targeted matric suctions aimed to include samples with matric suctions before, at and beyond the AEV of the material to capture the behaviour of the tailings under varying unsaturated conditions.

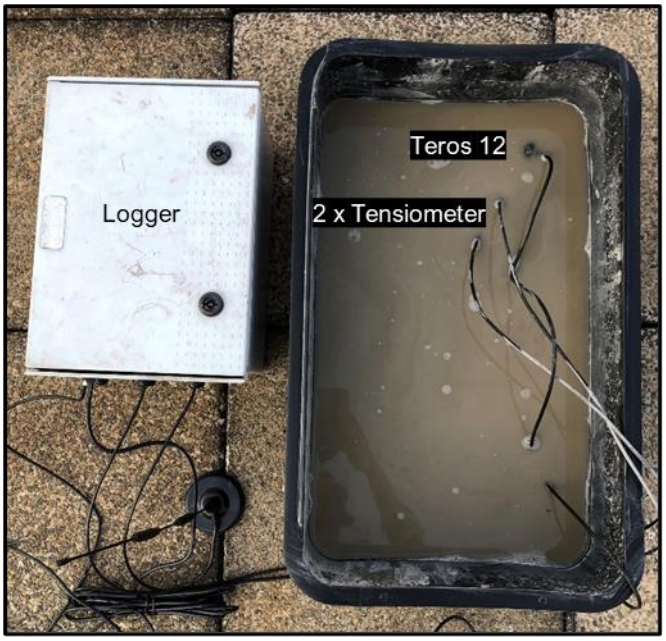

Figure 3.10: A 300mm x 600mm drying box filled with slurried platinum tailings instrumented with two tensiometers and one Teros 12 volumetric water content probe.

Samples were taken from the drying box by inserting a sampling tube with a diameter of 63.5 mm into the tailings. Samples were taken from the drying box by sealing the top of the sampler tube such that a partial vacuum formed within the tube as it was extracted from the tailings. It was challenging to take samples close to saturation as the combined effect of low strength, resulting from small matric suctions, and the relatively thin sample thickness (approximately 60 mm) required tilting of the sampling tube before lifting to prevent the sample from dropping out of the tube due to gravity. The tube and sample was then placed on a petri dish after removal from the drying box and carried to the DSS testing room. The sample was then extruded from the tube, trimmed to the correct height, and placed on the DSS pedestal (Figure 3.11).

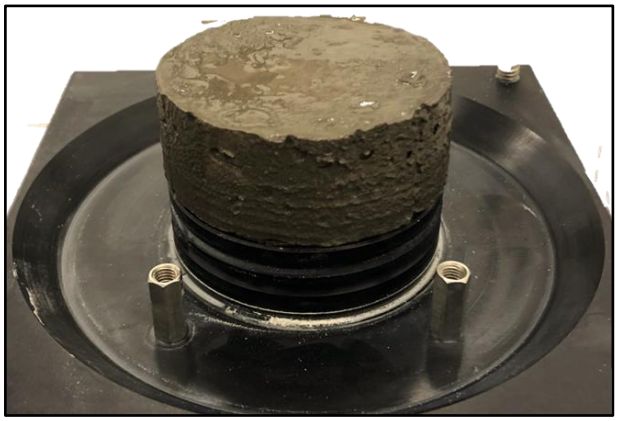

Figure 3.11: Tailings sample extruded onto the DSS pedestal.

A membrane, O-rings, top cap, and Teflon ring stack was then placed on the sample (Figure 3.12).

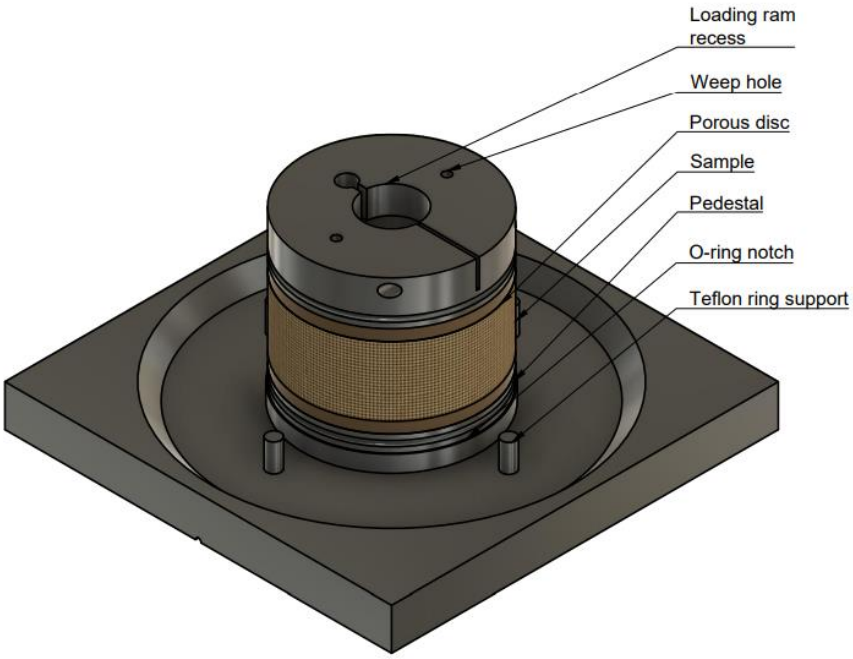

Figure 3.12: Schematic of a complete DSS pedestal and sample without the surrounding DSS rings, membrane and O-rings.

Samples with low suctions and low strength, were challenging to prepare as they tended to barrel under the weight of the top cap before the Teflon rings could be placed over the assembled sample and membrane. This caused large disturbances as the sample had to be extended to reduce its diameter to allow placement of the Teflon confinement rings over the sample (Figure 3.13).

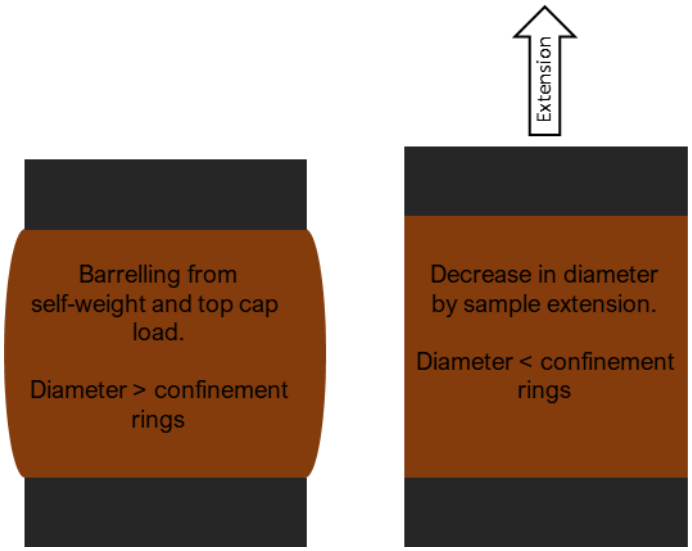

Figure 3.13: Barrelling of low-strength samples due to self-weight and top cap loading.

Pore pressure measurements in the drying box at the time of sampling and sample preparation were assumed to represent pore pressures in the sample before shearing as the time lag between sampling and shearing was less than an hour. Extensive desiccation, therefore increase of matric suctions within the sample, was prevented by keeping the sample sealed from the atmosphere as long as possible therefore reducing the effective time lag between sampling and shearing. Sample pore pressures after shearing were measured by placing a tensiometer on top of the sample. Sufficient contact between the sample and the tensiometer was achieved by placing a weight on top of the tensiometer (Figure 3.14 top). It was assumed that the differences in matric suctions between the top and the bottom of the sample were negligible due to the small sample height (less than 25 mm). Dilation can be seen in the matric suction measurements upon placement of the tensiometer on the sample, followed by pore pressure equilibration in the bottom figure of Figure 3.14.

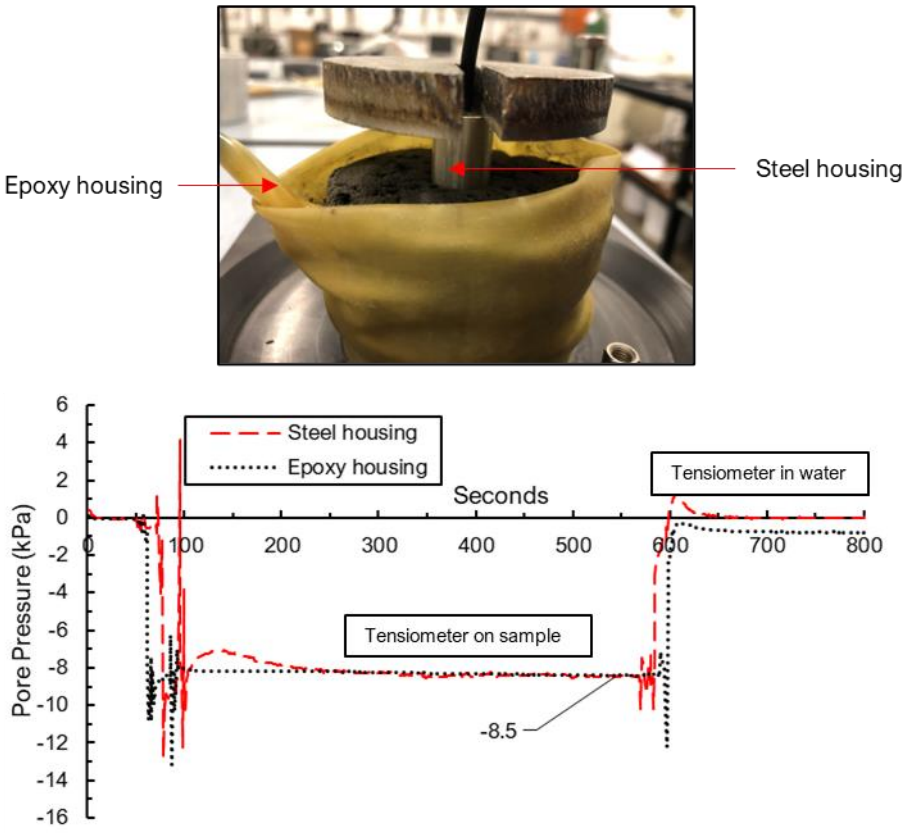

Figure 3.14: Placement of tensiometers on the sheared sample (top), example of pore pressure measurements after shearing (bottom).

The samples were sheared under a constant volume condition as it was expected that a peak in shear stress would be reached before strain softening to a residual strength. The samples were all consolidated to a total (vertical) stress of 50 kPa, an arbitrary value

expected to be small enough that the effect of matric suctions can still be observed. However, monotonic DSS results did not show any correlation between matric suction and shear strength due to the following reasons:

- Samples were prepared as a slurry and had low void ratios.
- Strong and rapid dilation completely overshadowed the effect of matric suction, resulting in very large vertical stresses being generated.
- Shear tests were done under constant volume conditions which were enforced by automatic correction of the normal stress applied by the DSS-apparatus. This resulted in noisy normal stress data as the DSSs PID system (proportional integral derivative controller) was not tuned for stiff materials, causing over-corrections.
- Samples taken at low matric suctions, especially at high saturation levels, had virtually no strength, collapsed, and barrelled during the sample preparation stage. However, samples that collapsed during preparation showed the highest strength. This is due to good horizontal confinement created between the sample and the DSS rings by the sample collapsing and filling the void between the confinement rings and the sample.
- Samples taken at high matric suctions had sufficient strength to remain relatively undisturbed. However, this compromised the horizontal confinement held by the DSS rings as a slight void existed between the sample and the rings. This caused a shear band to form upon shearing. The criteria for simple shearing was thus not met which resulted in low shear strength measurements.

The drying box was remixed to a slurry for a second time after the DSS was tuned to test stiff materials to reduce the noise in the normal stress measurements. However, control of dilation and horizontal confinement remained a problem.

3.3.2 Dense, moist tamped samples

The first shearing attempt showed the importance of horizontal confinement. Samples moist tamped directly in the DSS rings, instead of sampling, should be the preferred method when intending to achieve sufficient horizontal confinement. The samples were consolidated to and sheared under a total stress of 50 kPa, an arbitrary total stress value that would not completely overshadow the effect of matric suctions.

It has been shown that constant volume testing will not show the effect of matric suctions when considering the peak strength alone when samples dilate under shearing, as experienced in Section 3.3.1. The high densities caused by slurry deposition and

desiccation of the samples caused strong dilation. Therefore, the shear strength increased unrestrained. Had the samples contracted, a single peak shear strength value could be used to find the relationship between matric suction and unsaturated shear strength. A constant stress test, instead of a constant volume test, should be the preferred method as it would provide a single shear strength value.

The second attempt therefore tested moist tamped samples at a dry density of 2077 kg/m^3, which related to a void ratio of 0.68, but at varying water content percentages of 4, 8, 12 and 16%.

Samples were compacted in an assembled DSS pedestal within the membrane. Three equal amounts of tailings, mixed to the desired water content, was placed in the membrane and rings and compacted to the required height. Void ratio control during sample preparation was challenging due to the small sample volume (Ø=63.5 mm; H=25 mm). A 1 mm deviation from the correct sample height would cause a void ratio deviation of 0.1 therefore, final void ratios between 0.66 and 0.70 were deemed acceptable. Matric suctions were measured before and after shearing as before (Figure 3.15). The samples did not have enough time for the water content to reduce significantly during shearing therefore, the differences in matric suction before and after shearing as reported are assumed to only be due to effects caused by consolidation and shearing. Consolidation would reduce the void ratio, increase the degree of saturation, decreasing matric suction.

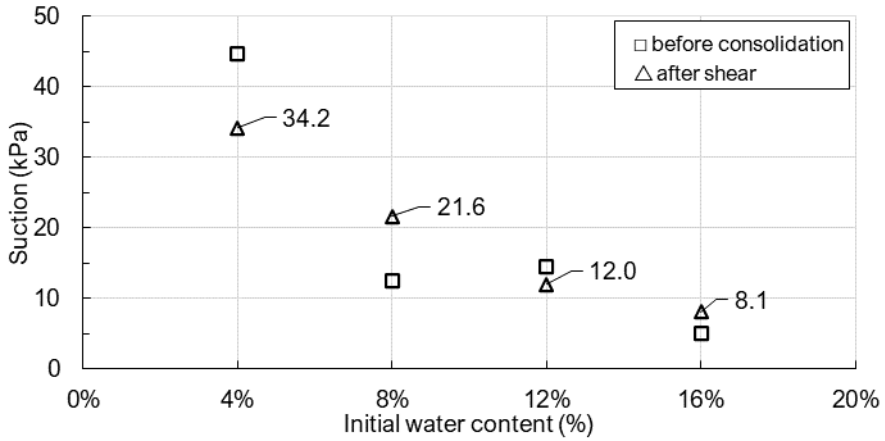

Figure 3.15: Matric suctions of the dense moist tamped samples measured with a tensiometer before and after shearing.

Shear test results showed unrealistic shear strengths with extremely high mobilized friction angles as seen in DSS tests at low stresses as discussed in Chapter 2. Once

again, the effect of matric suction on shear strength was not immediately clear and could not be studied from the shear data as interparticle friction, dilation, matric suction and particle interlock caused by sample compaction all simultaneously contributed to shear strength.

3.3.3 Loose, moist tamped sample

The second approach aimed to create moist tamped samples at varying matric suctions by changing the water content at which they were formed. However, this method caused varying over consolidation ratios due to the compaction energy required to reach the same void ratio across varying water contents. It is likely that horizontal stresses were locked in the samples from the second approach due to the abovementioned reason. Contributors to strength such as particle interlock, locking in of horizontal stresses and dilation all played a role which masked the effect of matric suction. However, these factors can be eliminated when samples are tested under loose, normally consolidated conditions.

Loose, normally consolidated samples would tend to contract upon shearing. This would result in a stress strain curve where the mobilised peak stress is similar to the residual strength. The remaining strength contributors would thus only be interparticle friction (in this case assumed to always remain constant regardless of the stress state) and matric suction allowing for investigation of the effect of matric suction on the shear strength.

Four sets, each set containing two identical samples, were formed at varying water contents. The matric suction in each sample was measured with a tensiometer before consolidation and after shearing. All the samples were nominally moist tamped. However, void ratios between sets varied due to the effect that the varying water contents had on the compaction energy required to reach a certain density. Only minimal tamping effort was required to ensure that all the samples would still be normally consolidated after consolidating to a vertical stress of 50 kPa. The compaction energy applied to the samples was not specifically measured, however, the author attempted to exert the minimum amount of compaction energy such that the samples could be handled without falling apart.

Each set comprised of two samples formed at the same water content and compacted to the same density. The one sample was tested unsaturated by consolidating to a vertical stress of 50 kPa before shearing. The other sample was tested saturated

(Measured Sr > 98%) by filling the DSS bath with water before consolidation to a vertical stress of 50 kPa before shearing.

Figure 3.16 plots void ratio against the initial formation water content of each sample. Two additional samples were tested, one completely dry sample (w = 0%) and another nearly saturated sample (w = 20%). The hollow symbols represents samples that were sheared unsaturated whilst the solid symbols represents the samples that were saturated before consolidation.

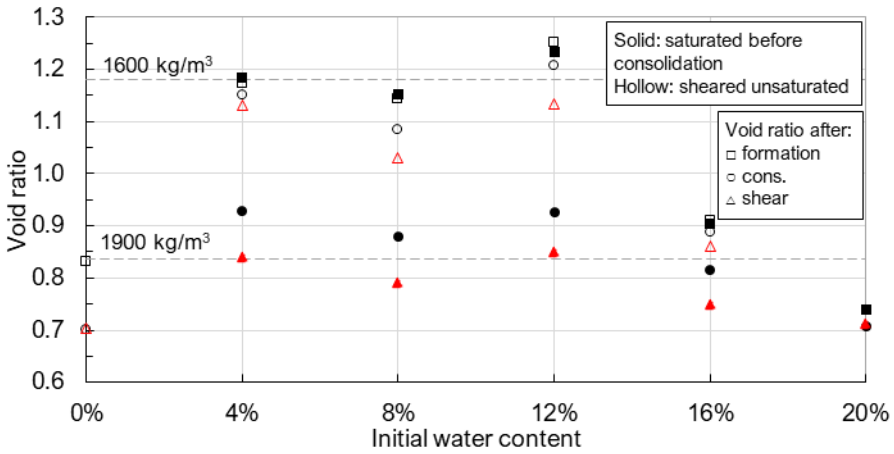

Figure 3.16: Void ratios achieved during formation, consolidation and shearing.

The samples that were saturated before consolidation all collapsed during the consolidation stage as opposed to the unsaturated samples which did not compress as much. Such large differences in the void ratio between the saturated and unsaturated samples were not expected and made the comparison of shear strengths impossible.

3.3.4 Slurry deposited samples

The testing strategies discussed above showed that the following aspects should first be considered when attempting to measure the effect of matric suction on strength when using a direct simple shear device without pore pressure control:

- Interparticle friction, fabric, interlock due to compaction, dilation and matric suction all play a role in the shear strength of soils. Achieving variation of matric suction without variation in the remaining contributors is challenging, especially when the pore air and water pressure cannot be controlled.
- Good contact between the sample and the DSS rings is required to achieve sufficient horizontal confinement. Inserting a fragile, undisturbed tailings sample into the rings without significant disturbance proved very challenging.

- Samples should preferably be tested under normally consolidated conditions to avoid locked in stresses from tamping.
- Strength gain due to overconsolidation associated with tamping masks the effect of matric suctions, making analysis challenging.
- Samples should be tested at the same void ratio as this is one of the main driving factors of shearing behaviour.

The requirements above lead to the final approach where tailings was slurry deposited in an assembled DSS ring stack and membrane. The slurry was mixed at a water content of 25% and placed inside the stretched membrane. The free water which rose to the surface was removed with a paper towel until the surface was visibly dry to speed up the desiccation process. Thereafter the matric suction in the sample was monitored using a tensiometer. It was assumed that the pore pressure gradient in the sample is negligible due to the low sample height. The tensiometers were removed once matric suctions reached a targeted value and the sample was covered with the top cap to be tested under constant stress conditions. Shrinkage was not a problem as the void ratio achieved during slurry deposition was below the shrinkage limit, therefore no gap formed between the sample and the DSS rings due to drying induced shrinkage. The result of this preparation technique were samples, at similar void ratios mentioned in Section 4.2, that could be sheared at varying matric suctions.

Figure 3.17 shows the duplicate tensiometers that were placed on top of each sample. Pore pressures were continuously monitored during the drying process. The tensiometers were removed once a targeted matric suction was reached and the sample was prepared for unsaturated testing. The pore pressure of each sample was also measured after shearing.

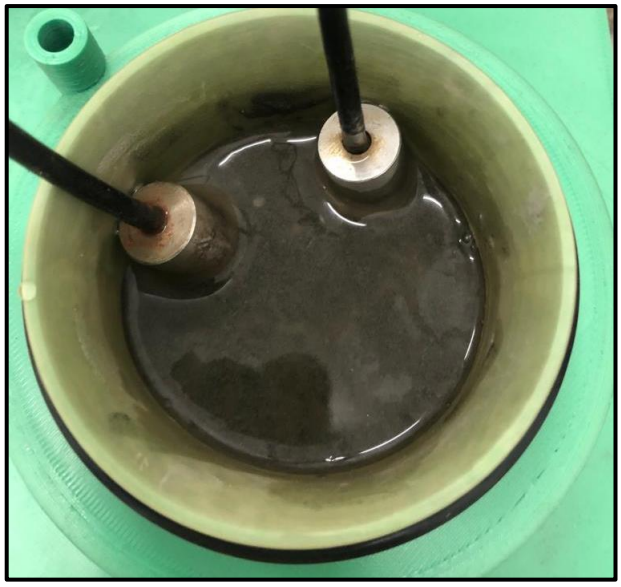

Figure 3.17: Tensiometers placed on top of a sample slurried into a membrane stretched over the DSS rings to monitor the generation of matric suctions during drying.

3.4 MONITORING THE UNSATURATED REGIME IN A TAILINGS DAM

The behaviour of matric suctions and water contents in active tailings dams had to be verified before being able to comment on the effect of matric suctions on the slope stability of these facilities. Therefore, matric suctions were measured using the University of Pretoria tensiometer (Jacobsz, 2018) (Figure 3.18) and water contents were measured with either a 5TM or Teros 12 probe (Figure 3.19) in tailings dams as deposition occurred. Tensiometers were placed side by side with water content sensors at different locations shown in Figure 3.23 and Figure 3.26. Sensors were installed on a platinum tailings dam and a gold tailings dam. The platinum tailings dam is a spigotted operation whilst the gold tailings dam is a day-wall operation. Sensors were placed along the beach of the platinum tailings dam and in the daywall of the gold tailings dam.

Figure 3.18 shows the construction and components of the in-house developed tensiometer (Jacobsz, 2018). The sensitivity and operating range of the sensor can be altered by the type of high air entry (HAE) ceramic and sensor used to suit requirements. The pressure sensor is commercially available with pressure ranges of 100 kPa, 700 kPa, 1.2 MPa, and 7.0 Mpa. Methods followed to saturate and calibrate the tensiometer are described by Jacobsz (2018).

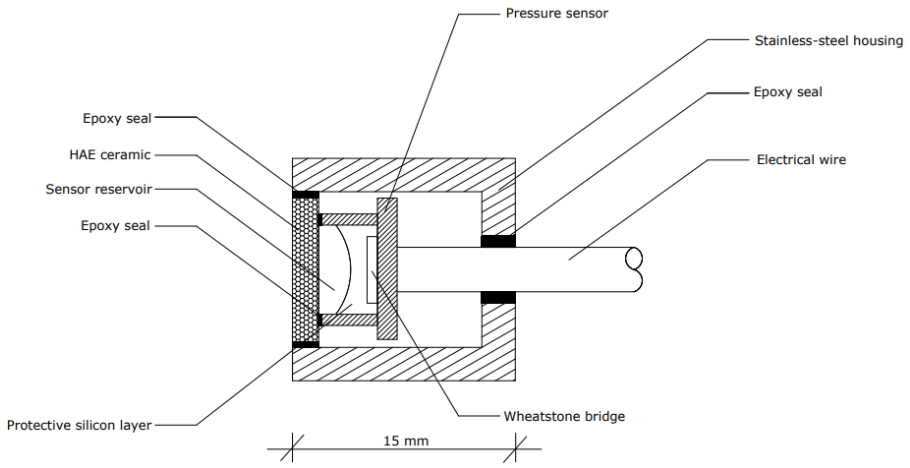

Figure 3.18: Schematic of the University of Pretoria high capacity tensiometer.

Two different sensors, the 5TM soil moisture sensor and the Teros 12, probe manufactured by Meter Group (Figure 3.19), were used in this study. Both the 5TM and Teros 12 have an accuracy of 3% when measuring volumetric water content with Topp's empirical equation for mineral soils (Meter Group, 2019) and both had the capability of measuring temperature. However, calibration is advised when working

with soils with abnormal mineralogy or high electrical conductivity, which might be the case when considering the relatively large quantity of heavy metals and chemicals in tailings (Rotta et al., 2020).

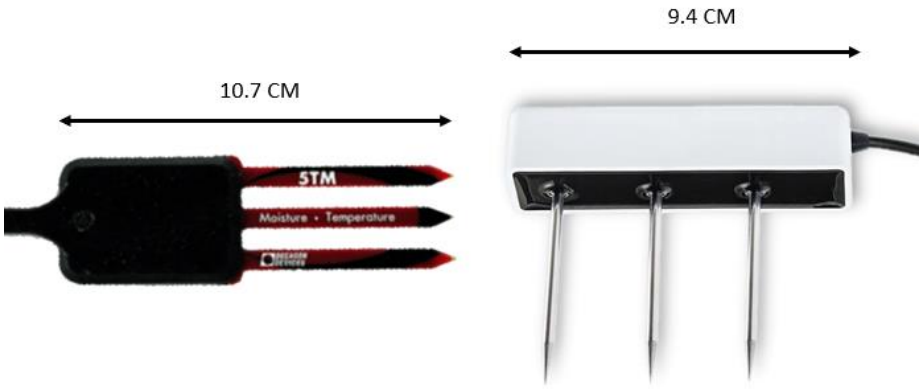

Figure 3.19: TDR volumetric water content sensors, 5TM (left), Teros 12 (right).

Calibration was done by placing tailings mixed at varying water contents in a container such that the bulk volume of the tailings is known. The volumetric water contents could then be calculated from soil phase relationships and compared with the dielectric permittivity of the soil measured by the sensor.

A polynomial curve was fitted to discrete calibration points and served as a new relationship between dielectric permittivity and volumetric water content for platinum and gold tailings. Coefficients for the calibration curve can be found in Figure 3.20. It was found that datasets of both materials had similar trendlines. It was therefore decided that, for practical purposes, a common trendline could be used. A third-degree polynomial was fitted to the dataset by minimizing the mean square error as it was found that Topp's equation tended to overpredict volumetric water contents at higher dielectric permittivity values in platinum and gold tailings. Void ratio was not considered in the calibration procedure of the probe as the exact void ratio in the field is generally not known and only estimated (Figure 3.21).

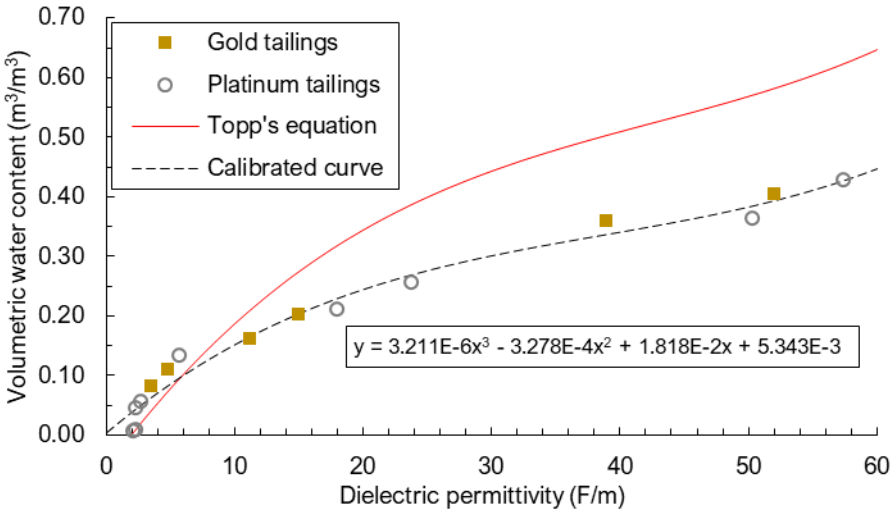

Figure 3.20: Calibration curve of the Teros 12 probe to gold and platinum tailings for volumetric water content.

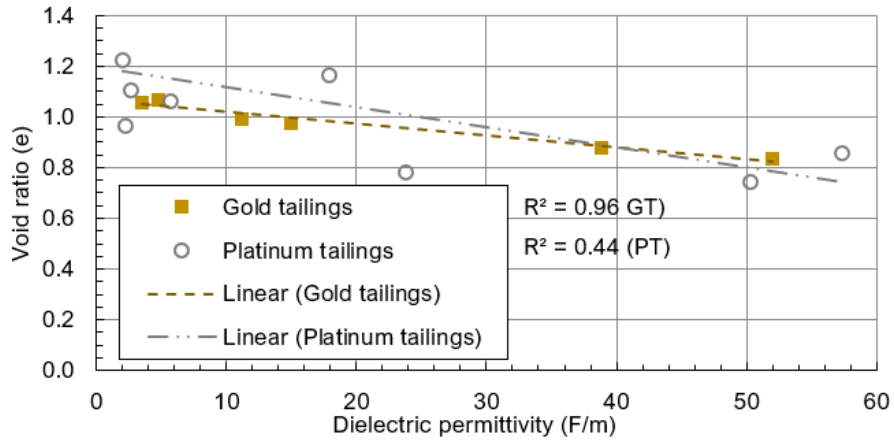

Figure 3.21: Variation in void ratio during calibration of the Teros 12 probe.

The depth of measurement increased as time progressed due to the additional tailings being deposited on the sensors by virtue of the operation of the tailings dams. This allowed for the estimation of a matric suction profile if the increase in measurement depth is considered. The matric suction versus depth profile was estimated by adding discrete, measured, increases in tailings depth to the probe depth. Minimum, 1st quartile, average, 3rd quartile and maximum values were determined for matric suction measurements at each discrete depth shown in Figure 3.22.

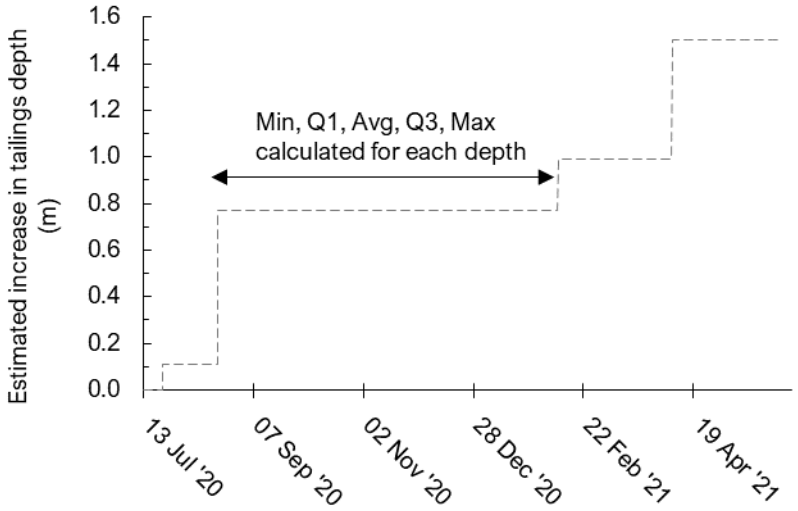

Figure 3.22: Measured increase of tailings depth at DAQ1.

Local increases in the measurement depth for the platinum case were recorded with every site visit. The increase in measurement depth for the gold tailings dam was estimated by the monthly increase in crest elevation (approximately 2 m/year) from the operators report. Monthly operators reports were also used for rainfall and piezometer data.

3.4.1 Platinum tailings dam

Matric suctions and water contents were measured on a platinum tailings dam located on the eastern limb of the Bushveld igneous complex in South Africa. Three loggers were installed all (DAQ1, 2 and 3) all along a cross section at varying distances from the pool (Figure 3.23).

Figure 3.24 shows the sensor configuration of the installation closest to the wall, which is of relevance to this study. Sensors were installed at varying depths to observe the vertical progression of the wetting front upon tailings deposition. The probes were installed in holes drilled with a hand auger. Installation procedures were followed according to the manufacturer's suggestions.

Figure 3.25 shows the sensor configuration of DAQs 2 and 3, although these were not relevant to this study which investigates slope stability. Surface, in-situ void ratios at each logger (DAQ) were measured and are listed in Table 3.1.

Figure 3.23: Data acquisitioning systems (DAQ) layout on a platinum tailings dam (Google Earth Pro, 2022).

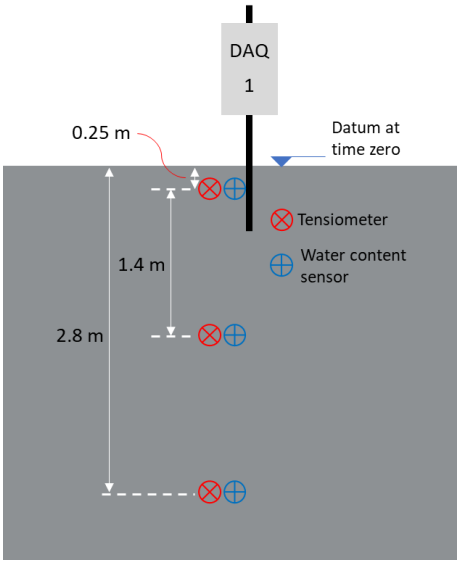

Figure 3.24: Sensor configuration at DAQ1 (not to scale).

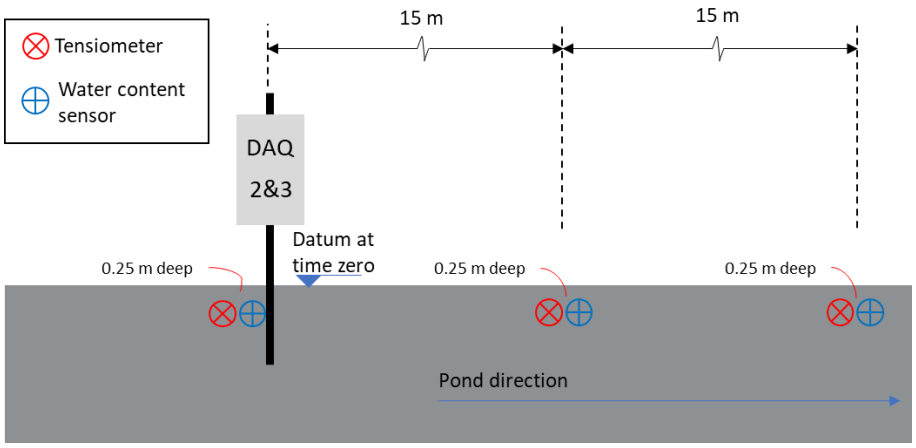

Figure 3.25: Sensor configuration at DAQ2 and DAQ3 (not to scale).

3.4.2 Gold tailings dam

The data acquisition system was installed on the slope of the gold tailings dam, located in the East Rand (East of Johannesburg), (Figure 3.26) with tensiometers and water content sensors placed in the bench, daywall and slope (Figure 3.27). The surface in-situ void ratio was measured as 0.99 (ρ_{dry} = 1456 kg/m^3) by measuring the mass of a block sample with a known volume.

Figure 3.26: Data acquisitioning system position on a gold tailings dam (Google Earth Pro, 2022).

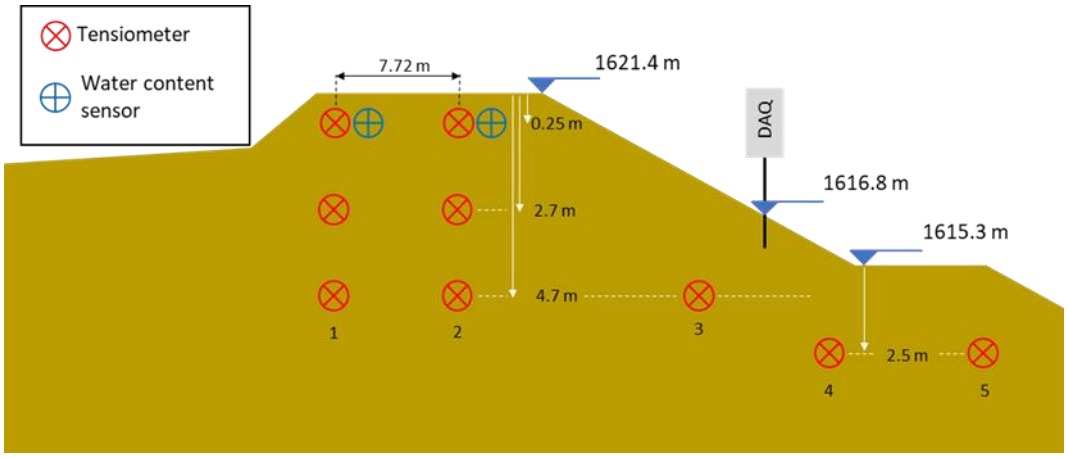

Figure 3.27: Sensor configuration (not to scale).

3.5 CONSIDERATION OF UNSATURATED SOIL MECHANICS PRINCIPLES IN SLOPE STABILITY ASSESSMENTS

The first objective of this thesis was to find a model that can predict the unsaturated shear strength of tailings as a function of matric suction. The second objective was to observe the trend of in-situ matric suctions and water contents on an active tailings dam as this would allow for the estimation of the in-situ, unsaturated shear strength gains originating from matric suctions.

The third objective was to find the effect of matric suctions on slope stability safety factors of active tailings dams which required the theoretical background from the first and second objectives.

The effect of matric suction on the slope stability factor of a tailings dam is considered for the platinum tailings case as well as for the gold tailings case. The safety factor of both the slopes, at the instrumentation locations, were calculated using a limit equilibrium slope stability program, SLOPE/W, from the geotechnical software package, GeoStudio. The phreatic surfaces of both the models were calibrated to standpipe piezometer measurements provided by the tailings dam operators. Piezocone probe test results from the platinum tailings dam showed a sub-hydrostatic increase in pore pressure below the phreatic surface at a rate of 5.14 kPa/m, caused by the flow of porewater. The water column height in the standpipe piezometer was therefore adjusted to account for the sub-hydrostatic pore pressure conditions such that a more realistic phreatic surface could be determined. The same pore pressure build up rate of 5.14 kPa/m was assumed for the gold tailings dam as no piezocone probing data was available for the gold tailings case. The slope stability safety factors were determined with the Morgenstern Price method.

Matric suctions were modelled in the unsaturated region by capping the suction profile according to average, measured field values (illustrated by the red, dashed line in Figure 3.28). Typical minimum and maximum suction values were also considered to find the sensitivity of the slope safety factor to fluctuations in matric suction.

The unsaturated shear strength model by Vanapalli et al. (1996) replaced the typical Mohr-Coulomb strength model in the modelling software to take the strengthening effect of matric suctions into account. Results from both the tailings dam slopes were compared to safety factors determined from a base case which only considered saturated soil mechanics (Mohr-Coulomb) assuming a cohesion of 0 kPa.

Two other methods of incorporating matric suctions into the analyses are also presented in the results of this study. The one assumed a cohesion value with the Mohr-Coulomb strength model equal to typical increases in the unsaturated shear strength of in-situ platinum and gold tailings, during deposition and in between depositions, which were calculated from the field data. The other used the unsaturated shear strength model by Vanapalli et al. (1996) which took matric suctions into account by assuming that the matric suction profile in the model would extrapolate at a rate of 9.81 kPa/m from the phreatic surface through the unsaturated region up to the outer surface of the slope (illustrated by the black, solid line in Figure 3.28).

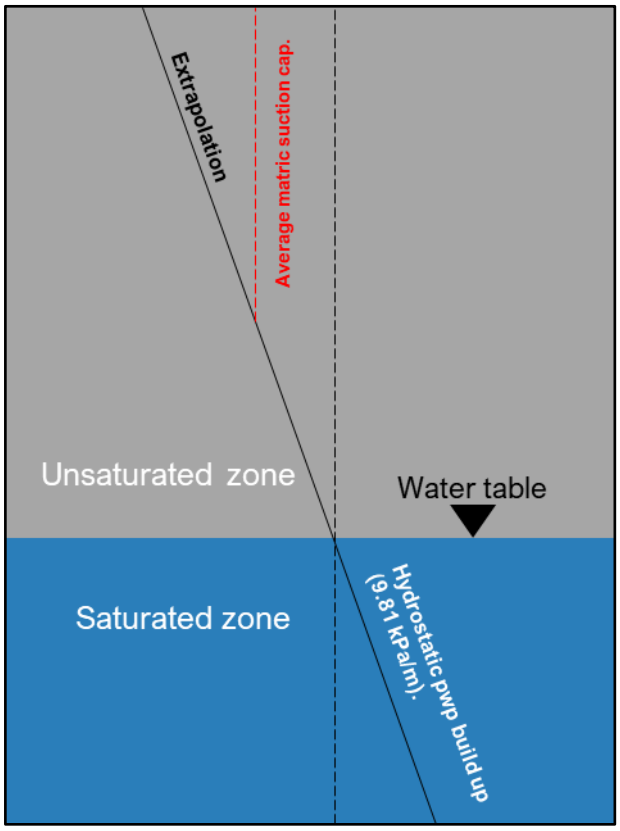

Figure 3.28: Extrapolation of the pore pressure build-up into the unsaturated region of a tailings dam slope.

The unsaturated shear strength model by Vanapalli et al. (1996) calculates the increase in strength from matric suction by finding the product between a soil's effective degree of saturation, suction and the tangential of the friction angle. The additional input parameters, as opposed to the Mohr-Coulomb model, are thus matric suction and volumetric water content.

The matric suction profile in all the models is a user defined parameter and thus defines the suction of each element. The volumetric water content of each soil element is found

by finding the water content relating to the matric suction of the element dictated by a SWRC. The SWRC, measured as stated in section 3.2.2 at a similar density to which the material was found in the field, was provided to SLOPE/W as a material parameter and assumed as a constant over the entire slope. The strengthening effect associated with matric suctions were thus included in the model by first assigning a pore pressure to each element, and then finding the water content of the element according to its suction and finally estimating the gain in strength from suctions with the unsaturated shear strength model by Vanapalli et al. (1996).

Comparisons between the cases where matric suctions were and were not considered had to be drawn between identical slip surfaces. The critical slip surface between the toe and each berm was thus found and the associated safety factor compared between the classical case (ignoring suctions) and the cases considering matric suction on the same slip surface. Figure 3.29 and Figure 3.30 show the analysed slopes with the all the considered slip surfaces. The phreatic surface in both slopes was calibrated to standpipe piezometer data and SWRCs shown in section 3.2.2 were used as material inputs. Other material parameters relevant to the slope stability assessments are summarised in Table 3.3. The horizontal permeability values for platinum and gold tailings taken from Maree (1987) and Blight (1981) respectively. The friction angle for gold tailings was taken from Crous (2021), the friction angle for platinum tailings was obtained from DSS testing.

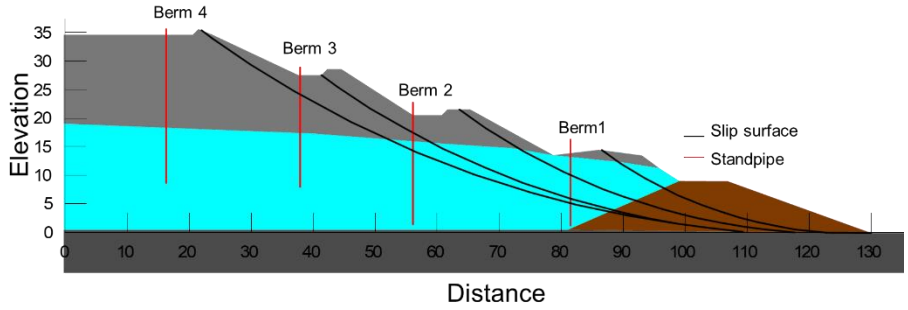

Figure 3.29: Cross-section of the analysed platinum tailings dam slope showing the slip surfaces considered.

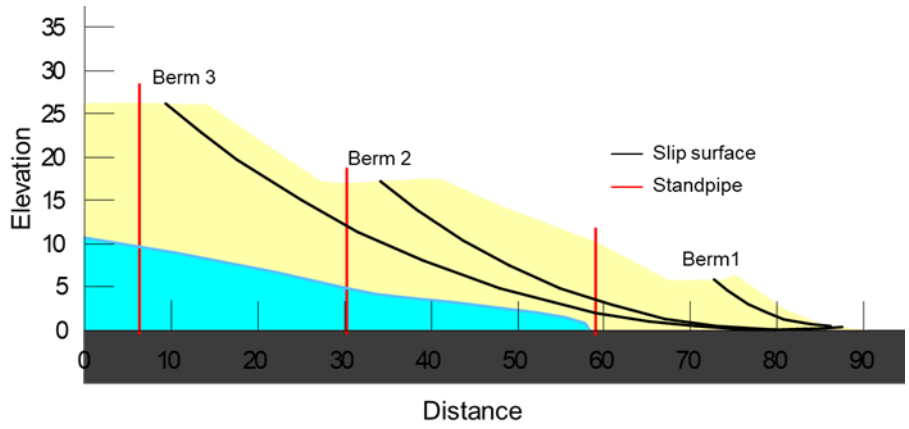

Figure 3.30: Cross-section of the analysed gold tailings dam slope showing the slip surfaces considered.

Table 3.3: Material parameters relevant to the slope stability assessments.

	Platinum tailings	Gold tailings
Gs	3.49	2.74
Permeability ($k_{x\ Sat}$ [m/s])	2.7e-5	9.5e-8
Anisotropy ratio (k_y/k_x)	1/3	1/3
Dry density (kN/m^3)	20	15
Friction angle (°)	35	33

SWRCs were modelled with the method proposed by Fredlund and Xing (1994) and are plotted in Figure 3.31. The models were fitted to measured data of which the resulting parameters are summarized in Table 3.4. Figure 3.32 plots the calculated increase in shear strength expected from matric suction by using the SWRC relationships plotted in Figure 3.31 as inputs for the unsaturated shear strength equation proposed by Vanapalli et al. (1996).

Table 3.4: Fitted parameters for the Fredlund and Xing (1994) model.

SWRC parameter	Platinum tailings	Gold tailings
a	16.82	48.32
m	1.408	4.705
n	3.710	0.762
θ_s (m^3/m^3)	0.530	0.519
θ_r (m^3/m^3)	0.007	0.035

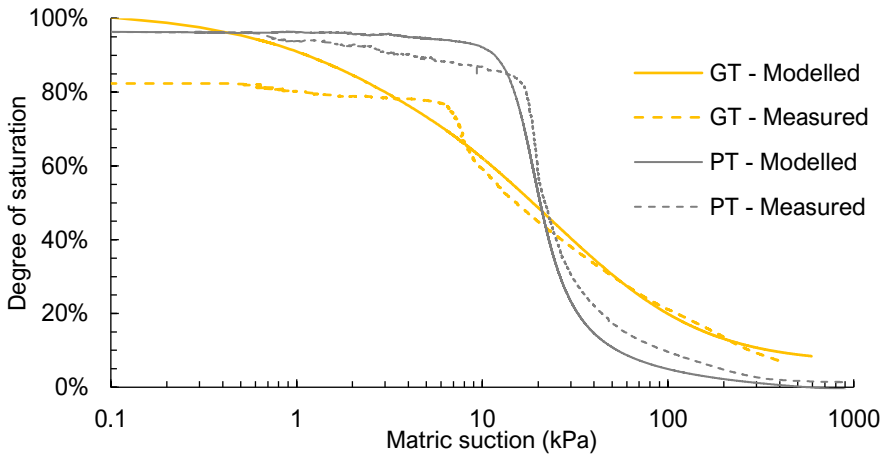

Figure 3.31: Soil water retention curves of gold and platinum tailings used in the GeoStudio analyses.

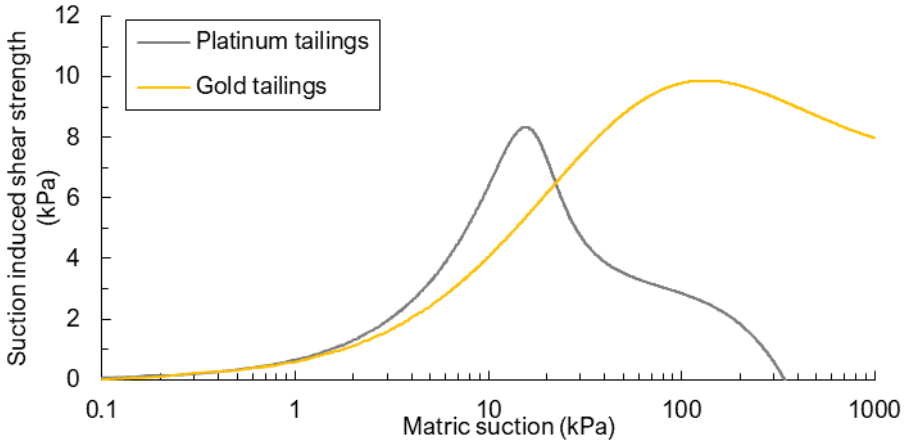

Figure 3.32: Increases in shear strength due to suction calculated from the SWRC.

4 EXPERIMENTAL RESULTS AND DISCUSSION

4.1 INTRODUCTION

The previous chapter discussed two important aspects regarding the effect of matric suction on slope stability.

Firstly, the verification of a suitable model that could predict the unsaturated shear strength of tailings. This was done by shearing platinum tailings samples in a DSS apparatus under varying matric suctions and comparing the measured shear strengths.

Secondly, the temporal behaviour of in-situ matric suctions and water contents on active tailings dams were verified. The contribution of matric suctions on the shear strength of unsaturated soil in slope stability calculations is often ignored due to the uncertainty in the magnitude and reliability of matric suctions. Events such as rainfall or tailings deposition, which increases in-situ water contents, will cause a loss in matric suctions. Therefore, it can be possible that a slope design may rely on additional strength, originating from matric suctions, which is not available anymore. Tensiometers and water content sensors were installed on a platinum and a gold tailings dam to monitor matric suctions and water contents to provide information on the reliability and behaviour thereof.

The effect of matric suctions on s”ope ’tability could be considered once a suitable unsaturated shear strength model had been verified. The in-situ measurements of matric suctions and water contents were compared to a SWRC measured in the laboratory to verify whether the measured SWRC could be applied in analyses to predict the relationship between matric suction and water content.

The slope stability models were run on Geostudio’s SLOPE/W and SEEP/W programs. SEEP/W was used to generate a porewater pressure regime required by the slope stability assessments. The model assumed that the pore pressure regime would extrapolate above the water table at the hydrostatic pore pressure gradient. A SWRC measured in the laboratory, provided as an input by the user, was used to match a water content value to each element in the model, in the unsaturated region, according to its assumed pore pressure. Typically, the conventional Mohr-Coulomb strength model is used in limit equilibrium analyses. However, it was replaced with the unsaturated shear strength model by Vanapalli et al. (1996) to consider the effect of matric suction. Factor

of safety values between cases where matric suctions were and were not considered were compared.

4.2 MONOTONIC DIRECT SIMPLE SHEAR TESTING RESULTS

This section discusses the results obtained from the direct simple shear tests. The effect of matric suction on the shear strength of platinum tailings was examined by changing the pore pressures of the samples by altering the water content under which they were sheared as explained in Chapter 3. Pore pressures were measured with tensiometers before and after testing.

4.2.1 Sampling from a drying box

Figure 4.1 plots the pore pressure data measured from the drying box shown in Figure 3.10. Samples were taken from the drying box, the effect of which are visible as the spikes in the pore pressure plot indicated in Figure 4.1, even though the samples were taken as far away as 40 cm from the tensiometers.

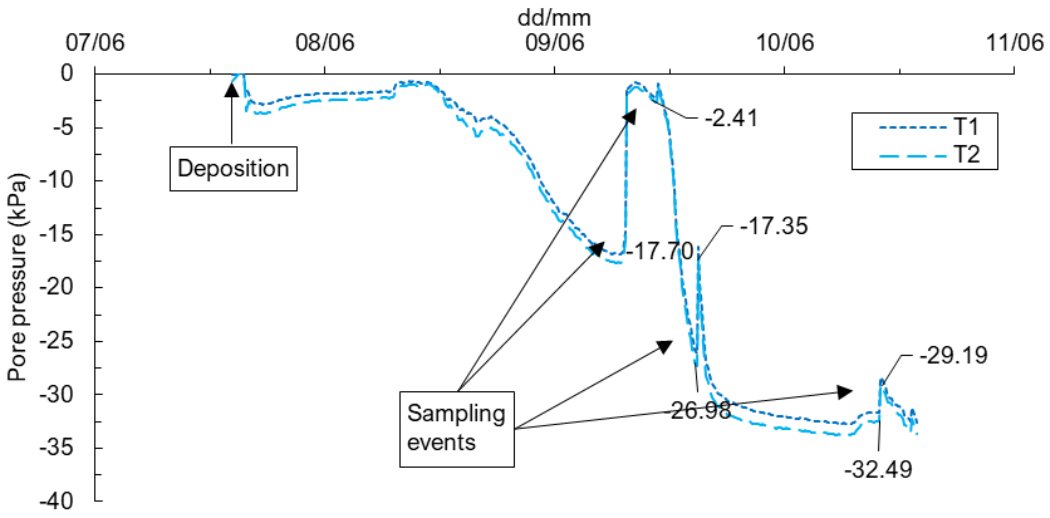

Figure 4.1: Pore pressure measurements from the drying box.

The changes in pore pressures were caused by straining of the soil due to the insertion of the sampling tube. Samples were taken approximately 30 to 40 cm away from the tensiometers showing that the pore pressure disturbances propagate through the entire drying box. This implies that samples that were to be taken in the future were already disturbed by sampling in the past. No comment can be made on the disturbance of the soil element within the sampling tube at the time of sampling. However, the sample cannot be considered as undisturbed due to the changes in pore pressure recorded by the tensiometers in the drying box due to sampling. In addition, the sample was further

disturbed by transportation to the DSS testing room, extrusion, trimming and placement of the sample in the DSS apparatus.

Figure 4.2 plots DSS test results of three samples taken from the drying box.

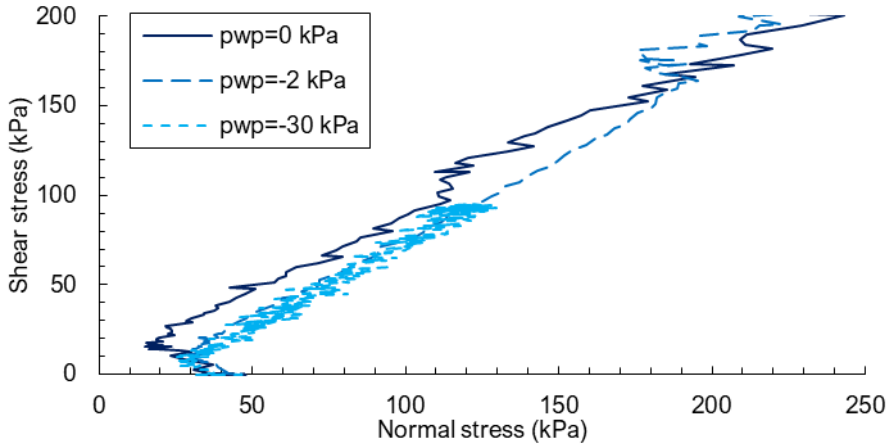

Figure 4.2: Monotonic DSS results on three samples taken from the dying box.

The samples were sheared monotonically under constant volume conditions (similar to undrained conditions in a triaxial apparatus) as it was expected that the tailings samples would strain soften. It was hoped that the results would have showed peak shear strengths which could be compared between samples with varying matric suctions to find a relationship between strength and suction.

Shearing data from the first approach appeared noisy due to the DSS apparatus not being tuned to test stiff materials causing over-corrections in the normal stress applied to the sample. The normal stress exerted onto the sample was controlled automatically by the DSS apparatus to keep the vertical height of the sample constant. It was also found that the diameter of the sampling device was slightly too small, resulting in a gap (less than 1 mm) between the sample and the DSS rings. This caused shear banding to form in samples that were taken at high matric suctions due to insufficient horizontal confinement, implying that the conditions for simple shear were not met.

However, samples taken at low matric suctions, in contrast to samples taken at higher suctions, showed low strength and collapsed under the weight of the top. This caused the sample to increase in diameter which filled the void between the sample and the confinement rings. Therefore, samples sheared at low matric suctions showed higher strengths compared to samples sheared at high matric suctions due to the improved horizontal confinement.

The drying box was remixed whichn the same manner as before after tuning the DSS apparatus for testing stiff materials to retry the first.

Figure 4.3 presents pore pressures and temperatures measured in the drying box after saturation and remixing.

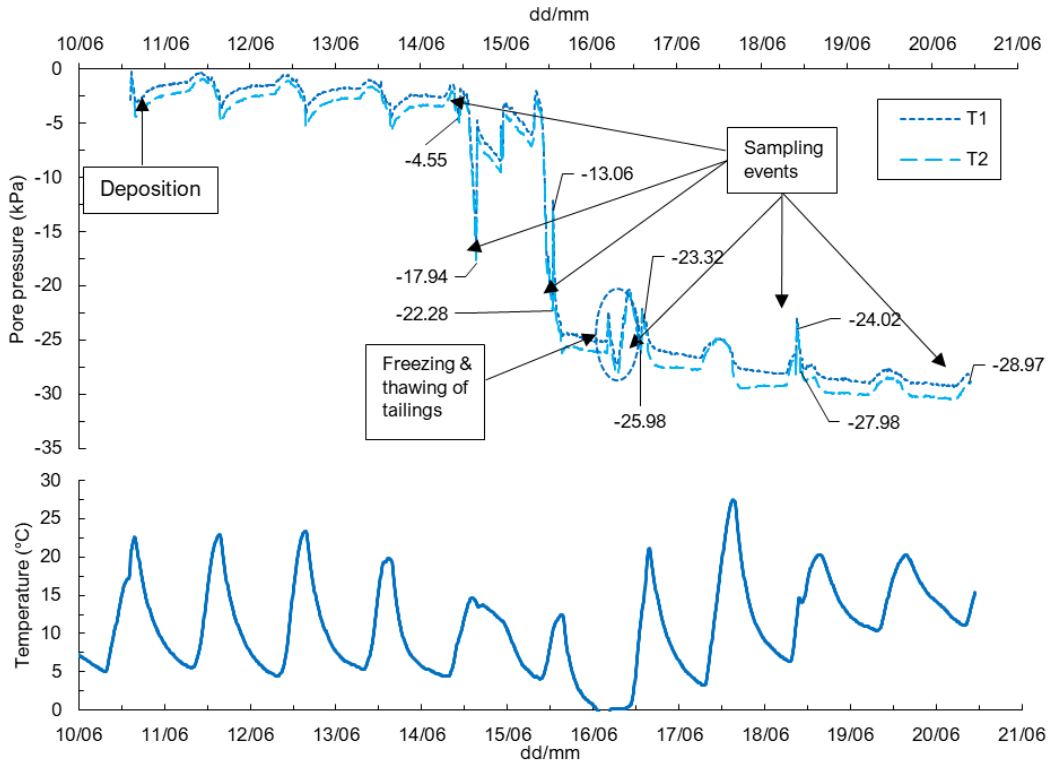

Figure 4.3: Pore pressures (top) and temperature (bottom) measurements from the drying box.

Disturbances caused from sampling can again be seen by the sudden changes in pore pressure. The magnitude in the pore pressure spikes reduced as the tailings in the drying box lost water due to evaporation.

On the morning of 16 June sampling was not possible as the tailings had frozen. This can be seen in Figure 4.3 and Figure 4.4 from the drop in temperature below zero, also reflected by the pore pressure fluctuations seen. The water content reduced slightly upon freezing as a fraction of the pore water had frozen. This reduced the dielectric permittivity of the soil, causing a reduction in the measured volumetric water content. The temperature of the tailings remained constant during thawing due to the latent heat absorption required for water to undergo a phase transfer.

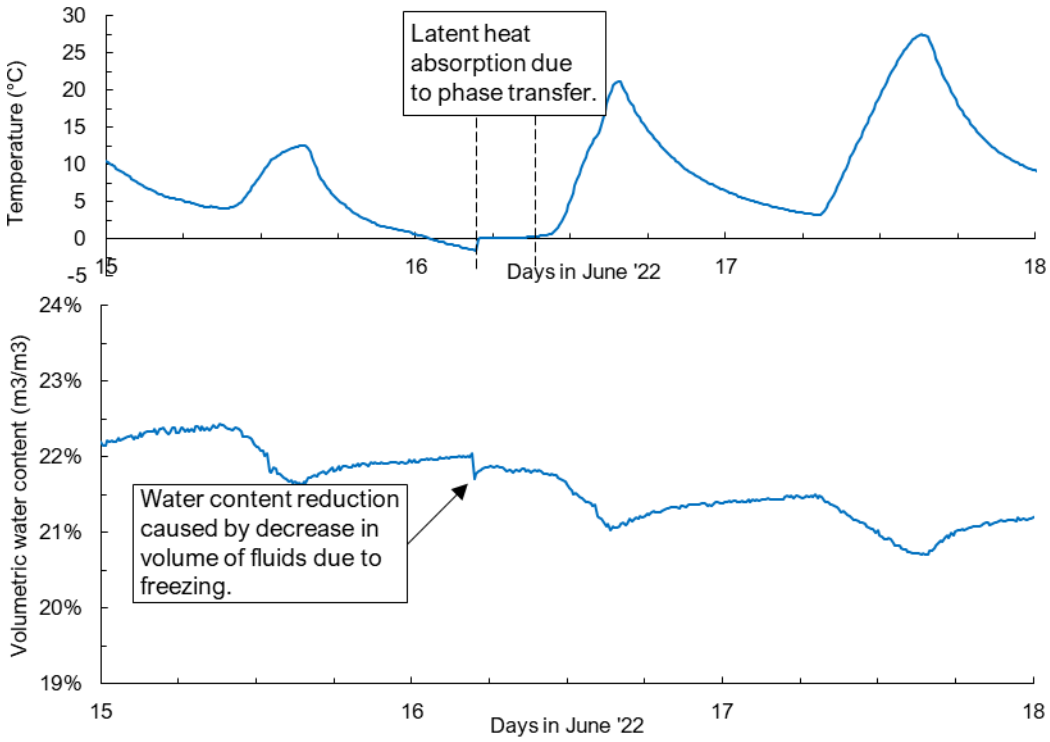

Figure 4.4: The effect of sub-zero pore water temperature on water content.

Figure 4.5 presents the DSS results. Noise reduction in the normal stress data was achieved after tuning the DSS for stiff materials as shown in the test results. However, unrestraint dilation and horizontal confinement proved problematic. Samples with low matric suctions and high degrees of saturation once again collapsed, barrelled and filled the DSS rings, creating good horizontal sample confinement whilst the dryer and stronger samples showed low shear strengths as shear banding again occurred, which was caused by ineffective horizontal confinement. The slurried samples tended to reach low void ratios. The combination of low void ratios with low confining stresses encouraged dilation which further masked the effect of matric suctions.

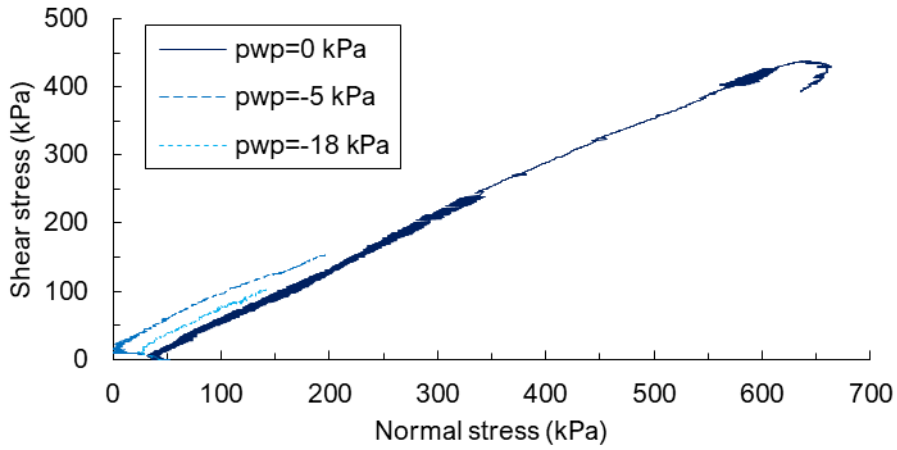

Figure 4.5: Monotonic DSS results of the second sampling attempt from the drying box.

It was mentioned in Section 3.3 that the results from the first approach were inadequate to demonstrate any relationship between matric suction and shear strength. In summary, reasons include the combined effect of high-density samples and shearing at low confinement stresses. The high density of the samples caused dilation which overshadowed the effect of matric suction on shear strength. Testing was done under constant volume conditions which is similar to an undrained triaxial test. This caused the strain hardening stress path to dilate unrestraint all along the critical state line. For example, Figure 4.5 shows how the normal stress applied onto the sample had thus increased from 50 kPa up to 650 kPa as the constant volume condition was enforced. The effect of matric suction is not discernible at such high stresses.

4.2.2 Dense, moist tamped samples

The second attempt at measuring the effect of matric suction on the shear strength of platinum tailings aimed to address the concerns observed during testing of samples taken from the drying box by changing the following aspects:

- Samples were sheared under constant stress conditions instead of constant volume conditions. Constant stress tests are similar to a drained triaxial test as this testing method allows for change in sample height and measures the change thereof during shearing, whilst the normal stress on the sample is kept constant. This would thus provide a single shear strength for a constant normal stress. Unrestraint dilation as observed in Approach 1 would not develop.
- The samples were moist tamped into the confinement rings, lined with a membrane, which ensured good horizontal confinement.

- Matric suctions were measured before consolidation in the DSS and after shearing.

However, testing moist tamped, unsaturated samples at the same void ratio proved challenging due to the varying amount of energy required to compact samples (at varying water contents to control matric suction) to the same density. Completely dry or nearly saturated samples all tended to reach void ratios at or below 0.7 requiring minimal compaction effort. The author noted, in contrast, that samples prepared at water contents near the optimal moisture content required a substantially higher amount of compaction energy to reach void ratios similar to that reached by the completely dry and wet samples. This implies that the samples would have been sheared at varying degrees of over consolidation.

Figure 4.6 and Figure 4.7 plots the results obtained from the unsaturated, moist tamped samples sheared monotonically under a constant normal stress of 50 kPa. Shear test results showed unrealistic shear strengths with extremely high mobilized friction angles as seen in DSS tests at low stresses as discussed in Chapter 2, section 2.5.3. Once again, the effect of matric suction on shear strength was not clear and could not be studied from the test results as interparticle friction, dilation, particle interlock and matric suction all simultaneously contributed to shear strength.

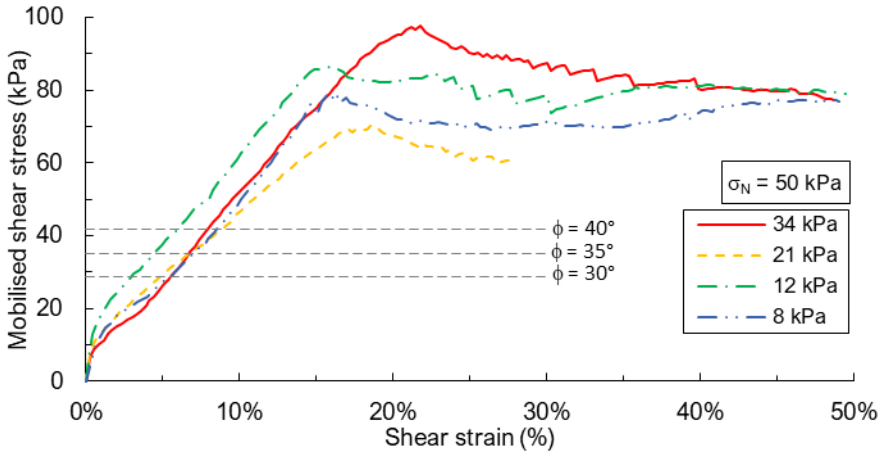

Figure 4.6: Monotonic DSS results of the second approach (Mobilised shear stress vs shear strain).

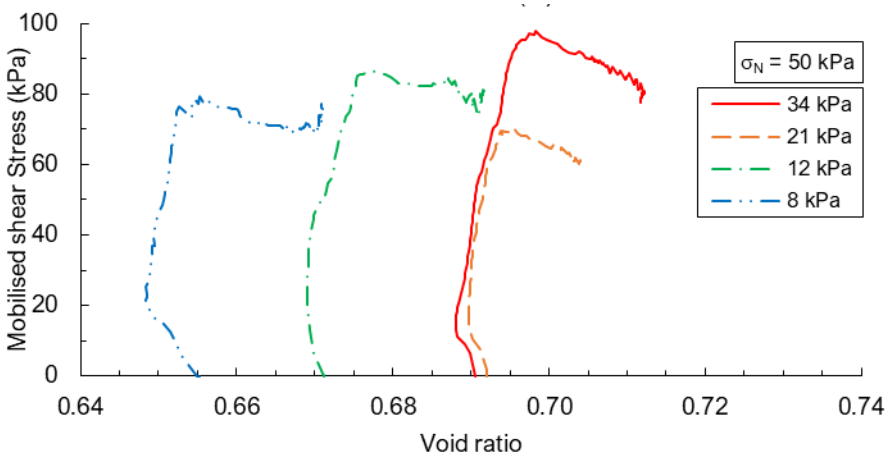

Figure 4.7: Monotonic DSS results of the second approach (Mobilised shear stress vs void ratio).

Figure 4.8 presents events associated with the vertical and horizontal stress developments in a sample during one dimensional consolidation. Tamping a sample into the DSS rings, lined with a membrane, would induce one dimensional consolidation conditions as the confinement rings would not allow the generation of radial stresses.

The act of compaction thus causes the stress path to transverse the one-dimensional compression line. Removal of the compaction stress would reduce the stress state to zero on the x-axis (vertical stress). However, the stress state would remain elevated and exist somewhere on the y-axis (horizontal stress) which represents locked in stresses. Therefore, compaction of the sample in the confinement rings could lock horizontal stresses therein which do not release, even after the removal of the compaction stress which generated the horizontal stress in the first place.

An application of the vertical stress underwhichch the sample would be sheared, equivalent to 50 kPa in this case, would thus result in a stress state which plots between the passive failure line and the one-dimensional compression line. It is therefore possible that the locked in stresses create larger than expected effective stresses in the soil resulting in the measurement of unconservative shear strengths.

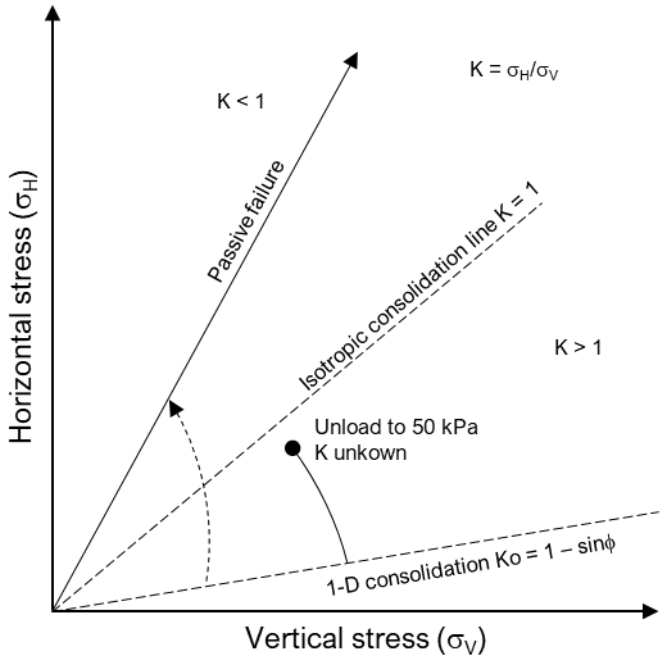

Figure 4.8: One-dimensional consolidation.

4.2.3 Loose, moist tamped samples

Previous testing showed the importance of controlling factors contributing to the shear strength of unsaturated soil, especially at high densities and low stresses. The testing strategy was changed to test under normally consolidated conditions with varying water contents. It was expected that testing under normally consolidated conditions would reduce the effect of contributions to shear strength which are not related to matric suction. Testing several samples at the same void ratio with varying water contents is challenging as varying amounts of energy is required to compact these samples to the same density. This implies that the samples would require varying degrees of overconsolidation to reach the same void ratio because of their respective water contents.

The effect of the consolidation stress history on the shearing resistance of saturated tailings under a total stress of 50 kPa can be seen in Figure 4.9. Two samples were formed at approximately the same void ratio and water content of 16% (Sr ≈ 80%), both saturated before consolidation. The only difference was that the one sample was sheared at an OCR of 1 and the other at an OCR of approximately 3.

Figure 4.9 shows how the normally consolidated sample reached its critical state at peak strength, showing no softening behaviour. The overconsolidated sample showed typical behaviour of a dense sample tested drained, where the stress path overshot the

critical state line before falling back to the critical state. However, the over-consolidated sample did not reach the critical state as clearly as the normally consolidated sample. Increases in the mobilised shear strengths at shear strains beyond 20% on the over-consolidated sample could have been mistaken for strength gains due to matric suction, whilst it originated from the fact that the sample was over-consolidated.

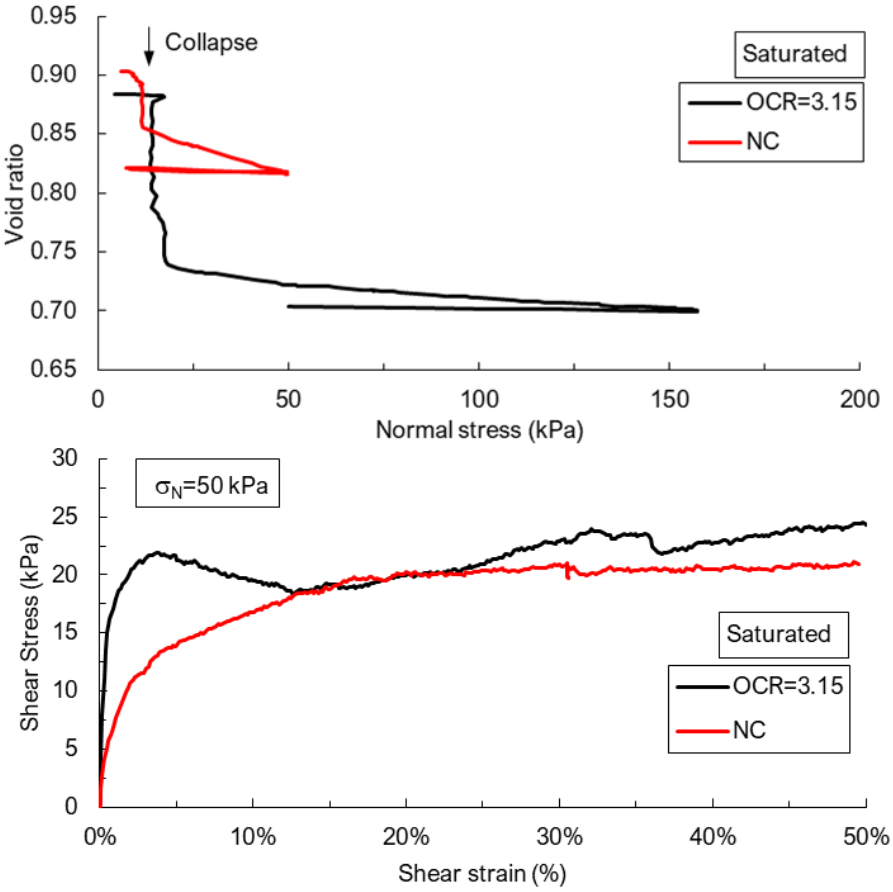

Figure 4.9: Comparison between overconsolidated and normally consolidated samples a) consolidation, b) shearing.

Samples for the third testing regime were therefore nominally moist tamped in an attempt to ensure normally consolidated conditions. Unsaturated shear strengths needed to be compared to a saturated strengths. Thus, each unsaturated sample required a corresponding counterpart formed at the same water content and void ratio. The only difference was that one of the two samples was saturated by submersion in the bath of the DSS before consolidation and tested under saturated conditions, while the other was consolidated and sheared unsaturated by keeping the bath dry. It was found that submersion of samples, prepared unsaturated at loose states, collapsed. Both the

unsaturated and saturated samples were consolidated to 50 kPa and sheared under the same constant total stress.

Figure 4.10 summarizes the void ratios achieved after consolidation. All saturated samples collapsed (solid, black lines), reducing their void ratios significantly, compared to their unsaturated counterpart (dashed, coloured lines).

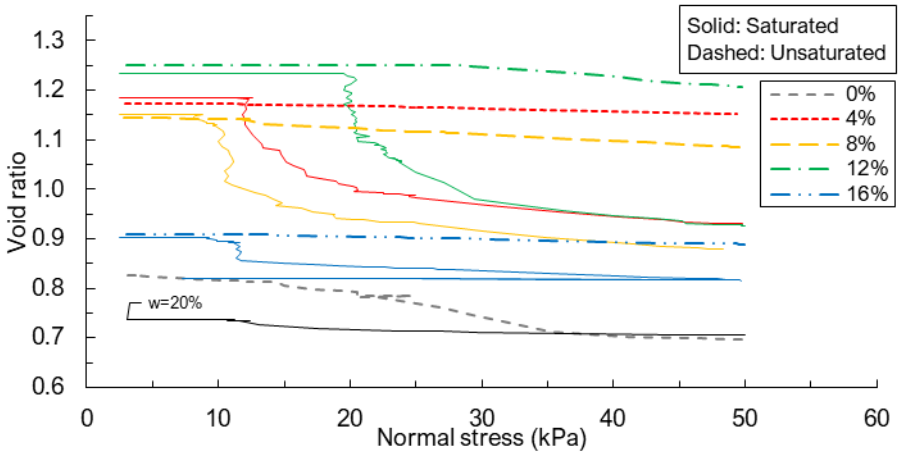

Figure 4.10: Consolidation of nominally moist tamped samples to 50 kPa vertical stress.

Figure 4.11 shows that matric suctions reduced after consolidation and shearing. The reduction in matric suction resulted from the increase in the degree of saturation due to compression of the sample during the testing process.

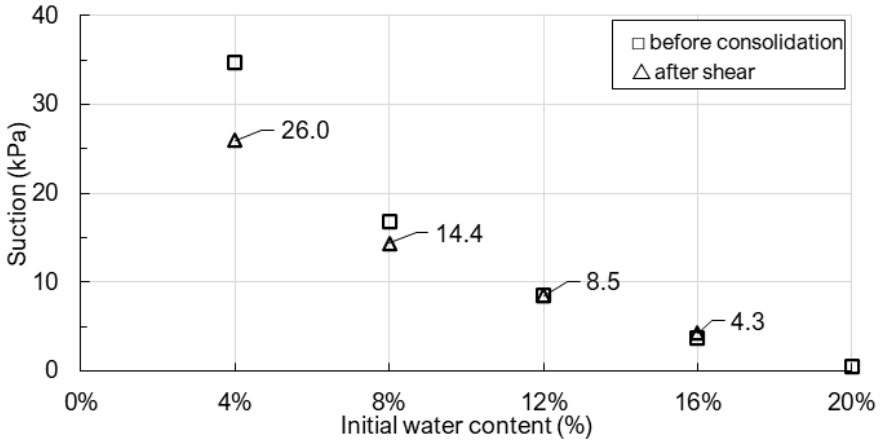

Figure 4.11: Matric suctions in the nominally compacted samples measured with a tensiometer before and after shearing.

It was found that varying void ratios between saturated and unsaturated tests complicated the comparison of strengths between samples and as shown in Figure 4.12

which plots the mobilised shear stress against void ratio for all the tests. Saturated samples, which were formed at similar void ratios than the unsaturated tests, all collapsed during saturation and consolidation. This shifted the mobilised shear stress plots (plotted in black) to the left, making direct strength comparison at equal void ratios impossible. However, shear strain contours show that matric suctions allowed the mobilisation of larger shear stresses at lower strains and densities.

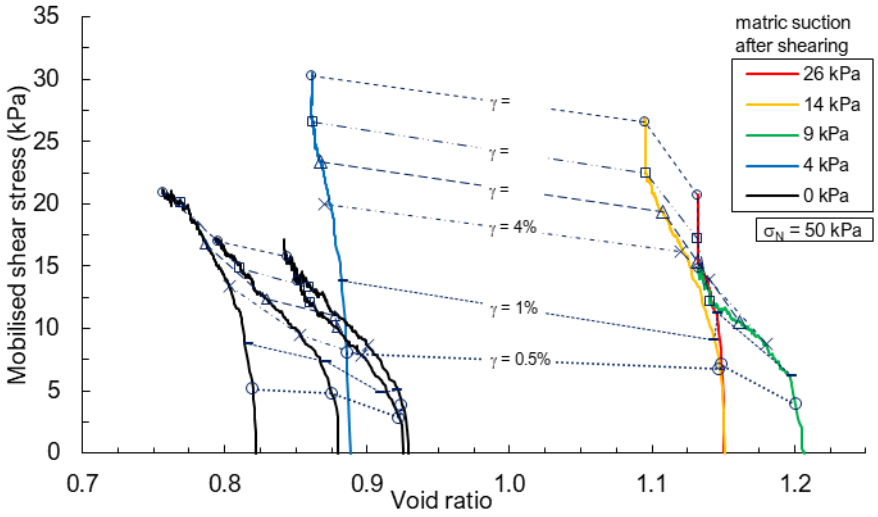

Figure 4.12: Drained, mobilised shear stresses of saturated and unsaturated, nominally moist tamped samples.

4.2.4 Slurry deposited samples

The first three attempts at measuring the effect of matric suction on shear strength all pointed towards slurry deposition as the preferred sample preparation method. Advantages of this method over other methods include the following:

- The fabric of slurried samples can be expected to most closely represent that in the field.
- The gap between the sample and the confinement rings, caused by an undersized sampler, would not occur in this case as the samples reached void ratios below the shrinkage limit of the material upon deposition in the rings.
- Matric suctions were controlled by varying the drying time of each sample.
- The dry-out process of the samples would undergo a stress history similar to that which a soil element would experience in the field.
- Sample strengths could be compared with each other as all the samples reached similar void ratios (0.67 to 0.71).

Figure 4.13 plots the pore pressures measured by the tensiometers during drying of the three samples which were tested. Data logging was stopped once a targeted matric suction was reached and the tensiometers were removed from the sample before preparation for testing.

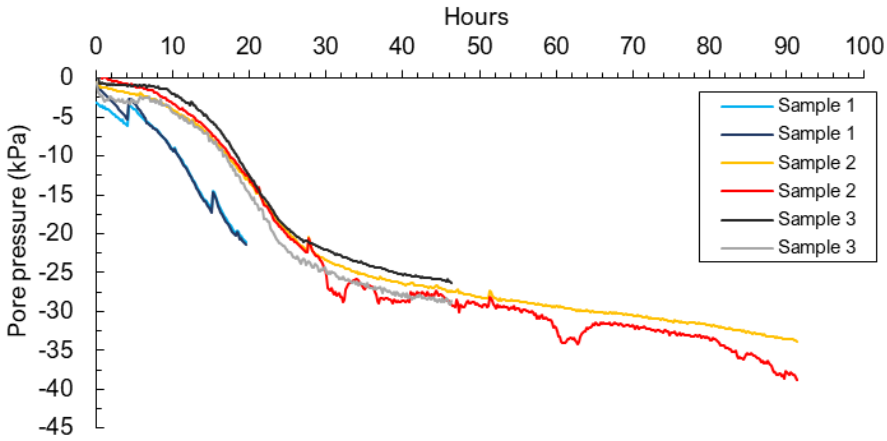

Figure 4.13: Pore pressure measurements from the samples slurried into the assembled DSS rings.

Figure 4.14 represents matric suctions measured in the sample before and after shearing. Matric suctions measured after shearing are probably the most representative of the true suctions in the samples as a trend similar to what one would expect from the SWRC is followed by these datapoints. These were used when relating shear strength to matric suction. Two cases at water contents of 8% and 16% showed an increase in matric suction after shearing which may be caused by a loss of water content during sample testing.

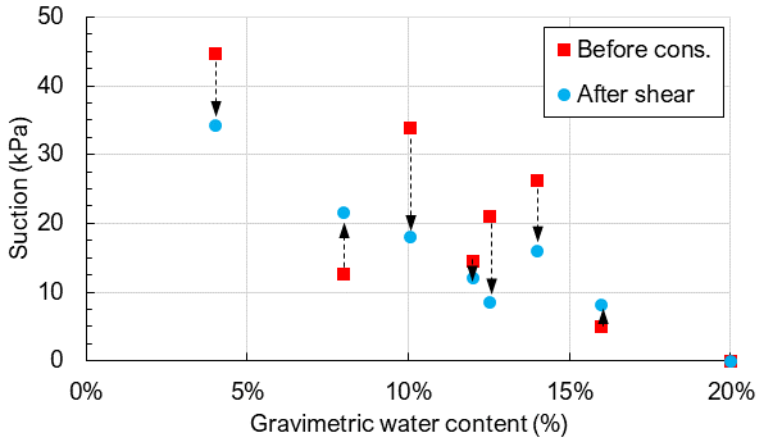

Figure 4.14: Matric suctions measured before consolidation and after shearing versus gravimetric water content.

Models used to predict the gain in shear strength due to matric suction are all dependent on some aspect of the SWRC. Therefore, a SWRC was fitted to suction vs water content data, from the sheared samples, to find a corresponding AEV. Pore pressures were measured before consolidation and after shearing as equipment limitations did not allow matric suction measurements during testing.

A Fredlund and Xing SWRC was fitted to the matric suction values measured after shearing by minimizing the sum of the mean squared errors. The input parameters for the SWRC *a*, *n* and *m* converged to 16.92, 3.751 and 1.875 respectively. The three encircled datapoints in Figure 4.15 – plotting matric suction measured after shearing versus degree of saturation together with a continious SWRC measured in the laboratory – were excluded from the curve fitting algorithm to achieve a more realistic SWRC. SWRCs measured in the laboratory showed air entry values in the order of 10 kPa, similar to that which is found with the fitted curve.

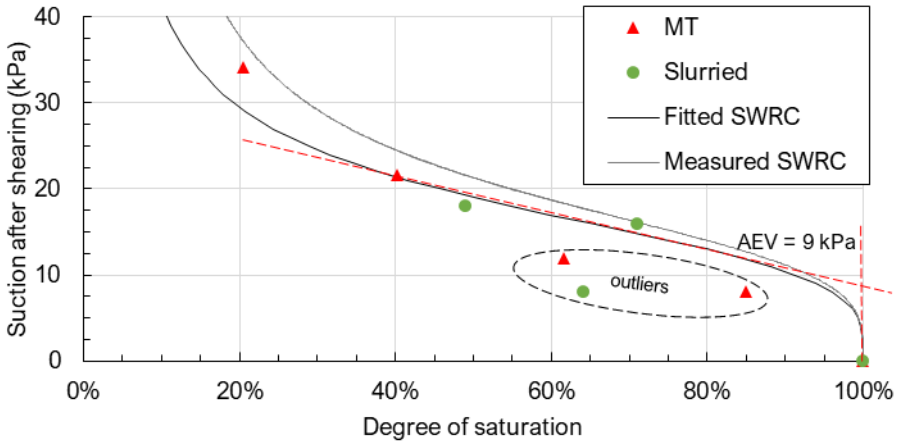

Figure 4.15: SWRC fitted to datapoints relating to matric suctions and degrees of saturations measured from the sheared samples.

Comparing the SWRC, fitted to single datapoints in Figure 4.15, with a continuous drying curve measured on the same material in the laboratory is shown in Figure 4.16. This provides additional confirmation of correct curve fitting. The intersection of the

diagonal, red construction lines with the vertical construction line represents the AEV of both datasets. Both curves showed similar AEVs.

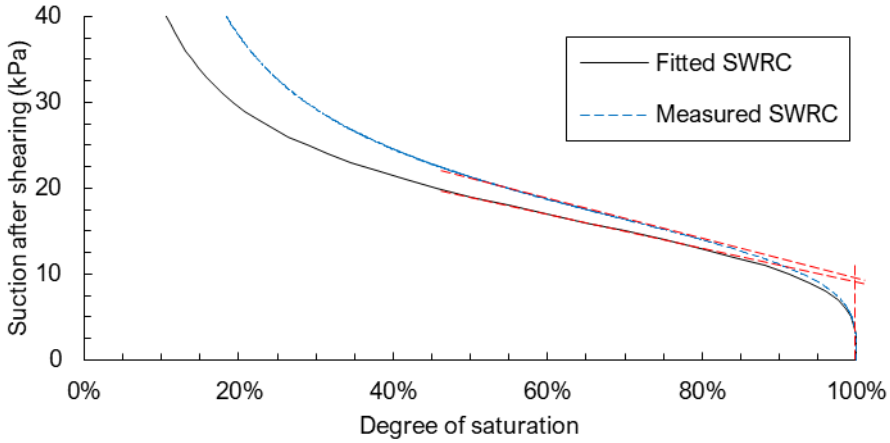

Figure 4.16: Comparison between the SWRC measured in the lab at in-situ densities and the SWRC fitted to data presented in Figure 4.15.

Figure 4.17 plots the mobilised shear stress over shear strain of each sample which was tested under a constant normal load of 50 kPa. Figure 4.17 contains three unsaturated shear strain curves and one saturated curve. Porewater pressure is abbreviated as "pwp" in the legend of the plot.

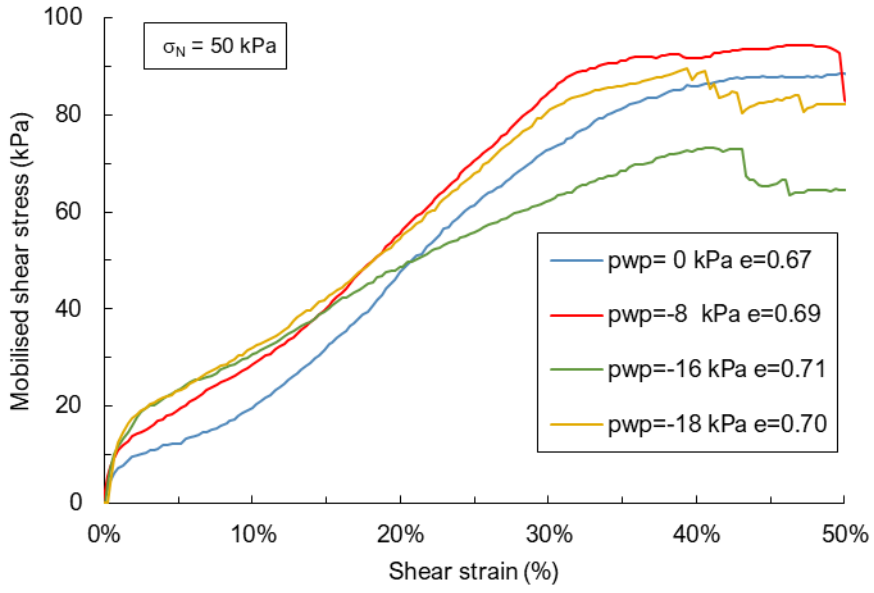

Figure 4.17: Shear stress measurements from drained, monotonic DSS testing on undisturbed slurry deposited tailings samples.

The effect of matric suctions on shear strength of the slurried samples is once again not immediately visible in Figure 4.17. Strong dilation overshadowed the effect of matric

suctions and no clear relationship between matric suction and shear strength could be drawn.

Figure 4.18 plots the mobilised shear stress against void ratio. Volume change during testing shows how all the samples underwent initial contraction followed by dilation.

The inflection points of the mobilised shear stress vs void ratio curves relate to a point of zero dilation as no volume change occurred at this point. No strength is gained from sources other than matric suction during zero dilation, therefore comparison of strengths is desirable at this, the phase transfer point. The phase transfer points between the datasets are linked with a straight dashed line as all the inflection points were found to occur near the same shear strain with one outlier reaching phase transfer at a slightly higher strain of approximately 7% instead of 5%. This point could also be identified by finding the shear strain where the dilation angle is zero as seen in Figure 4.19. Al Tarhouni and Hawlader (2021) also used the point of zero dilation to find the friction angle studying the simple shear behaviour of sand under low stresses. The instantaneous angle of dilation plotted with shear strain is found in Figure 4.19 and shows how all but one of the samples, relating to a negative pore water pressure of 16 kPa, reached zero dilation within a small shear strain range, in the order of 4% as the datasets approached the x-axis.

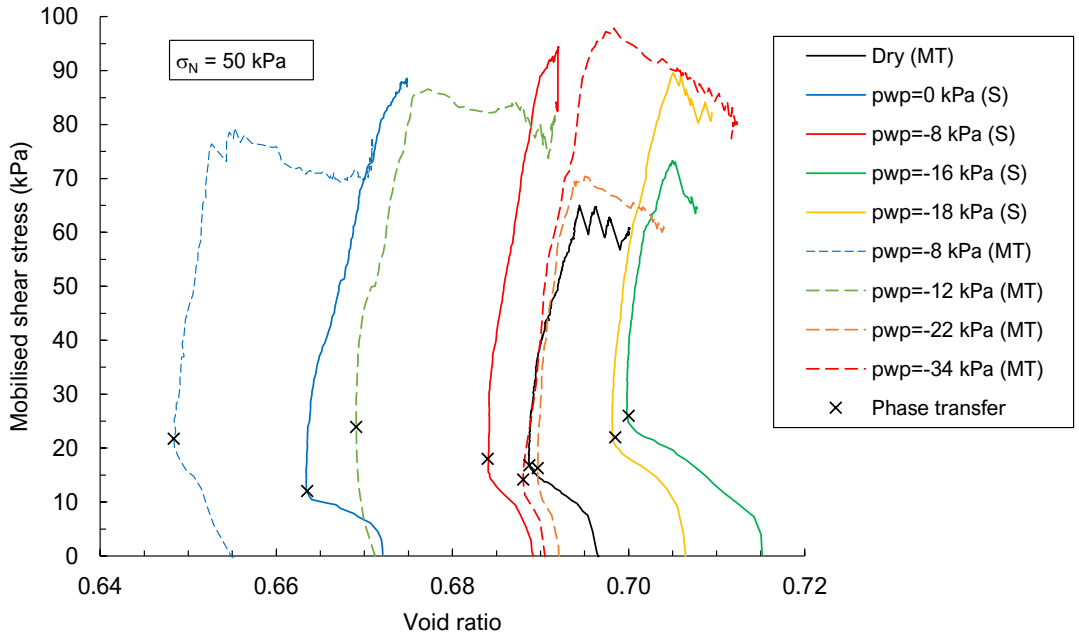

Figure 4.18: Mobilised shear stress plotted against void ratio of drained, monotonic DSS tests on undisturbed slurry deposited samples.

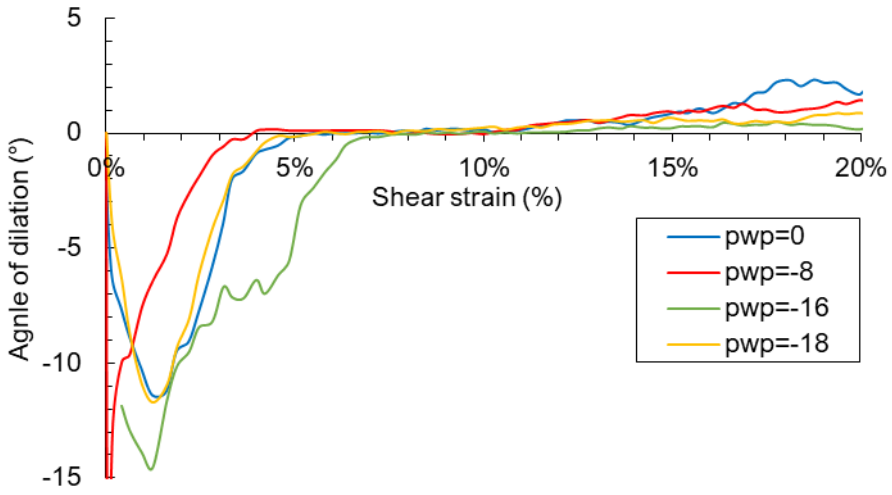

Figure 4.19: Plot of the dilation angle used to find the phase transfer point.

It was found that the dense, moist tamped samples, which achieved similar void ratios to the slurried samples, could also be used to observe the effect of matric suction on shear strength when considering the mobilised shear strength at the phase transfer point.

The mobilised shear stress vs void ratio datasets for all the unsaturated samples are plotted in Figure 4.20 from which mobilised shear strengths at phase transfer (marked with x) were extracted and plotted against matric suction measured after shearing in Figure 4.21 for the slurried samples and Figure 4.22 (for the moist tamped samples), respectively.

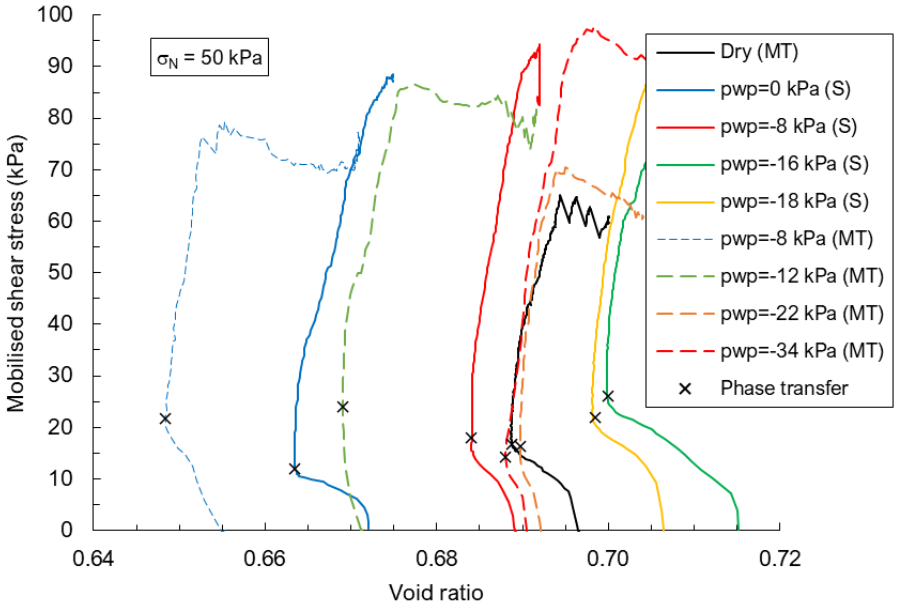

Figure 4.20: Shear stress results plotted against void ratio for dense platinum tailings samples.

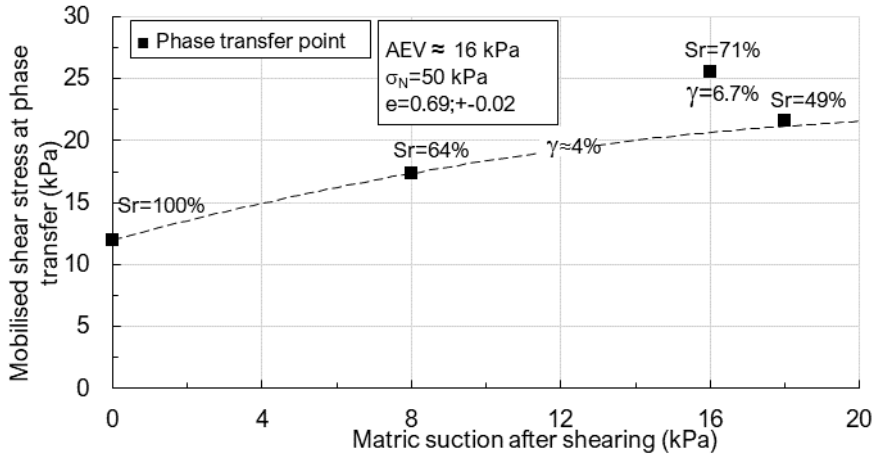

Figure 4.21: Mobilised shear stress at phase transfer for unsaturated slurried tailings at varying matric suctions, measured after shearing.

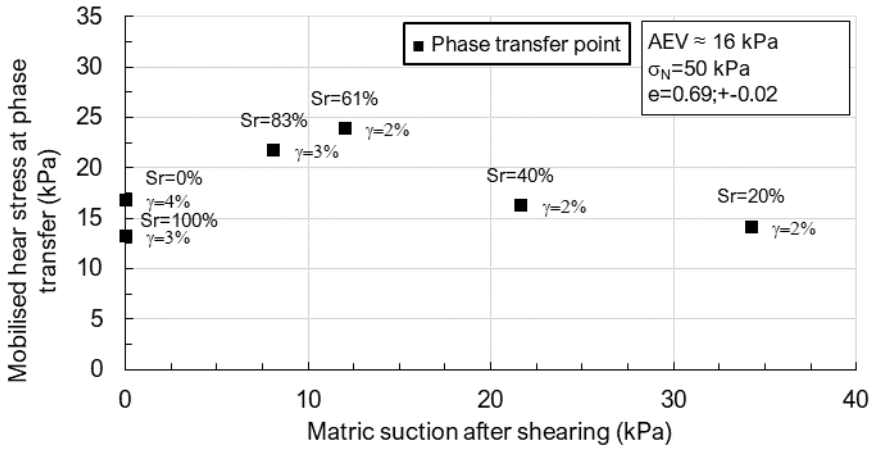

Figure 4.22: Mobilised shear stress at phase transfer of unsaturated moist tamped tailings at varying matric suctions measured after shearing.

All phase transfer points in Figure 4.21 occurred at a shear strain of 4% for the slurried samples shown in Figure 4.18 with one apparent outlier at 6.7%. Examination of the test results of samples prepared by moist tamping revealed the phase transfers occurring at shear strains between 2% and 4%. A strong positive correlation between matric suction and the mobilised shear stress at the phase transfer point was found, demonstrating the strengthening effect of matric suction on the shear strength of tailings.

4.2.5 The effect of matric suction on the mobilised shear stress at the phase transfer point

A summary of the justifications of mobilised shear strength comparison at the phase transfer point is listed below:

- Dilation or contraction do not contribute to strength at phase transfer, reducing the uncertainty regarding the origin of strength gain.
- Shear strains at phase transfer were all well below 10%.
- There was a clear trend between the mobilised shear stress at phase transfer and matric suction for both the moist tamped and slurried.
- The variation in void ratios between dense samples were within a range of ± 0.02 and which was deemed acceptable for strength comparison, unlike the loose samples.

It was found that the shear strain at phase transfer for the moist tamped samples tended to vary between 2% and 4%. However, a relationship between mobilised shear strength

and matric suction was still found (Figure 4.22) which was in accordance with the literature (Donald, 1957).

Figure 4.23 presents the mobilised shear stress of both the moist tamped and slurried samples plotted over matric suctions. A large proportion of the unsaturated shear strength models discussed in Section 2.4.1 included three mathematical terms, the first corresponding to cohesion, the second corresponding to a saturated strength component and the third corresponding to an unsaturated strength component. For example, in the model by Vanapalli et al. (1996) ($\tau = c' + \sigma_n tan\phi' + \psi\left(\frac{\theta-\theta_r}{\theta_s-\theta_r}\right) tan\phi'$), the saturated strength originates from the second term and the unsaturated strength originates from the third term.

The saturated strength component could be assumed as a common variable across all tests due to the fact that all the samples were sheared under a constant normal stress of 50 kPa and similar void ratios. This allows for the estimation of the unsaturated component found by subtracting the saturated strength component from the total measured strength. The hatched area below the datapoints in Figure 4.23 represents the assumed saturated strength of 12.75, kPa applicable to all datasets as the datapoints corresponding to zero matric suction had an average mobilised shear strength of 12.75 kPa corresponding to an effective friction angle of 14°. The unsaturated strength component is thus represented by the area above the hatched section.

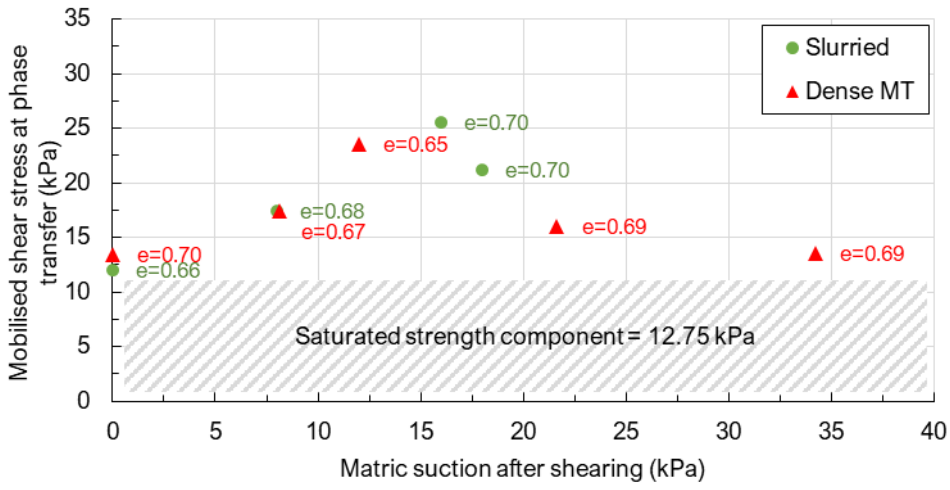

Figure 4.23: Mobilised shear stress at phase transfer of dense, unsaturated tailings plotted versus matric suction.

The AEV from the fitted SWRC was found to be in the order of 9 kPa (Figure 4.15). Figure 4.24 shows that an AEV of 13 kPa would have been expected, as the AEV is the

point where matric suctions are converted to effective stress the most efficiently. The literature shows that the peak strength due to matric suction is often found at the air entry value. Deviation from this value could be caused by the fact that the curve was fitted through SWRC datapoints which plotted on scanning curves for the moist tamped samples. Determination of the AEV is somewhat an arbitrary method using construction lines which may also cause deviations between AEVs. Another potential explanation are the different stress histories experienced by the slurried samples due to the development of matric suctions during the desiccation process. Differences in the fabric of slurried and moist tamped samples could also contribute to strength differences.

The contribution of matric suctions to shear strength reduced once suctions exceed the air entry value as stated by Öberg and Sällfors (1995). This implies that the shear strength gained from matric suctions will increase linearly with matric suction up to the AEV, which is the case from the data in Figure 4.24 between matric suctions of 0 and 16 kPa. Air dried samples crumbled effortlessly when handled, showing the loss of strength under residual conditions. This suggests that the strength gain from matric suctions will eventually have to reduce to zero.

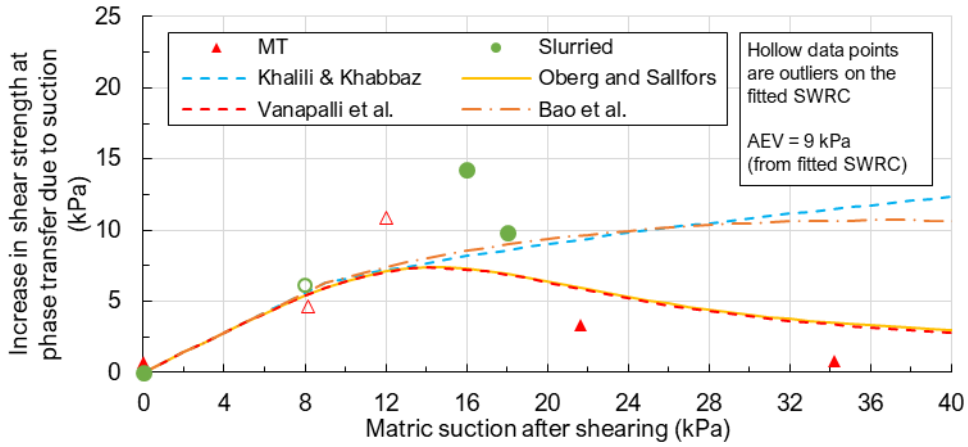

Figure 4.24: Increase in shear strength at the phase transfer point of dense, unsaturated tailings samples plotted over matric suction.

Table 4.1 statistically summarizes the performance in predicting the unsaturated shear strength of tailings of the four evaluated equations.

Table 4.1: Statistical performance of the considered unsaturated shear strength models.

Statistical parameter	Khalili and Khabbaz	Öberg and Sällfors	Vanapalli	Bao
# of datapoints	9	9	9	9
CI	43.5%	43.8%	53.7%	44.5%
R^2-value	0.03	0.877	0.909	0.061
Slope	0.022	0.266	0.291	0.084

Models proposed by Khalili and Khabbaz (1998) and Bao et al. (1998) overpredict shear strength at matric suction values larger than air entry and have the lowest confidence intervals at 43.5% and 44.5% respectively. The model by Vanapalli et al. (1996) fits the experimental data better as it takes the decrease in shear strength at matric suctions beyond air entry into account, increasing the confidence intervals to 53.7%. The models by Vanapalli et a. (1996) and Öberg and Sällfors (1995) are similar as both estimate the unsaturated shear strength by finding the product of pore pressure and an expression of the effective degree of saturation, therefore the similar shape.

The model proposed by Öberg and Sällfors (1995) is based on Bishop's (1959) unsaturated effective stress equation: $\sigma'=(\sigma-u_a) + \chi(u_a-u_w)$, as discussed in Section 2.4.1. Assuming the pore air pressure (u_a) as zero, leads to: $\sigma'= (\sigma) + \chi\psi$, where the parameter ψ represents matric suction and χ a parameter between 0 and 1, depending on the degree of saturation and soil type. The result is a simple equation capable of predicting the drained shear strength of unsaturated, non-clayey soils sufficiently accurately for practical engineering purposes: $\tau' = c' + \sigma\tan\phi' + S_r\psi\tan\phi'$.

The same case can be made for the similar equation proposed by Vanapalli et al. (1996), the only difference being that the degree of saturation is replaced by an effective degree of saturation, $\left(\frac{\theta-\theta_r}{\theta_s-\theta_r}\right)$. The shear strength equation by Vanapalli et al. (1996) was used in analyses due to it giving the highest confidence interval with the experimental data as presented in Table 4.1.

4.3 FIELD MEASUREMENTS

Matric suction, temperature and volumetric water content were measured on a platinum and gold tailings dam. The data gathered was then used to estimate the magnitude of the shear strength gain attributed to matric suctions as deposition and desiccation cycles occurred.

4.3.1 Platinum tailings (Spigotted operation)

Probes measuring water content, pore pressure and temperature were installed close to the outer wall of the platinum tailings dam at depths of 0.25 m, 1.4 m, and 2.8 m as described in Chapter 3 (Figure 3.24). The depth of measurement increased by approximately 1.5 m throughout the duration of the study due to deposition but was not continuously measured. Figure 4.25 plots the measured in-situ field data gathered from DAQ1 over a period of 13 months. Deposition events are characterised by sudden increases in water content in August, October and March. Deposition routinely increased the calculated degree of saturation from 20% to approximately 45%. The degree of saturation was based on void ratios measured from cube samples taken.

Matric suction and temperature data gathered within the first month of commissioning appears noisy due to the daily fluctuation in temperature. It is known that temperature and matric suction have a fundamental thermodynamic relationship, causing the observed fluctuations (Likos and Lu, 2004). This phenomenon can also be seen in the drying box data presented in Figure 4.3. Measured thermal fluctuation reduced once tailings thickness increased after the first deposition event which increased the instrumentation depth by approximately 0.8 m. Interestingly, deposition of fresh tailings never caused suctions to entirely dissipate. The effect of deposition and rainfall on matric suction decreased as time progressed, once again due to the increase in measurement depth. Matric suctions across all depths tended to gradually decrease with time as the instrumentation depth increased, possibly associated with the migration of moisture in the tailings.

The first part of the deposition event in August 2020 was not recorded as the logger's battery had to be replaced. There is an indication of matric suctions decreasing from approximately 30 kPa to between 20 and 10 kPa. However, thereafter suctions never dissipated completely following deposition. This is due to the deposition method. Spigotted operations tend to form a delta of meandering slurry streams upon deposition. It is therefore possible that a stream can either flow directly over or around the probes,

both causing different effects on the matric suctions recorded. The nature of deposition is such that it is unlikely to cause a total dissipation of matric suctions over a large area.

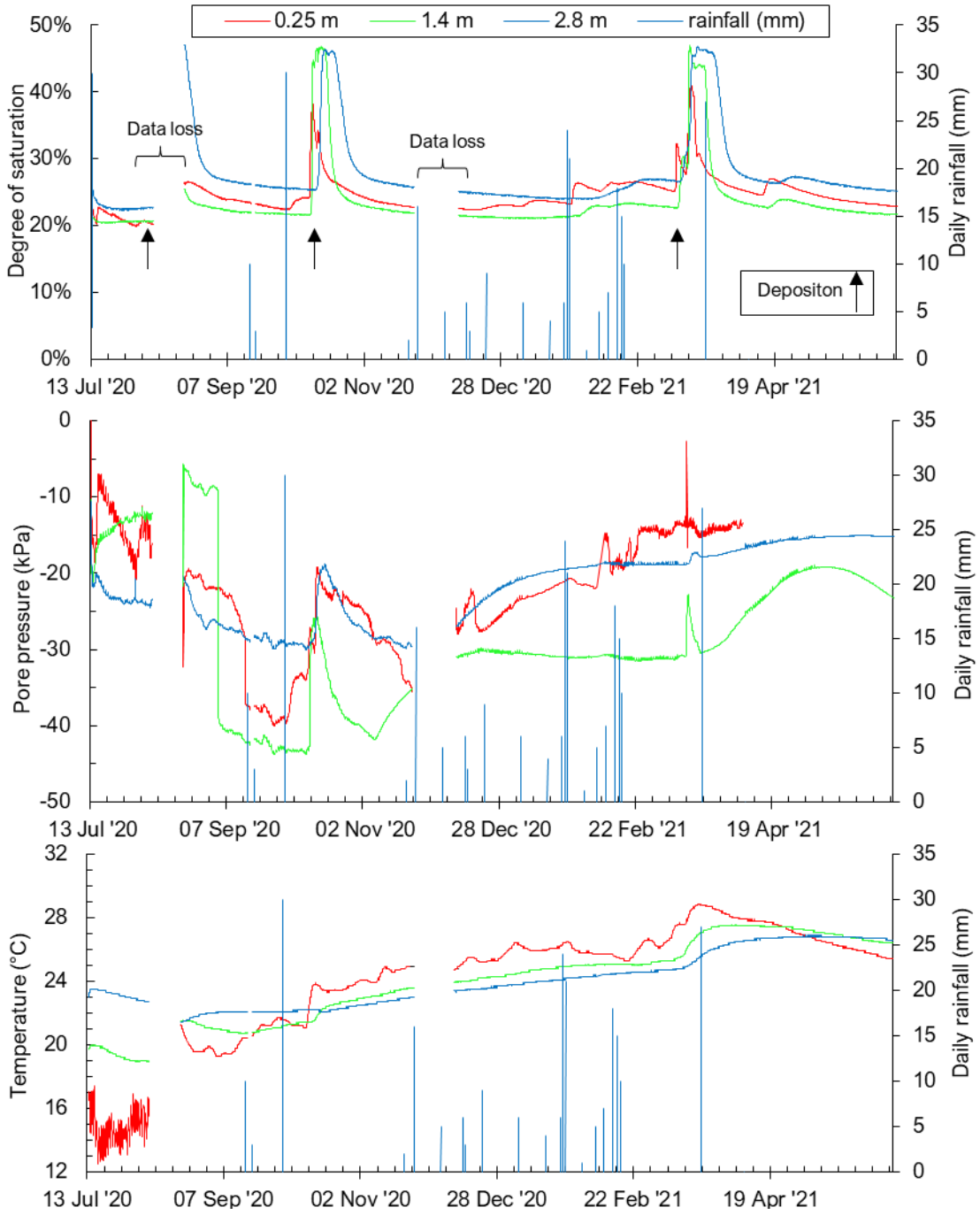

Figure 4.25: Degree of saturation, pore pressure and temperature monitored at varying depths near the wall of a platinum tailings dam.

An example of the matric suction response due to rainfall can be seen between September 2020 and October 2020 marked by the 30 mm rainfall event. The shallowest matric suction measurement decreased from 39 kPa to 35 kPa after the rainfall had occurred whilst the remaining, deeper, matric suction measurements continued increasing. The response in degree of saturation coincides with the decrease of matric suction in the shallow measurement and can be identified by the discontinuity in the dataset after the rainfall event indicating an increase in water content. The remaining, deeper, degree of saturation measurements continued decreasing. The rainfall event caused an approximately 4 kPa reduction in matric suction in the shallowest measurement, with a reducing effect as the measurement depth increased.

Daliri et al. (2016) showed that matric suctions dissipated entirely upon deposition of a new tailings layer in a drying box. Also, fluctuation in water content measurements after deposition tended to decrease as the tailings depth above the point of measurement increased. Both these cases were not observed in the field measurements. To the contrary, matric suctions never dissipated entirely, and the water contents all increased approximately to the same value following repeated depositions, not reaching full saturation, regardless of the measurement depth considered. A possible explanation for this might include a more permeable material, the effect of the deposition methods, drainage conditions and the presence of vast volumes of unsaturated, underlying tailings able to accept porewater.

Figure 4.26 shows how the degree of saturation changed with time due to two deposition events. Both measurements were at depths of 0.25 m (top), 1.4 m (middle) and 2.8 m (bottom), plotted in Figure 4.26, showed a rapid response to deposition. The deepest measurement showed a reaction delayed by approximately one week. The shallowest measurement reached a peak degree of saturation of the order of 45% before showing reversal in water content after a short period of time. Measurements at a medium depth increased to and remained at S_r = 45% for approximately five days, suggesting that the layer has reached a steady state as the water content in the top layer reduces whilst that of the bottom layer increases. The increase in the water content of the bottom layer stopped as soon as the middle layer started dewatering again. Thereafter, the water content of the bottom layer once again remained constant at a degree of saturation of 45%. The effect of antecedent water contents cannot be seen in Figure 4.26 as the calculated degree of saturation before deposition events was approximately between 20 and 27 % for all cases and not large enough to show any effects on post deposition behaviour.

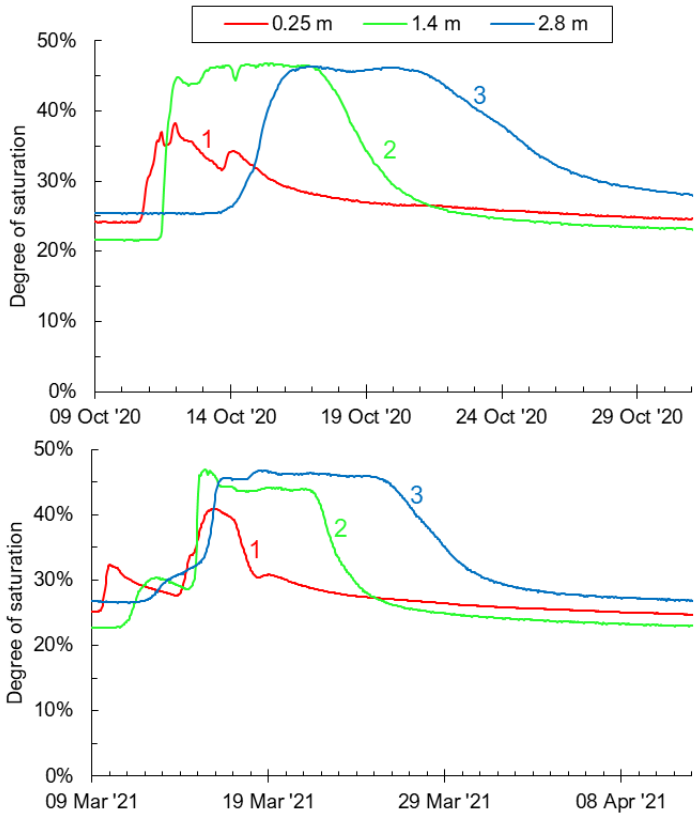

Figure 4.26: Two different cases of water infiltration behaviour after tailings deposition measured from the same installation.

The matric suction and degree of saturation relationships observed during both the deposition events in October 2020 and March 2021, showed in Figure 4.26, are plotted with a drying SWRC measured in the laboratory in Figure 4.27. The bottom figure in Figure 4.27 is an enlargement of the area over which the water content changes occur. The SWRC was measured at a dry density of 1700 kg/m^3, close to the field density at the instrumentation installation point. The wetting and drying curves from the deposition events plot below the drying curve, which is expected as scanning curves plot between the wetting and drying curves. This also shows that a SWRC measured in the laboratory, at a density close to which is found in the field, can be used during evaluation of infiltration models or matric suction related aspects in slope stability analyses due to good agreement between field and laboratory data. The flat shape of the SWRC over the funicular regime coincides with the water content ranges found in the field and shows why matric suctions did not change much upon deposition of tailings. For example, a change in degree of saturation from 90% to 20% will only result in a 50 kPa increase in matric suction from 10 kPa to 60 kPa.

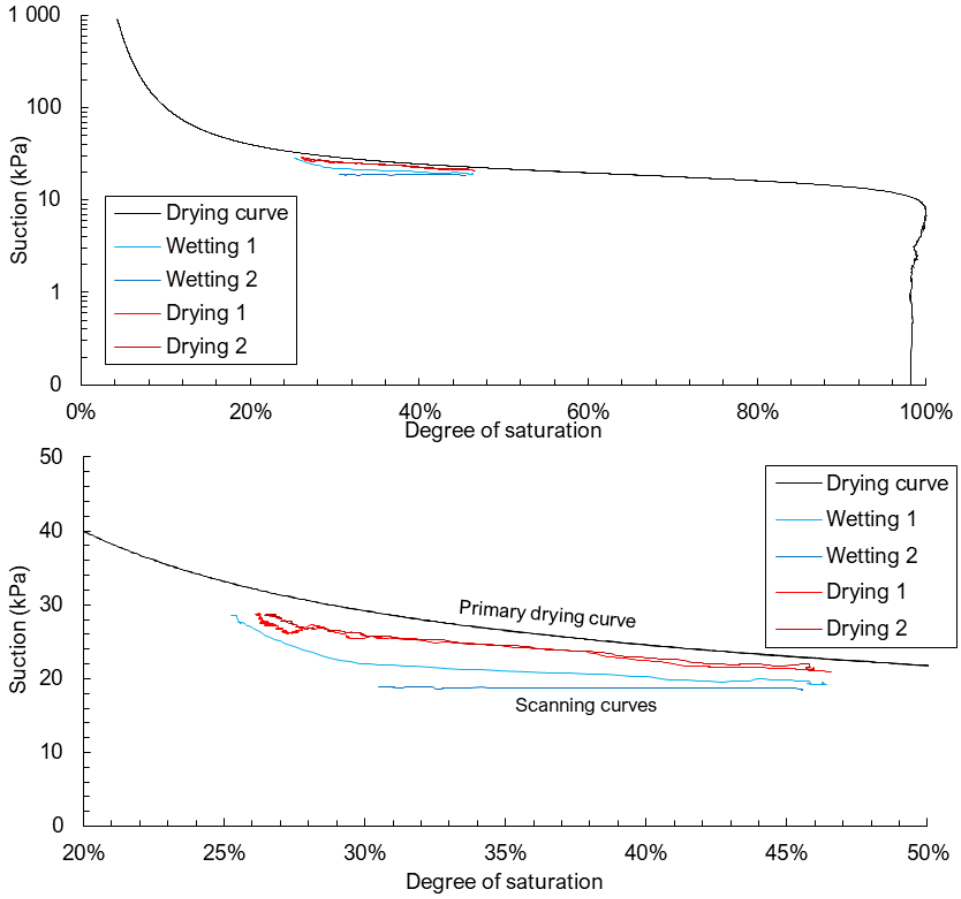

Figure 4.27: Comparison between laboratory and in-situ soil water retention behaviour.

Figure 3.22 shows how the measurement depth for all the sensors at DAQ1 increased by 1.5 m during the monitored period. The measurement depth increases for the tensiometers at DAQ1 were from 0.25 m to 1.75 m for the shallowest tensiometer, 1.4 m to 2.9 m for the medium depth tensiometer and 2.8 m to 4.3 m for the deepest tensiometer.

Figure 4.28, Figure 4.29 and Figure 4.30 show estimated matric suction versus depth profiles at DAQ1 (near the wall of the platinum tailings dam). Each figure presents matric suction data measured by a single tensiometer as the measurement depth increased. Figure 4.31 plots the coefficient of variation for the total measurement depth (0.25 m to 4.3 m). The four figures below show that matric suction fluctuations tend to reduce with depth as the coefficient of variation reduced from 0.3 at a depth of 0.25 m to values below 0.1 at depths greater than 3.7 m.

However, there was no clear trend in the matric suction measurements apart from the average matric suction measurement ranging between 12 kPa and 25 kPa for all depths

with an overall average of 20 kPa and a coefficient of variation of 0.32. Overall maximum and minimum suction values were 11 kPa and 25 kPa for the entire measurement depth with coefficient of variations of 0.72 and 0.34 respectively, showing higher variability in low suction ranges due to the larger coefficient of variation.

The minimum suction values, in Figure 4.28 and Figure 4.29, plot relatively far from the 1st quartile values indicating that big losses in matric suction due to deposition are quick and matric suction is recovered soon after the wetting event has occurred. All the values plotted in Figure 4.30 plot close to each other showing how the variability in matric suction decreases with depth. The minimum matric suctions plotted at depths of 0.25 m, 1.4 m and 2.8 m are not considered as representative values as they relate to the first wetting events after installation. A single hole was augered in which the tensiometers were installed, this initially created a preferential flow path for pore water causing a larger than expected loss in matric suction. The effect of the augered hole reduced as time progressed.

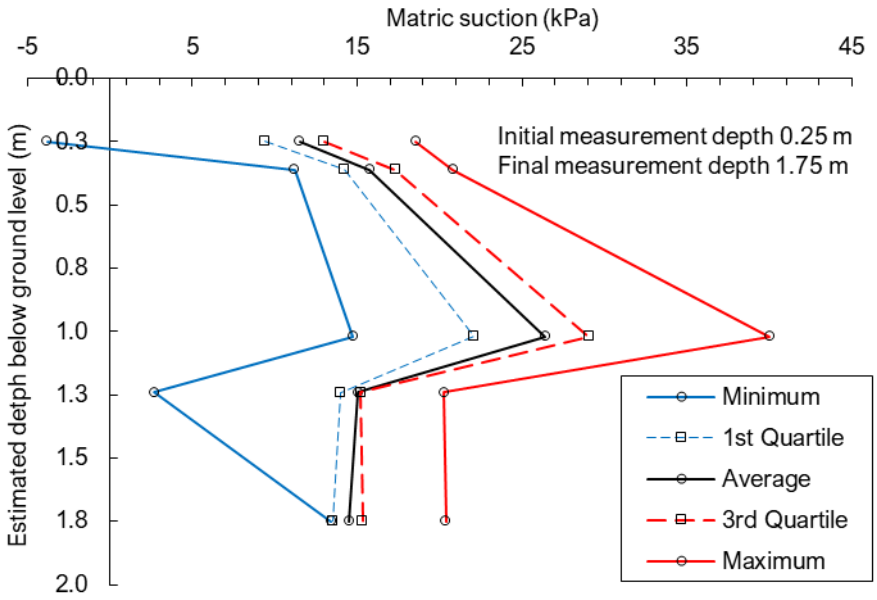

Figure 4.28: Matric suction profile for suctions measured between depths of 0.25 m and 1.7 m at DAQ1.

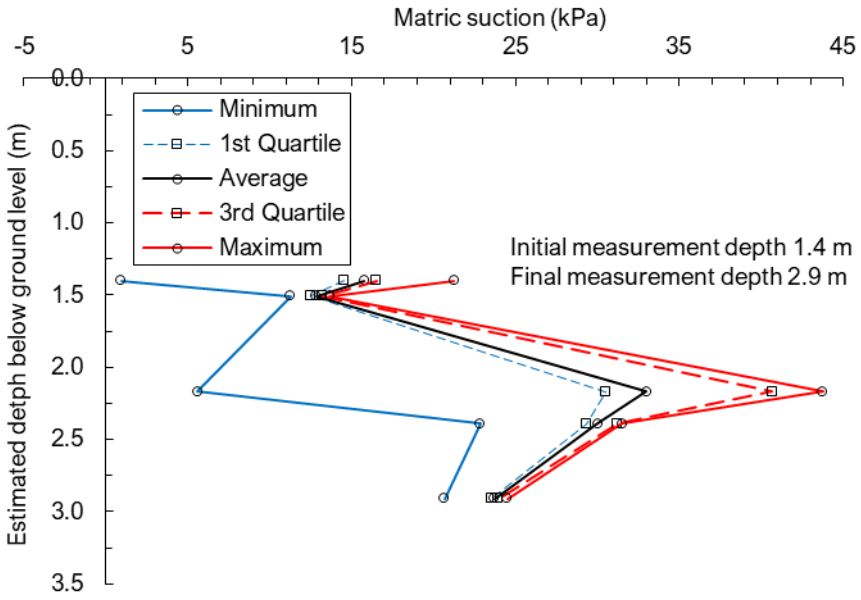

Figure 4.29: Matric suction profile for suctions measured between depths of 1.4 m and 2.9 m at DAQ1.

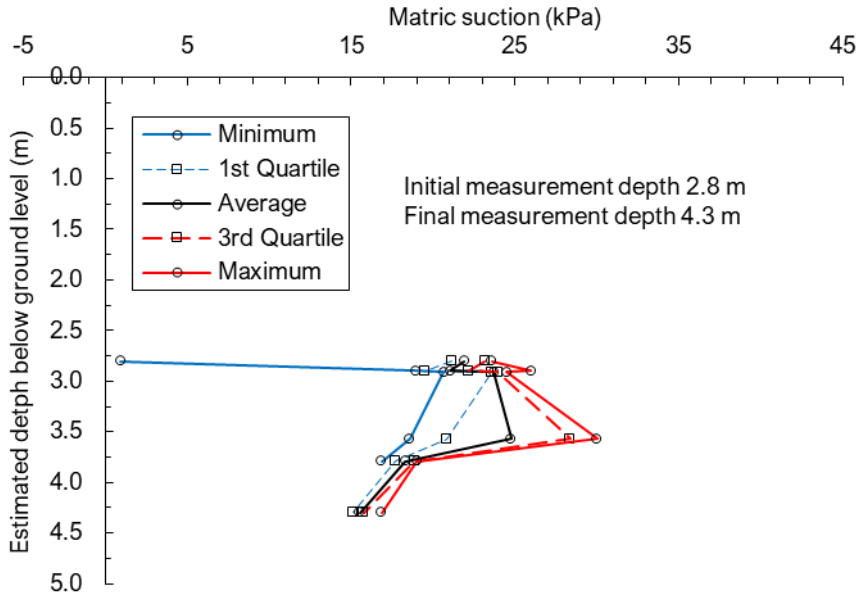

Figure 4.30: Matric suction profile for suctions measured between depths of 2.8 m and 4.3 m at DAQ1.

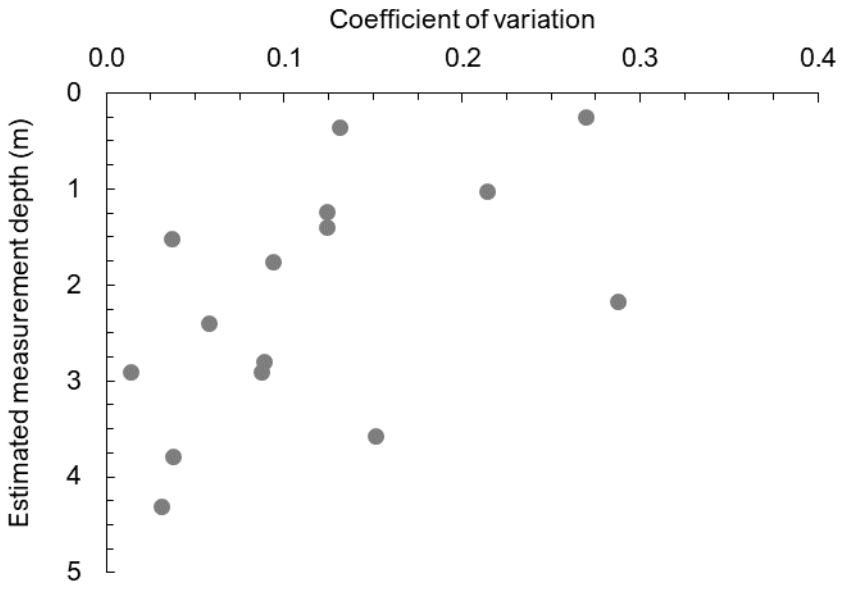

Figure 4.31: Calculated coefficients of variations in matric suction plotted versus measurement depth at DAQ1.

Figure 4.32 presents data gathered halfway along the beach of the platinum tailings dam from DAQ2 (Figure 3.23). The minimum degree of saturation is generally higher the closer the measurement was to the pool due to the higher prevailing water contents. Calculated degrees of saturation reached maximum values of approximately 48%.

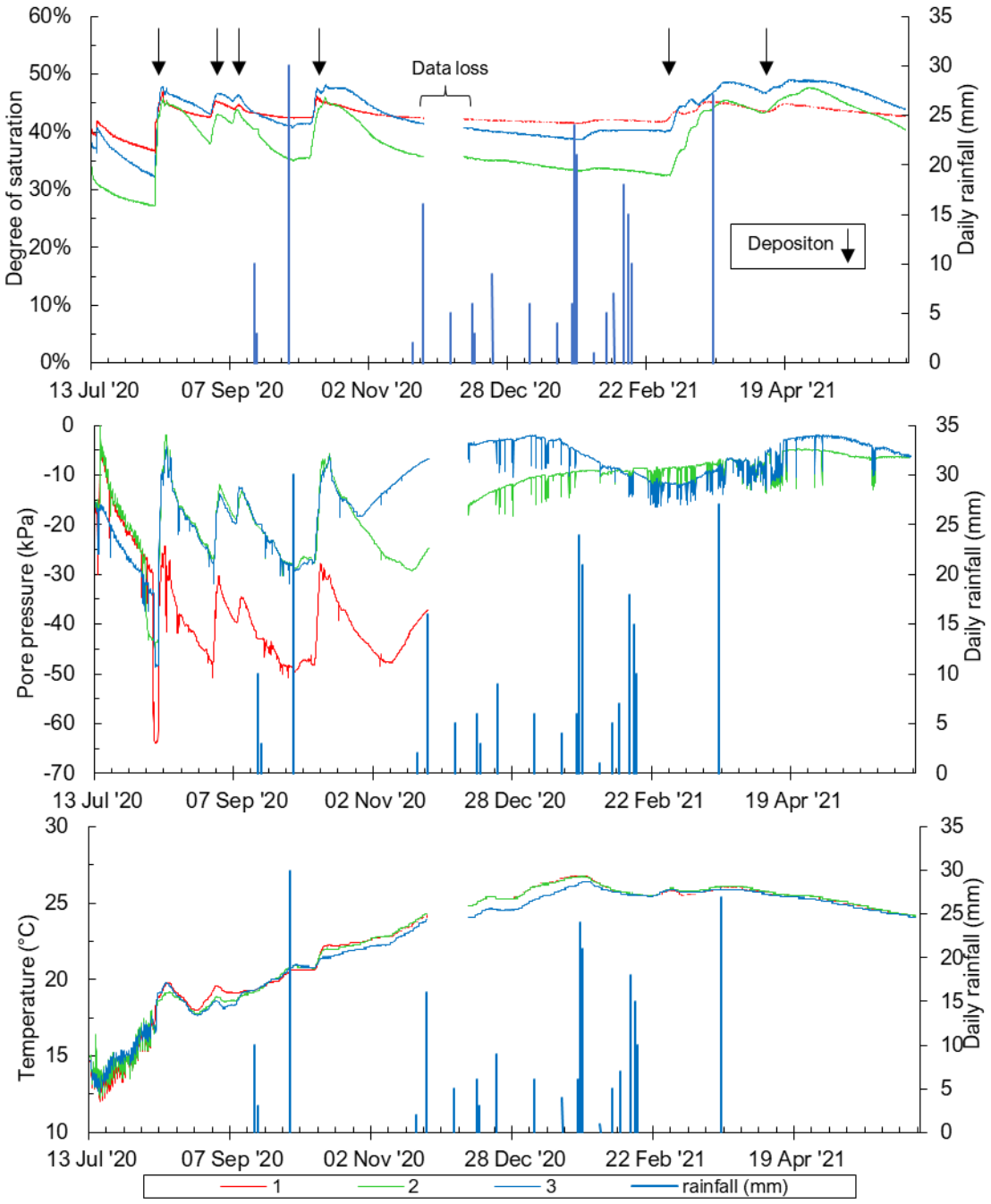

Figure 4.32: Surface measurements of water content, pore pressure and temperature halfway along the beach of a platinum tailings dam (DAQ2).

An additional deposition event is seen in September 2020 (Figure 4.32) which was not sensed by the probes near the wall (Figure 4.25). This is due to deposition occurring from elsewhere along the perimeter of the dam wall far enough from the probes at the wall such that its effect can only be observed by measurements taken in the beach. The effect of the meandering slurry streams can also be seen in Figure 4.32, resulting from

to the variation in water content and matric suction as probe pairs were installed 10 m apart, even though they were installed at the same depth.

The same rainfall event discussed in Figure 4.25, between September 2020 and October 2020, can be seen in Figure 4.32. The measurement taken from the probes in the figure above were all taken at the same depth. The probes were installed at the same depth (0.25 m) as the shallowest measurements near the wall (DAQ1). However, the response measured by DAQ2 shows a somewhat different reduction in matric suction. The degrees of saturation and measured matric suctions showed a short plateau caused by the rainfall event. Where water contents and matric suctions remained constant until the occurrence of the next deposition event.

Figure 4.33 shows matric suctions measured at depths estimated between 0.25 m and 1.75 m at DAQ2. The matric suction profile again tended to reduce with time, converging to a value of approximately 5 kPa at a depth of 1.75 m. The variability in the matric suction measurements also reduced with depth as the distance between the 1st and 3rd quartile values reduced as the measurement depth increased. However, minimum matric suction values, less than 2 kPa, appear more often from the data gathered by DAQ2 (halfway across the beach of the platinum tailings dam) compared to the data gathered by DAQ1 (near the wall of the platinum tailings dam). This may be due to the proximity of the measurements to the tailings discharge point. Tailings deposited from spigots close to DAQ1 may flow around the probes in single channels and would thus not cause matric suctions to dissipate entirely. However, the area of influence may increase with distance from the spigots as the slurry stream has had time to spread out causing a larger loss in matric suctions in the beach area. Average matric suction values also appeared to be higher at DAQ1 compared to DAQ2 for the same reason. Comparisons between DAQ1 and DAQ2 in terms of matric suction versus depth profiles were drawn between Figure 4.28 and Figure 4.33 as both the figures show equal initial tensiometer installation depths.

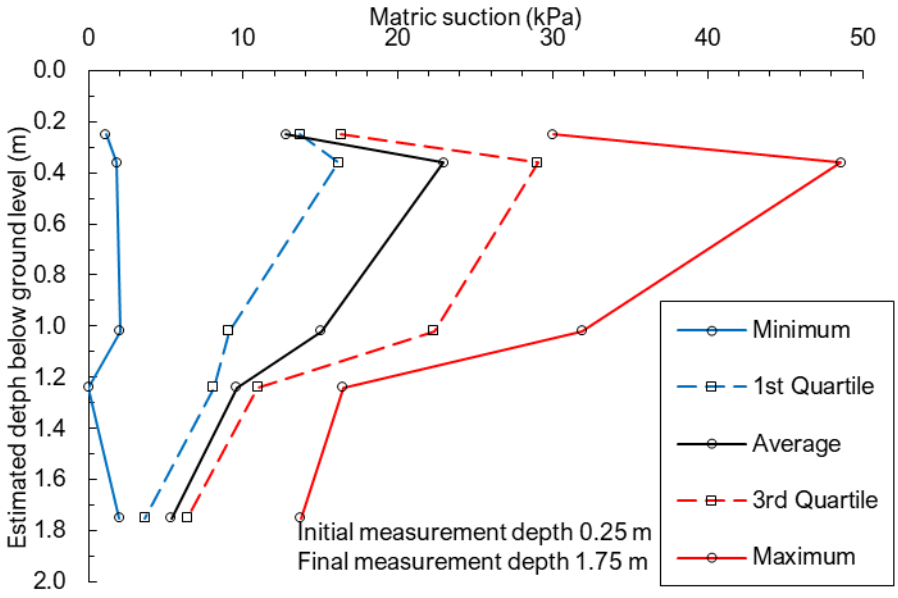

Figure 4.33: Matric suction profile for suctions measured between depths of 0.25 m to 1.75 m at DAQ2.

Figure 4.34 presents degrees of saturation calculated from the measured volumetric water content, pore pressures and temperatures gathered next to the tailings dam pond. Positive pore pressures were generated during the August deposition event as the pool size increased and extended over the tensiometers. Data recording at the pool stopped prematurely as the consistency of the tailings did not allow access for battery replacement and data retrieval.

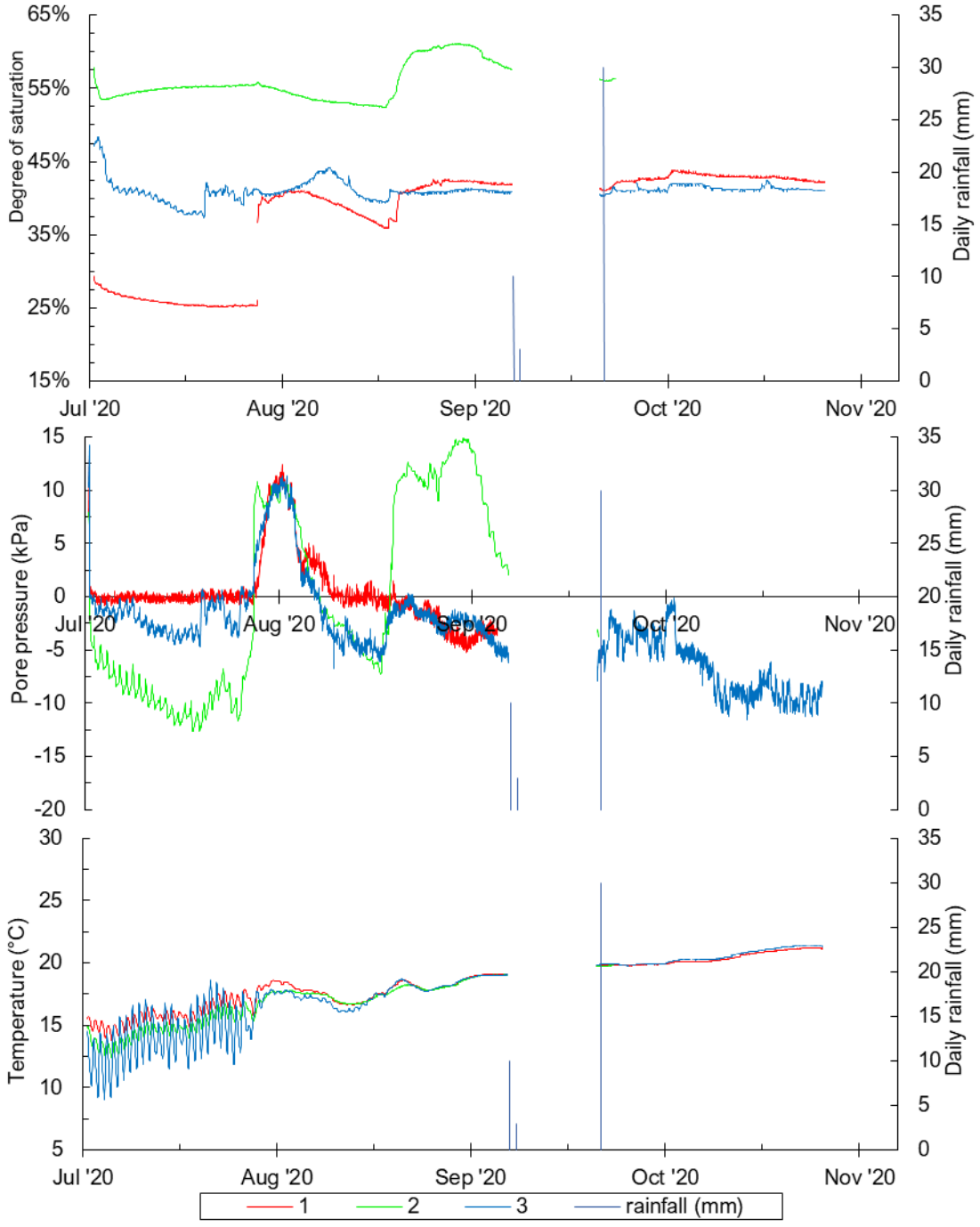

Figure 4.34: Surface measurements of water content, pore pressure and temperature on the pool edge of a platinum tailings dam (DAQ3).

4.3.2 Gold tailings (Daywall-Paddock operation)

The placement of the nine tensiometers and two water content sensors that were installed in a gold tailings dam is shown in Figure 4.35. Tensiometers were installed at depths of 0.25 m, 2.7 m and 4.7 m in the daywall to observe the effect of deposition in the daywall on matric suctions with depth. The three remaining tensiometers were installed either beneath the slope or below the bench. This is to measure the lateral

change in matric suctions the closer they are measured to the outer slope. Two water content sensors were placed next to two tensiometers in the daywall to observe the fluctuations in water content due to deposition and drying cycles.

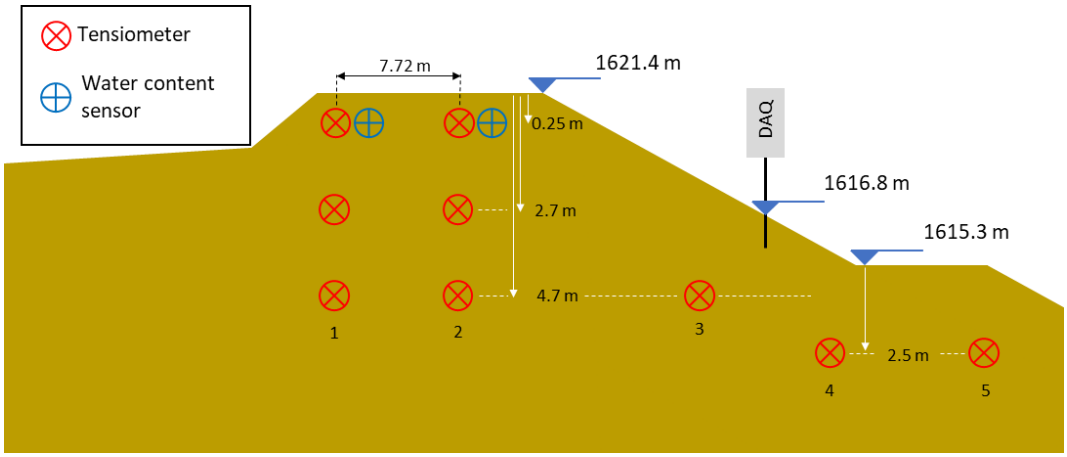

Figure 4.35: Sensor configuration of the probes in the daywall of a gold tailings dam, repeated from Figure 3.26.

Figure 4.36 plots matric suctions across time corresponding to measurements taken near the inside of the daywall (closest to the pond annotated with "1" in Figure 4.35).

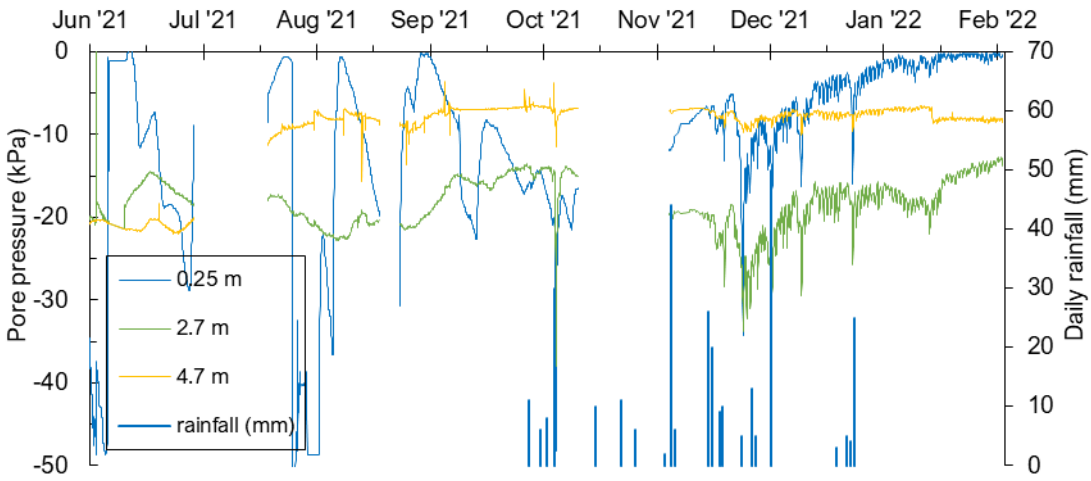

Figure 4.36: Matric suctions measured at varying depths on the inside of the daywall.

Matric suctions measured at varying depths in the inside of the daywall showed a typical negative pore pressure profile where there is infiltration from the top. Low values near the surface, higher at intermediate depths and low again at deeper depths. Matric suctions measured closest to the phreatic surface were insensitive to deposition. The measurement taken at a medium depth was generally higher than the bottom

measurement with a slight sensitivity to deposition due to the increased proximity to the surface. Measurements taken at the surface showed the largest variations reaching the largest absolutes upon drying and wetting ranging between 0 and 70 kPa. Matric suctions measured at the surface dissipated entirely during depositions unlike the case of the platinum tailings dam. This is due to the different deposition method. Daywall operations deposit tailings in compartments on top of the slopes, containing the deposited slurry, forcing water to drain downwards through the tailings as opposed to running off onto the beach.

Figure 4.37 plots matric suctions across time corresponding to measurements taken in the daywall (Figure 4.35). Tensiometers placed in the daywall, closest to the outer slope are plotted in black and labelled as “Slope side”, whilst measurements taken near the inside of the slope are plotted in grey and labelled as “Beach side”.

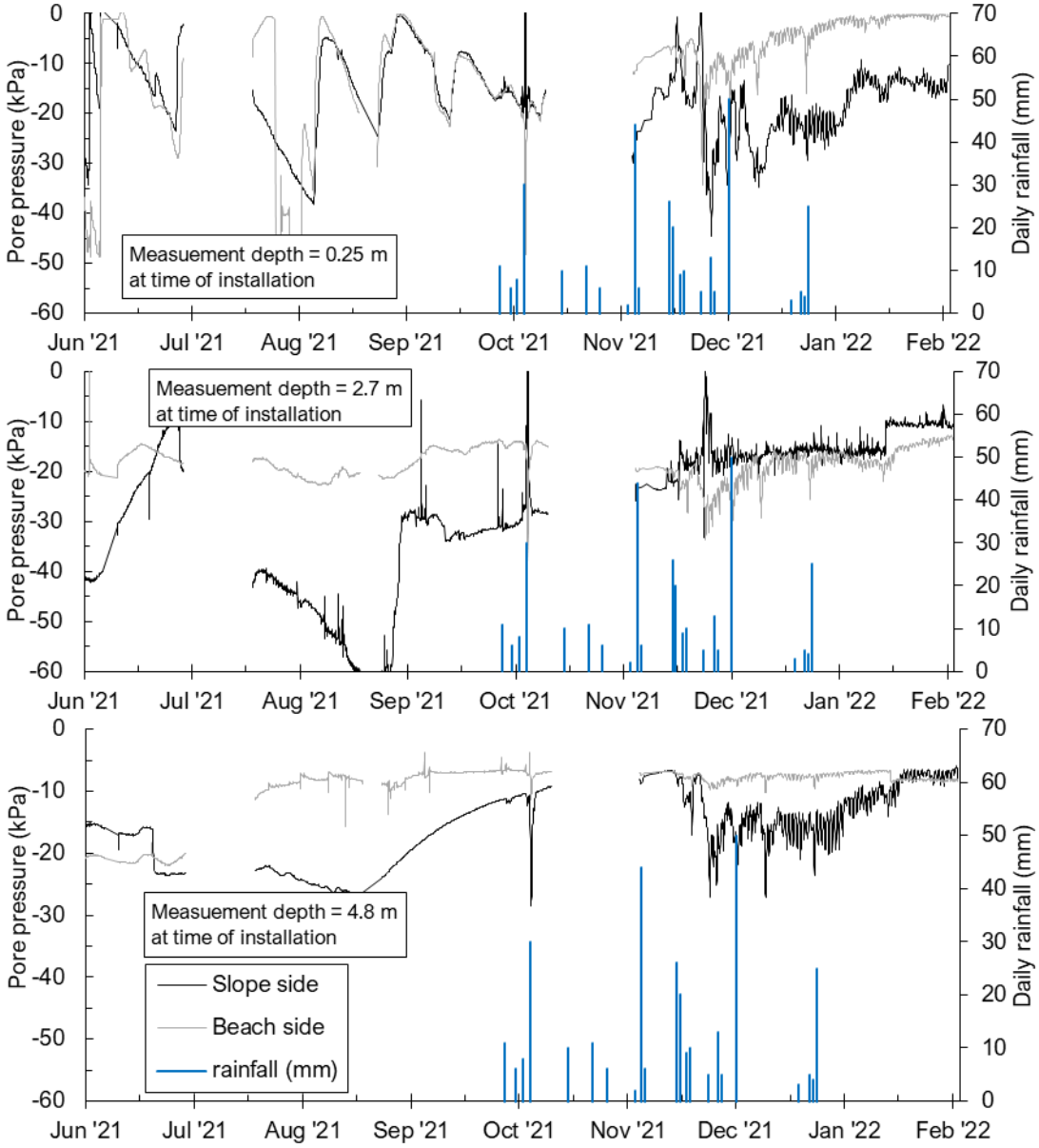

Figure 4.37: Matric suctions measured on the outer and inner edge of a gold tailings dam daywall.

Matric suctions measured closer to the outer slope often measured higher matric suctions due to the increased drying surface of the outer slope. The shallow tensiometers, initially buried at a depth of 0.25 m, showed large fluctuations. Matric suctions reduced to zero after deposition whereafter drying generates matric suctions in the order of 25 kPa after approximately two weeks. Once again, the variation in pore pressure decreases with an increase in depth, up to a point where suctions do not dissipate entirely during deposition, and the maximum matric suction reached before deposition reduces, at a depth of 4.8 m.

Pore pressures measured at a depth of 2.7 m upon installation fluctuate less compared to the shallow measurements, the tensiometer on the beach-side of the daywall constantly measured matric suctions around 20 kPa. The deepest beach-side case, 4.7 m upon installation, showed a constant matric suction of 10 kPa since August 2021.

Figure 4.38 and Figure 4.39 plot matric suction and degree of saturation near the surface of the daywall. Reductions in matric suction are driven by an increased saturation level. Matric suctions respond faster and more significantly to deposition in the case of the gold tailings dam as opposed to the case with platinum tailings as the area of deposition is more concentrated.

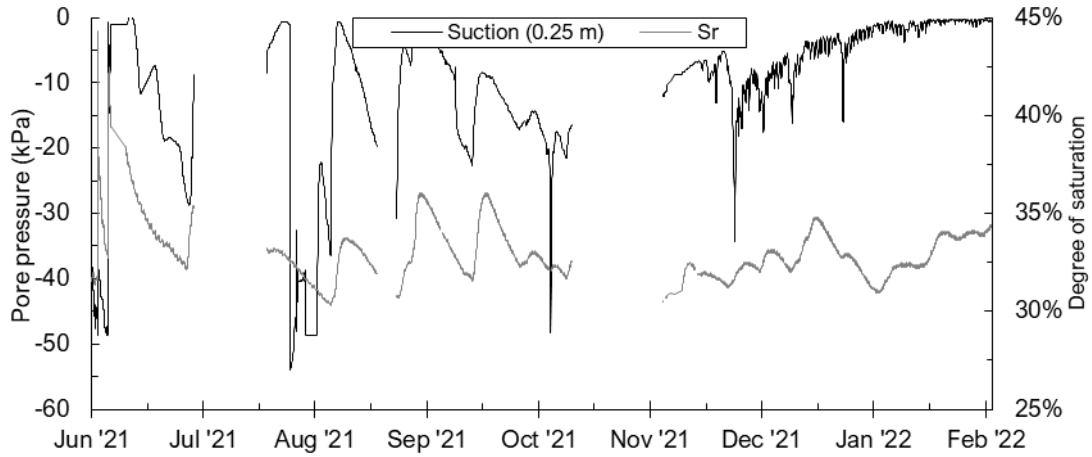

Figure 4.38: Pore pressure and degree of saturation measured in a daywall closest to the pool.

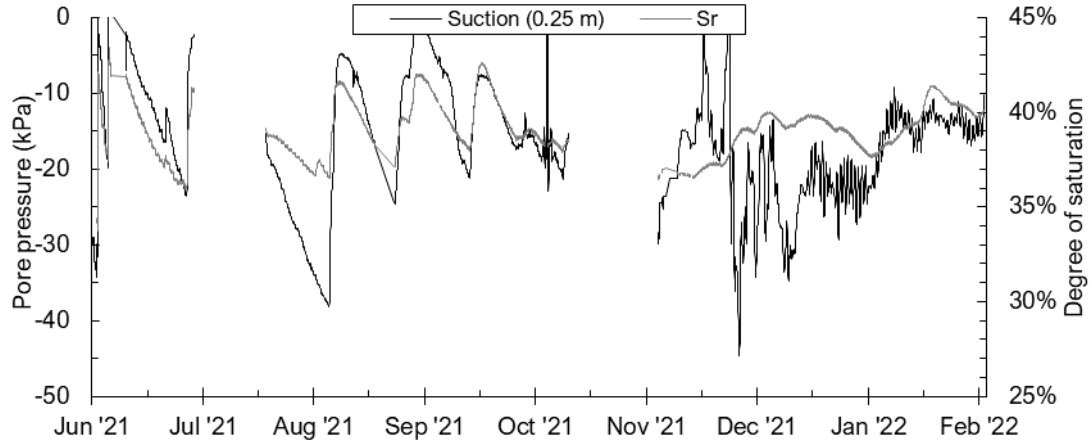

Figure 4.39: Pore pressure and degree of saturation measured in a daywall closest to the outer slope.

Figure 4.40 plots a SWRC measured in the laboratory overlayed with in situ soil water retention behaviour from the gold tailings dam. The platinum tailings showed good

agreement between the SWRC measured in the laboratory and the field data (Figure 4.27). However, this is not the case for gold tailings. Matric suction measurements in the daywall of the gold tailings dam, plotted in Figure 4.38 and Figure 4.39, often reduced to 0 kPa upon tailings deposition. The degree of saturations, calculated from void ratio and volumetric water content from the Teros 12 probe, shows that the zero suction measurements occurred between degrees of saturation of 35% to 40% and is considered as unrepresentative.

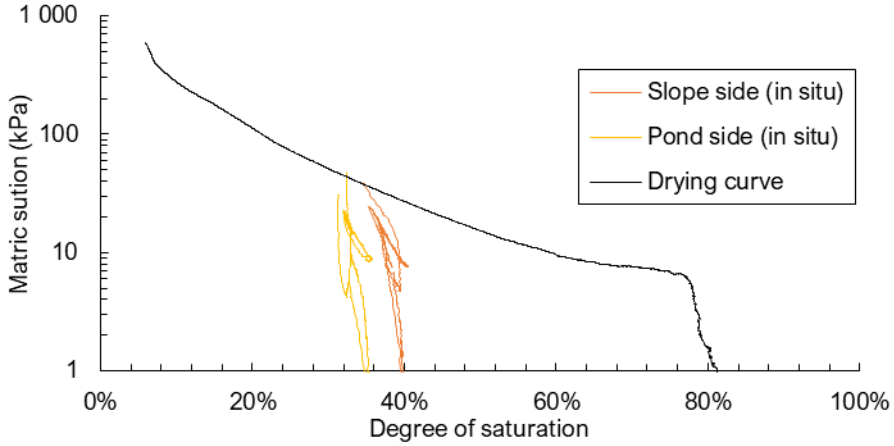

Figure 4.40: Comparison between in situ soil water retention behaviour and a drying curve measured on moist tamped material in the laboratory.

Figure 4.41 is a picture of desiccated gold tailings with crystal growths and shows the high dissolved salts content in gold tailings of which the yellow colour indicates the presence of some form of sulphuric compound. The volumetric water content of a soil is inferred from the dielectric permittivity of the soil medium of which the amount of porewater has the largest influence. Dissolved salts may influence the electrical behaviour of porewater and its effect on the measured dielectric permittivity is unknown. The Teros12 probe was calibrated to gold tailings by fitting a curve between discrete water content and dielectric permittivity datapoints. However, calibration was done on tailings samples taken from a drying box in which infiltration events were modelled. It is thus possible that most of the dissolved compounds were leeched from the tailings before it was used for calibration of the probe resulting in incorrect calibration curves.

Another explanation for the unrepresentative water content measurements may be due to the high variability in tailings dams caused by deposition. Deposition of tailings causes layering of which the particle size distribution in these layers may range from sand-size particles to silt-size particles. It could thus be the case that the water content

probe would report low water content values if the probe was placed in a coarse layer sandwiched in between fine layers. The water content in a finite soil element tends to vary as matric suctions equilibrate. Therefore, the fine layers would be wetter than the coarse layer due to its higher propensity to retain water at a certain matric suction compared to the coarse layer causing the probe to measure unrepresentative water contents.

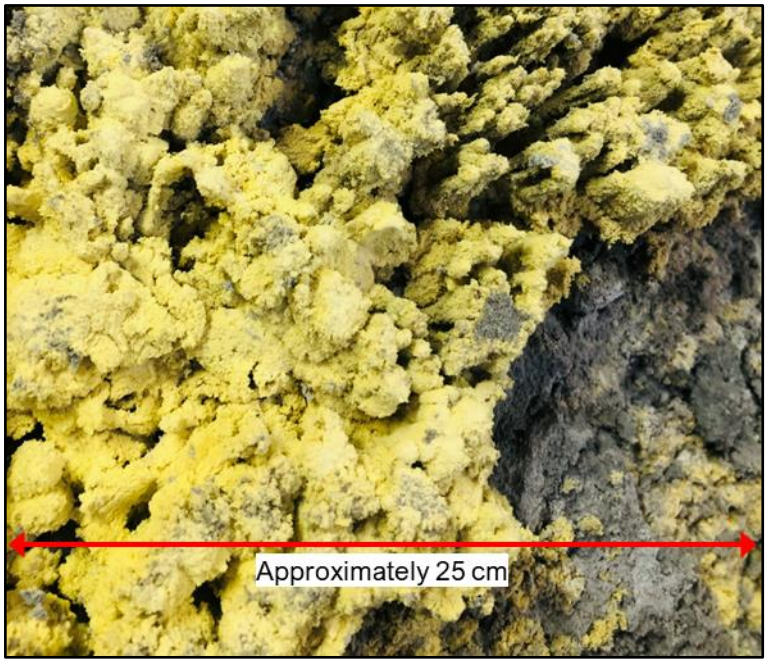

Figure 4.41: Cristal growth on a gold tailings sample.

Figure 4.42 shows a matric suction versus depth profile of the gold tailings dam ranging from a depth of 0.25 m to 5.90 m. Measurements taken with three different tensiometers, initially installed at depths of 0.25 m, 2.7 m and 4.7 m are all plotted on the same figure. No clear trend between matric suction and measurement depth is evident apart from the fact that the variability in the suction measurements tends to reduce as the measurement depth increases. Figure 4.43 plots the coefficient of variation in the matric suction measurements with depth. At shallow depths, the coefficient of variation is in the order of 1.0 and reduces to values below 0.3 at depths greater than 3 m. An average matric suction of 13 kPa was calculated from the profile in Figure 4.42. The average of both the minimum and maximum values are 7 kPa and 23 kPa respectively. Calculated minimum, average and maximum values are used as matric suction caps in the slope stability analyses to assess the effect of matric suction on slope stability.

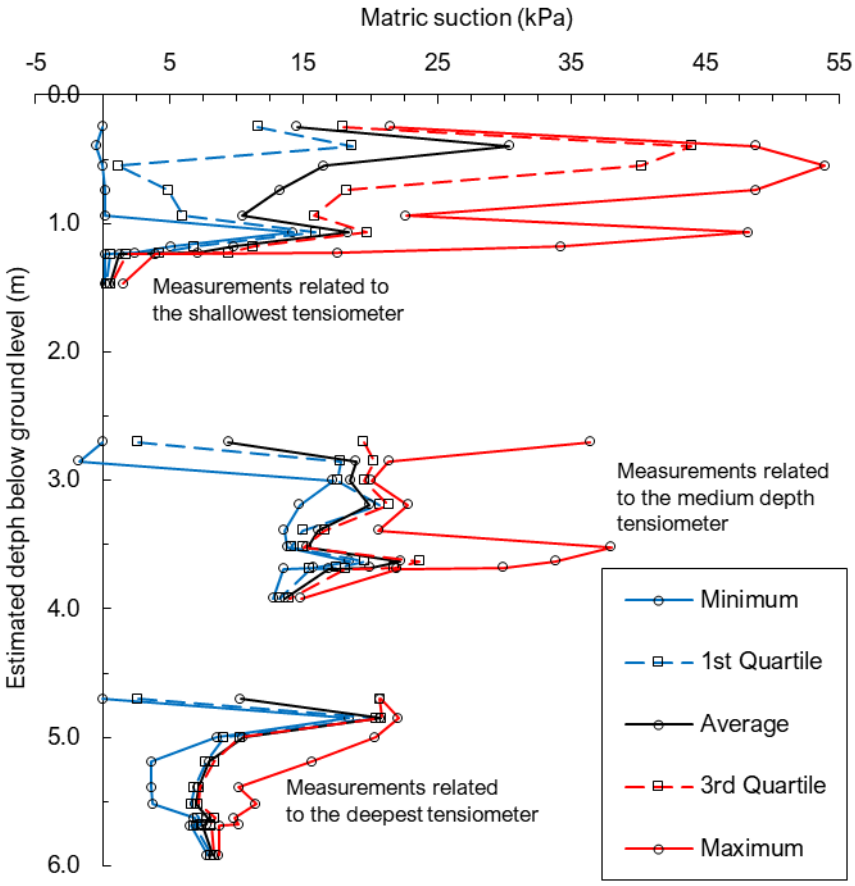

Figure 4.42: Matric suction profile for suctions measured between depths of 0.25 m to 5.90 m on the gold tailings dam.

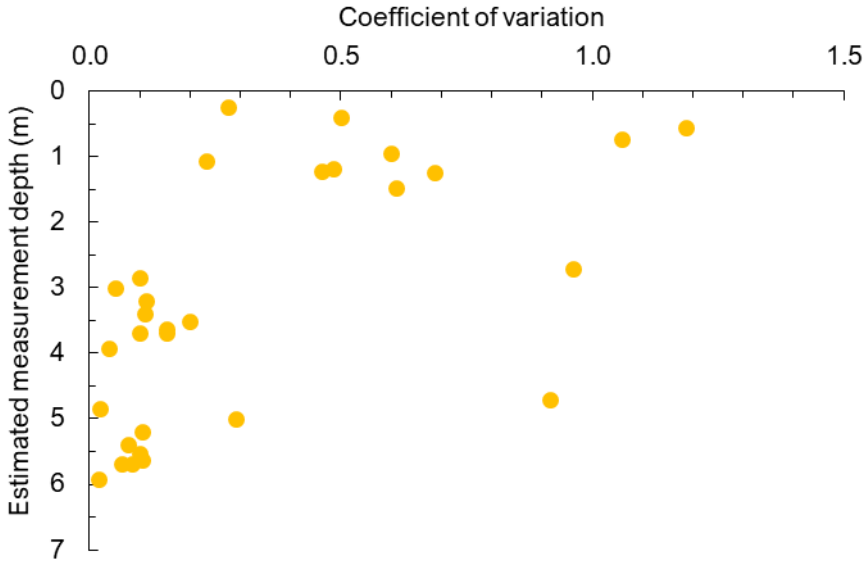

Figure 4.43: Calculated coefficients of variations in matric suction plotted versus measurement depth on the gold tailings dam.

Figure 4.44 plots coefficient of variation values from both the platinum and tailings dam matric suction measurements. The coefficient of variation in the gold tailings data is much larger than platinum tailings dam case for shallow measurements. This is due to the different SWRCs of the two materials combined with the different methods of operation. However, an upper bound value in the coefficient of variation of 0.3 can be taken for both the platinum and gold tailings dam cases for depths greater than 2 m.

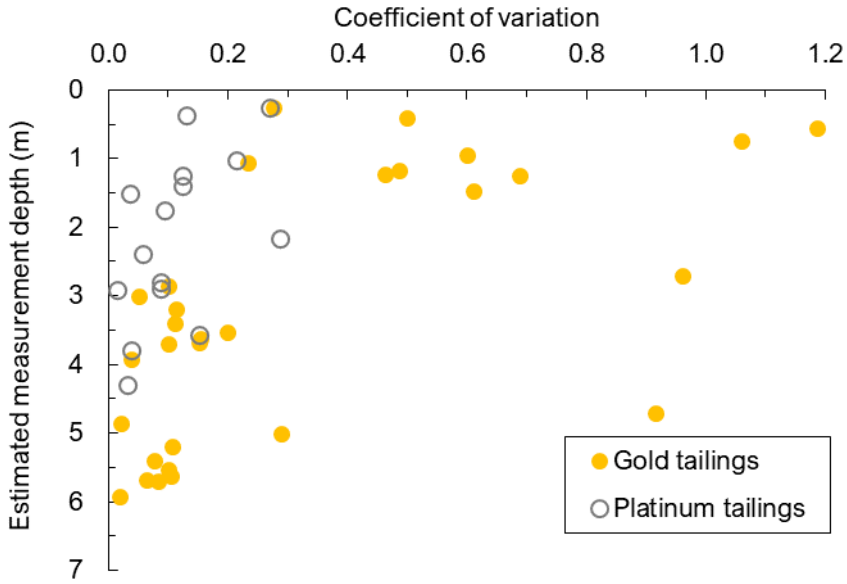

Figure 4.44: Comparison in the variability of matric suction measurements in gold tailings and platinum tailings.

4.3.3 In-situ, unsaturated shear strength behaviour of platinum and gold tailings

The contribution of matric suction to shear strength was estimated by use of Vanapalli et al. (1996) unsaturated shear strength equation:

$$\tau = c' + (\sigma_n - u_a)tan\phi' + (u_a - u_w)\left(\frac{\theta-\theta_r}{\theta_s-\theta_r}\right)tan\phi' \qquad (4.1)$$

Where:

c’ = drained cohesion intercept (assumed as 0 for tailings from practical experience)

$(\sigma_n - u_a)$ = net normal stress

ϕ’ = drained friction angle

$(u_a - u_w)$ = matric suction

θ = volumetric water content

θr = residual volumetric water content

θ_s = saturated volumetric water content

Vanapalli et al.'s (1996) equation consists of three terms, the first is the drained cohesion parameter, the second is related to a saturated, net stress component and the third to an unsaturated, matric suction component. Figure 4.45 estimates the increase in shear strength due to matric suctions near the wall (DAQ1) of the platinum tailings dam. Figure 4.47 serves the same purpose as Figure 4.45 but with data gathered from the beach (DAQ2) of the platinum tailings dam. The solid lines represent shear strength and the dashed lines represent the degree of saturation for both figures. These estimations are made by using the measured field data as inputs for equation 4.1 and the friction angles listed in Table 3.3. Only the third term of equation 4.1, relating to matric suction, is plotted.

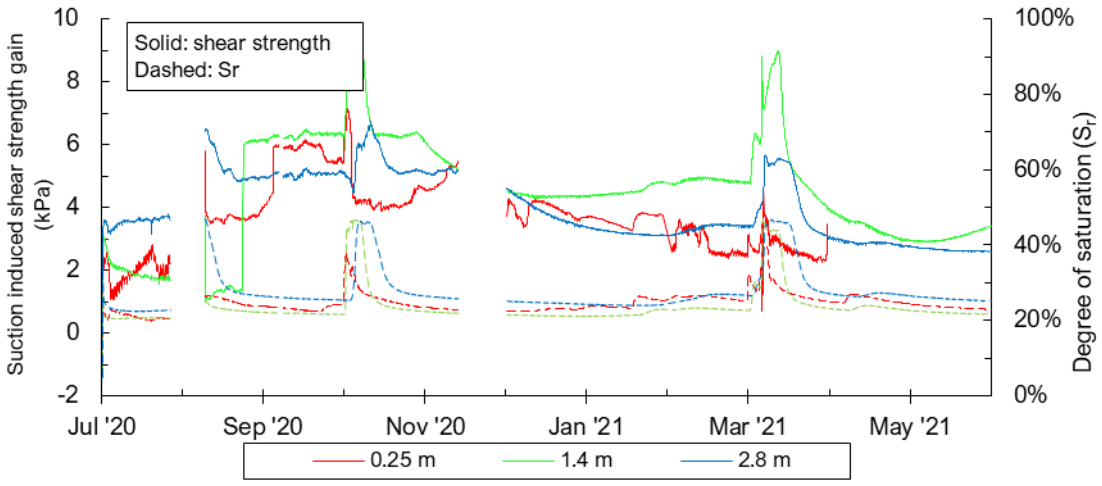

Figure 4.45: Shear strength gained from matric suctions at varying depths near the wall of a platinum tailings dam.

The calculated in-situ shear strength gain due to matric suctions is small for platinum tailings, between 2 kPa and 6 kPa. The fact that the suction stress increases upon wetting is counterintuitive. This can be explained by the large fluctuation in water content compared to the relatively small change in matric suction upon tailings deposition, suctions also never totally dissipated. Figure 3.7 plots the SWRCs corresponding to DAQ1 and DAQ2, the elongated flat portion of the plot shows how a large change in water content will cause a small change in matric suction. Thus, a higher degree of saturation allows for the conversion of a larger proportion of matric suctions to shear strength. Figure 4.46 further summarizes this phenomenon by plotting the gain in shear strength from matric suctions calculated from the SWRC of platinum

tailings with an AEV of 16 kPa. The increases in strength from matric suction in Figure 4.46 is calculated by solving the third term of equation 4.1 with inputs from a SWRC measured in the laboratory. Typical matric suction values during periods in between depositions are beyond the peak of the curve. Figure 4.46 clearly shows how a reduction in matric suction, caused by tailings deposition, would cause an increase in strength.

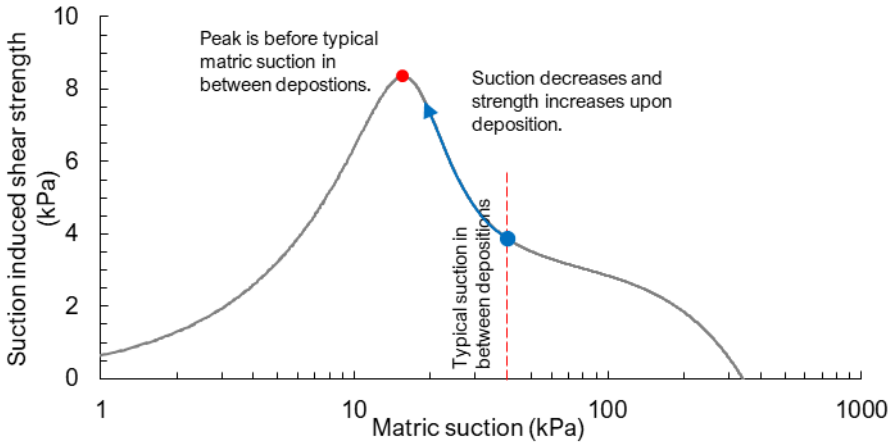

Figure 4.46: Increase in shear strength from matric suction calculated from the SWRC of platinum tailings.

Average increases in shear strength due to matric suction are estimated to be in the order of 3 kPa, increasing to 6 kPa upon deposition induced wetting. The strength increase lingers for approximately two weeks before reducing to its original value before deposition (around 3 kPa to 4 kPa) and relates to the duration of the effect of the wetting event on the measured water content.

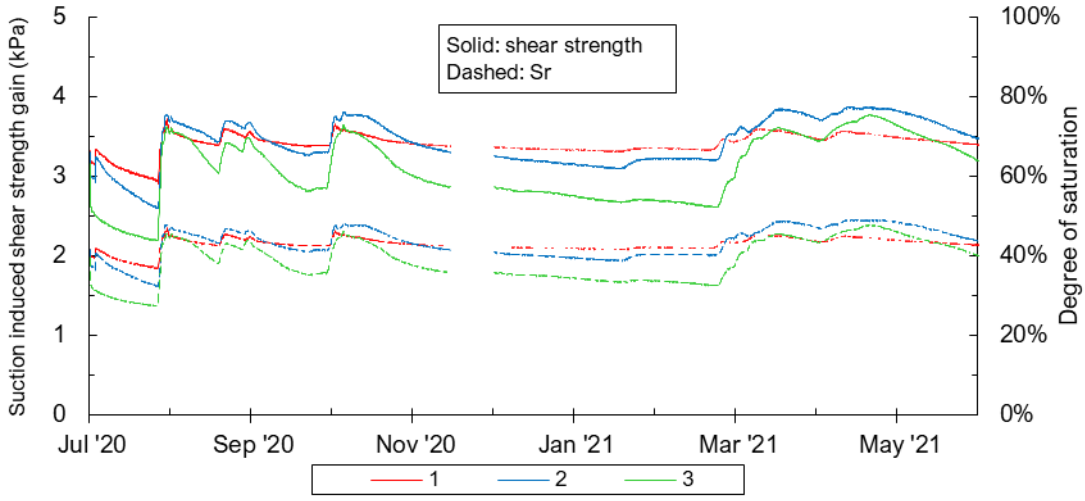

Figure 4.47: Shear strength gained from near-surface matric suctions measured on the beach of a platinum tailings dam.

The estimated gain in shear strength on the beach of a platinum tailings dam is between 3 and 4 kPa. The reason for a lower peak compared to the estimated values near the wall can be ascribed to the lower average water content and matric suctions caused by the increased proximity to the pond. Matric suctions in Figure 4.47 from which shear strengths were estimated, were measured approximately 120 m from the slurry discharge points. Therefore, by the time the tailings has reached the tensiometers the slurry is spread out over a larger area, causing a more uniform increase in water content but with lower peaks. The duration of strength increase once again lingers for approximately two weeks before reducing.

Shear strengths were not estimated with the measurements taken near the pool as the state of the material is mostly saturated, relating to low matric suctions and low strengths.

Figure 4.48 plots the matric suction related increases in shear strength from the measurements taken in the daywall of a gold tailings dam. The underreported water content measurements are compared with water contents estimated from the SWRC according to the matric suction measured with a tensiometer. It was found that the variability caused by the different water contents ranges between 2 kPa and 4 kPa. The plot calculated from water content values inferred from the SWRC was used for slope stability calculations as the value measured with the Teros12 probe is considered as unrepresentative.

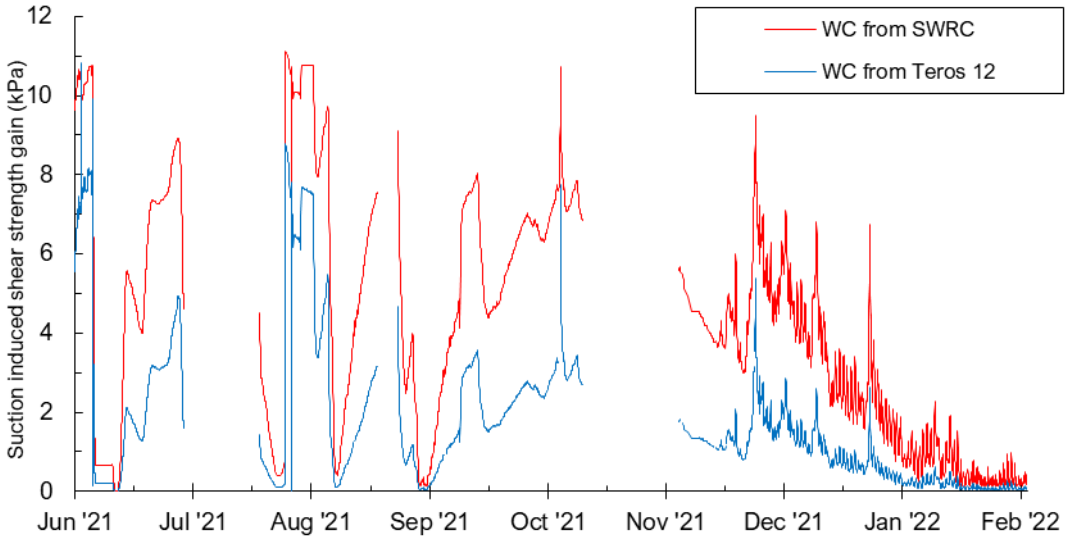

Figure 4.48: Comparison between matric suction induced shear strength gains, both estimated from matric suctions but with water contents measured with the Teros12 probe and inferred from the SWRC.

The behaviour of matric suction induced shear strength in the paddock of a gold tailings dam is different from that which is seen near the wall of a spigotted operation. Shear strength gains due to matric suctions in a paddock reach higher peaks during drying compared to the platinum tailings dam case. Matric suctions often dissipated entirely upon deposition causing a total loss of strength due to suction, the opposite is observed in the case of the platinum tailings dam. Comparing the platinum tailings SWRC with that of gold tailings helps explain why this is the case. Unlike platinum tailings, a large change in water content will relate to a large change in matric suction of gold tailings. The SWRC of gold tailings does not have an elongated, flat portion and will therefore cause a larger change in matric suction (Figure 3.8).

Figure 4.49, like Figure 4.46, helps explain the difference in behaviour between the two methods and plots the increase in shear strength calculated from matric suction of gold tailings. Unlike platinum tailings, a reduction in the matric suction of gold tailings would cause an immediate decrease in strength due to the shape of the curve of Figure 4.49.

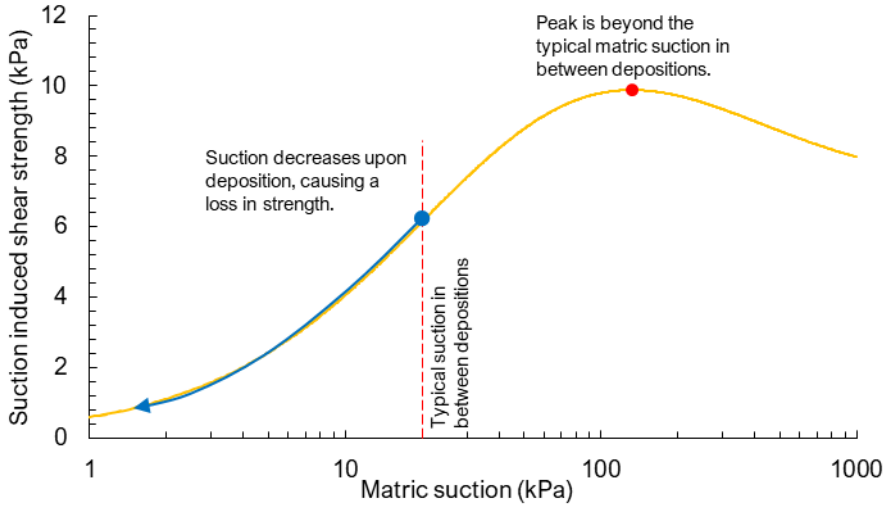

Figure 4.49: Increase in shear strength from matric suction calculated from the SWRC of gold tailings.

Shear strength gained from matric suctions in the paddock of a tailings dam ranged between 0 kPa and 10 kPa (Figure 4.48). However, the loss of strength due to suction decrease is prompt and strength is regained within a matter of days as a reduction in water content occurs rapidly.

4.4 CONSIDERING MATRIC SUCTION IN SLOPE STABILITY ASSESSMENTS OF TAILINGS DAMS

Section 4.3.3 shows how matric suction contributes to shear strength in active tailings dams. An attempt was made to capture the effect thereof on both slopes where in-situ data was collected. A counterintuitive increase in shear strength due to matric suction is estimated to range between 3 kPa in between deposition events and up to 8 kPa upon deposition for platinum tailings and 0 kPa upon deposition to 6 kPa in between depositions for gold tailings.

The phreatic surface of both profiles were calibrated to standpipe piezometer levels provided by the tailings dam operators. The safety factor of the slopes, from the toe to each berm, was determined by means of limit equilibrium slope stability analyses. The profile of the platinum and gold tailings dam slopes are shown in Figure 4.50 and Figure 4.51 respectively with curves showing the critical slip surface, identified by the software, from the toe to each berm. Site inspections at the platinum tailings dam showed a very shallow bedrock (less than 2 m deep). Stability analyses therefore assume that the slip surfaces would not extend beyond the foundation. This assumption was also made for the case of the gold tailings dam.

Safety factors were compared between cases where matric suctions were and were not considered. Section 3.5 discusses the different methods used to consider the effect of matric suction on slope stability in detail. These methods are summarised in the list below for quick reference:

- The material in the model was split into two different regions divided along the phreatic surface. The saturated region was assumed to have zero cohesion. The region above the phreatic surface was considered unsaturated in which matric suctions were modelled as a cohesion in the Mohr-Coulomb model with its magnitude relating to typical increases in unsaturated shear strength in between slurry depositions and during depositions. Cohesion values for the platinum tailings dam were 3 kPa and 8 kPa in between deposition and during deposition respectively. Cohesion values for the gold tailings dam were 6 kPa and 0 kPa in between deposition and during deposition respectively. This accounted for two of the six scenarios.
- Matric suctions were extrapolated into the unsaturated region starting at 0 kPa from the phreatic surface increasing by 9.81 kPa per vertical meter up to the outer surface.

- Matric suctions were extrapolated into the unsaturated region but capped to typical minimum, average and maximum matric suction values, shown in Section 4.3.1 and 4.3.2, accounting for the three remaining scenarios. The Mohr-Coulomb strength model in the unsaturated region was replaced with the model by Vanapalli et al for all the cases where matric suctions were extrapolated indefinitely or capped to typical values.

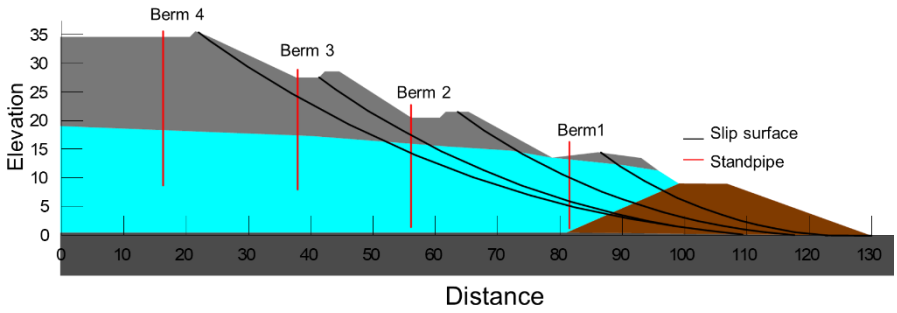

Figure 4.50: Analysed profile of the platinum tailings dam with the considered slip surfaces.

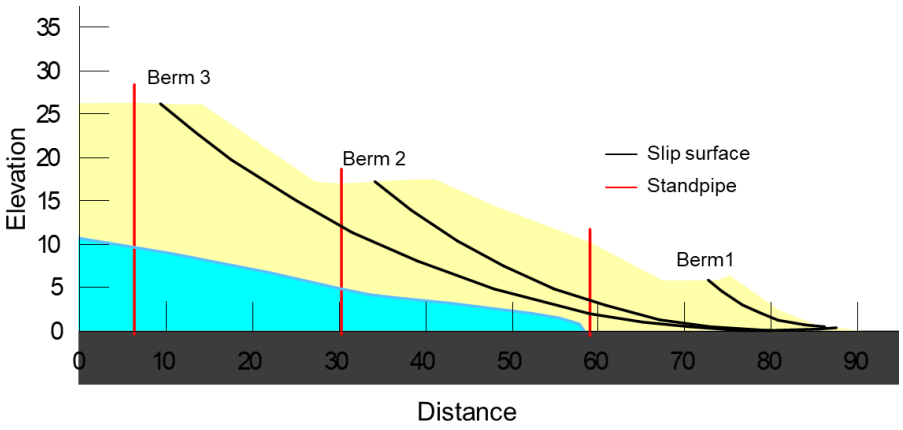

Figure 4.51: Analysed profile of the gold tailings dam with the considered slip surfaces.

The custom matric suction profiles, capped to typical values, required the manual provision of a spatial porewater pressure function over the entire model in the SLOPE/W analysis. It was thus important to ensure that the porewater pressure in the saturated region of the slope is equal across all scenarios as different positive porewater pressures will result in varying effective stresses which will influence the resulting safety factor.

Figure 4.52 and Figure 4.53 plot the porewater pressure at the bottom of each slice in each slip surface of the platinum and gold tailings dam respectively. These plots show that the porewater pressure in the saturated region of the slip surface is equal for all cases and the difference in safety factor between the listed scenarios are thus only due to matric suction.

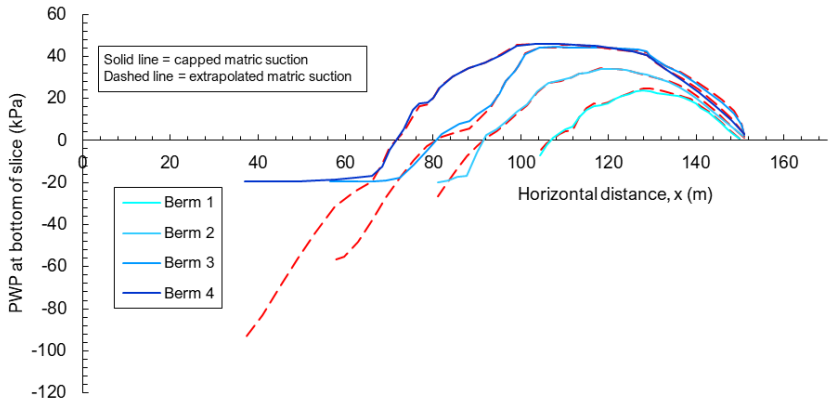

Figure 4.52: Calculated porewater pressure at the bottom of each slice of each slip surface on the platinum tailings dam.

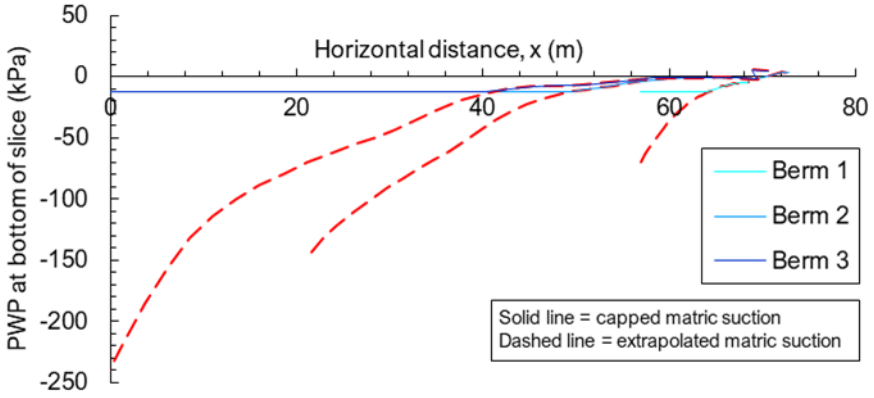

Figure 4.53: Calculated porewater pressure at the bottom of each slice of each slip surface on the gold tailings dam.

The phreatic surface of the platinum tailings dam is considerably higher, in terms of its proximity to the slip surfaces, compared to the gold tailings dam. The effect thereof on the porewater pressure along the slip surfaces can clearly be seen in the figures above. Figure 4.52 (corresponding to the platinum tailings dam) shows positive pore pressures up to 50 kPa in its slip surfaces as opposed to Figure 4.53 (corresponding to the gold tailings dam) which shows almost no positive pore pressures along its slip surfaces.

This is likely due to a blockage in the draining system of the platinum tailings dam as excessive seepage was encountered above the starter wall. A blocked drainage system reduced the drainage capacity of the slope and increased the elevation of the phreatic surface which caused a large proportion of the slip surfaces to slice through the saturated zone. The effect of the higher phreatic surface in the platinum tailings dam can be seen in the figures below as the resulting safety factor is lower than that of the gold tailings dam.

The calculated safety factors from the toe to each berm of the platinum tailings dam are plotted in the bar chart of Figure 4.54. Six matric suction scenarios were compared to the saturated case in the platinum tailings dam to verify whether there is a significant difference the method used to model matric suction profiles on slope stability.

A factor of safety (FoS) of 1.82 was calculated for the entire slope when ignoring matric suctions and increased to 1.88 (3.3% increase) when average matric suctions, capped to 20 kPa, were considered. The calculated FoS is insensitive towards the matric suction cap used as minimum, average and maximum values showed similar results for practical purposes.

The suction stress, calculated from the platinum tailings dam field data, was 3 kPa in between deposition events and 8 kPa upon deposition. These increases in strength were modelled by setting c’ equal to 3 kPa in between deposition events and 8 kPa upon deposition in the Mohr-Coulomb strength model. The safety factor of the entire slope was 1.85 (1.6% increase) in between depositions and increased to 1.89 (3.8% increase) during deposition. Figure 4.54 also shows how the calculated safety factor increased from the first berm to the fourth berm. This is due to the decrease of the overall slope angle. Extrapolation of matric suctions from the phreatic surface resulted in an overall FoS of 1.85 (1.6% increase).

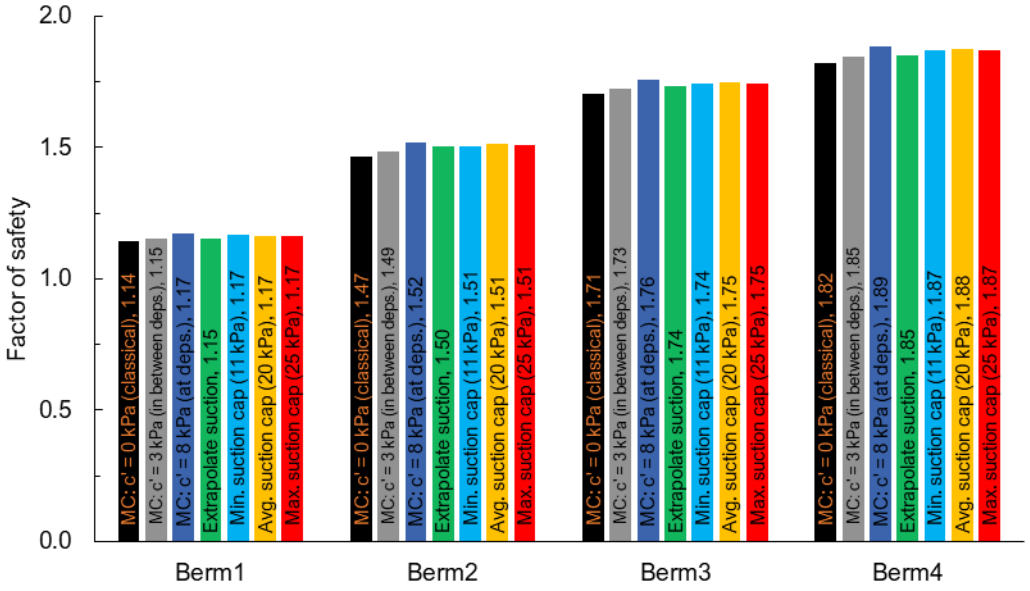

Figure 4.54: Safety factors of the platinum tailings dam.

Figure 4.55 shows a bar chart of the safety factors calculated for the gold tailings dam slope. A FoS of 2.16, when ignoring matric suctions, was calculated for the entire slope and increased to 2.32 (7.4% increase) when average matric suctions of 13 kPa were considered by replacing the Mohr-Coulomb strength model with the model by Vanapalli et al. (1996). However, unlike the platinum tailings dam, the slope stability of the gold tailings dam showed higher sensitivity towards the chosen matric suction cap. A minimum matric suction cap showed an increase in FoS from 2.16 to 2.28 (5.6% increase) and a maximum matric suction cap resulted in a FoS of 2.37 (9.7% increase). The large difference between safety factors when considering minimum, average and maximum values, compared to the platinum tailings dam case, is due to the fact that the entire slip surface is unsaturated. Figure 4.49 also shows how increases in shear strength from matric suctions are sustained for longer as the peak in strength gain only occurs at matric suctions in the order of 100 kPa.

The suction stress was calculated as 6 kPa in between deposition events and 0 kPa upon deposition for the gold tailings dam. The suction stress at deposition is thus considered as being equal to the saturated case and ignored. The safety factor of the entire slope when c’ = 6 kPa increased to 2.44 (13.0% increase), similar to the results obtained when capping suctions to typical maximum values of 23 kPa. Extrapolation of matric suctions from the phreatic surface resulted in an overall FoS of 2.39 (10.6% increase).

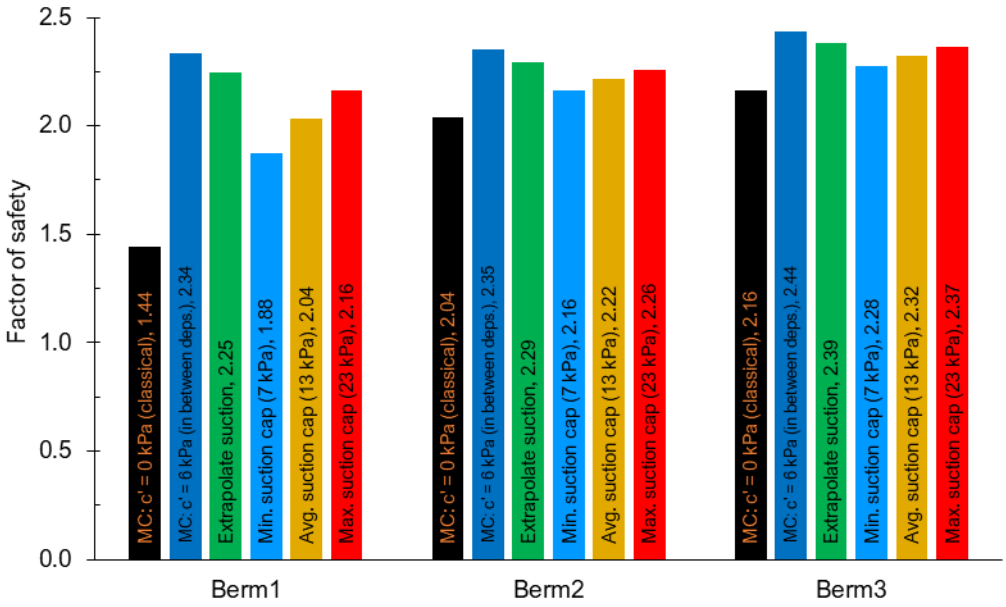

Figure 4.55: Safety factors of the gold tailings dam.

Figure 4.56 plots the increases in shear strength due to matric suctions at the typical minimum, average and maximum values measured on the platinum tailings dam and explains why the calculated FoS of the platinum tailings dam does not vary significantly. Typical minimum, average and maximum matric suction values occurred over the peak in Figure 4.56 (at 11 kPa, 20 kPa and 25 kPa respectively) and resulted in similar shear strength increases of 7 kPa, 8 kPa and 6 kPa respectively causing low variability in the calculated FoS.

The cohesions assumed from increases in shear strength, calculated from field data (Figure 4.45) and used in the Mohr-Coulomb model, were 8 kPa during deposition and 3 kPa in between depositions. Therefore, FoS results from typical matric suction values correspond to the FoS calculated for the case where a cohesion of 8 kPa is assumed as it plots near the peak of Figure 4.56. Indefinite extrapolation of matric suctions into the unsaturated regime resulted in maximum suctions as large as 170 kPa, which relates to a shear strength increase of approximately 2 kPa. The case where a cohesion of 3 kPa is assumed in the Mohr-Coulomb model will thus show similar results to the case where matric suctions are extrapolated indefinitely.

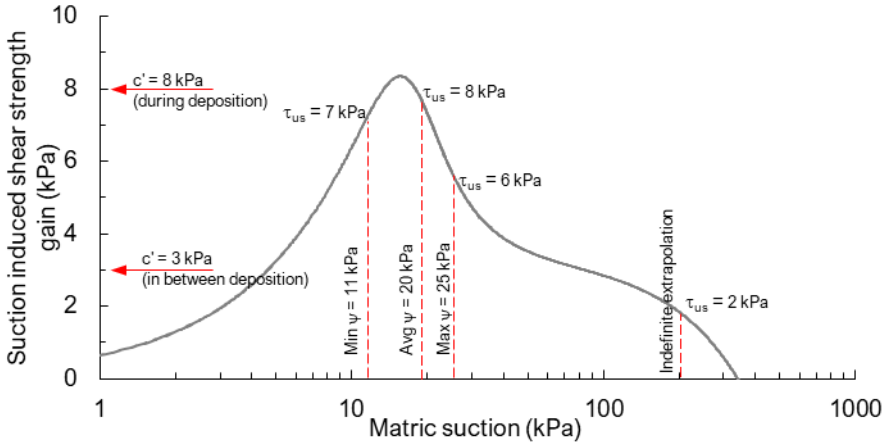

Figure 4.56: Increases in shear strength due to matric suctions at the typical minimum, average and maximum values measured on the platinum tailings dam.

Figure 4.57 plots the increases in shear strength due to matric suctions at the typical minimum, average and maximum values measured on the gold tailings dam. Safety factors calculated for the slope of the gold tailings dam, by capping matric suctions to the abovementioned typical values, are staggered due to the peak plotting after the typical matric suction values in Figure 4.57. Extrapolating matric suctions in the gold tailings dam caused suctions to reach maximum values as high as 240 kPa which plots closer to the peak in Figure 4.57 and explains why the calculated FoS is larger than that for the typical matric suctions.

Choosing a single cohesion value to represent a typical increase in shear strength in between depositions, calculated from the field data, was challenging. A conservative value of 6 kPa was chosen and still resulted in the highest FoS. This may be explained by the fact that the entire unsaturated portion of the slip surface immediately experiences the strengthening effect as it is modelled with a constant cohesion. Cases where the Vanapalli et al.'s (1996) model is used does not calculate a large, immediate increase in shear strength in the unsaturated region immediately next to the phreatic surface as matric suctions zero at the phreatic surface and increase gradually.

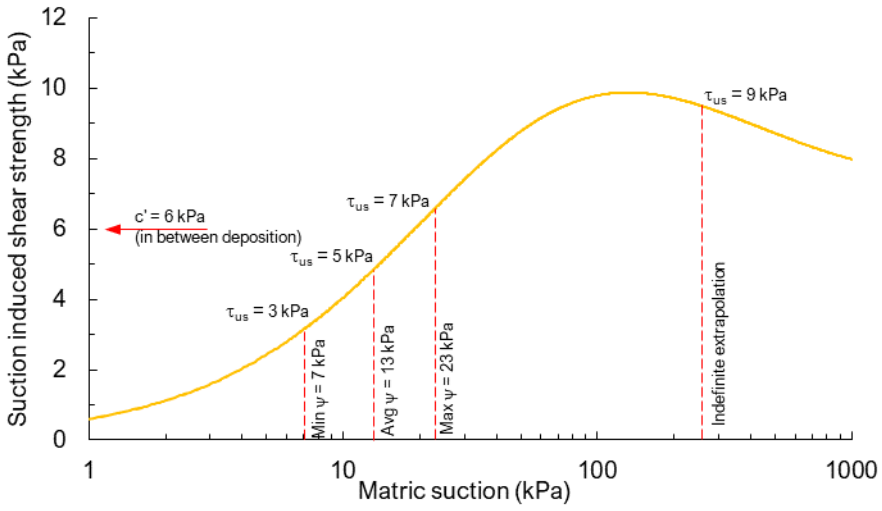

Figure 4.57: Increases in shear strength due to matric suctions at the typical minimum, average and maximum values measured on the gold tailings dam.

4.5 DISCUSSION SUMMARY

This chapter presented and discussed in-situ matric suction data from a platinum and gold tailings dam with the goal to comment on the effect thereof on the stability of tailings dam slopes.

This first required the identification of an unsaturated shear strength model from literature that could predict the strengthening effect of matric suctions on tailings. The effect of matric suction on the shear strength of platinum tailings was found by shearing various samples with a DSS apparatus under a constant normal stress but at varying matric suctions. Matric suctions were measured with a tensiometer and were varied by varying the initial moisture contents at which the samples were prepared for the moist tamped samples and varying the drying time for the slurried samples.

In-situ matric suctions were measured with a tensiometer and water contents with a probe using TDR technology over various months on active platinum and gold tailings dams. This allowed for the monitoring of the response of tailings in the unsaturated zone to observe the influence of tailings deposition and rainfall on matric suction. The identification of an unsaturated shear strength model enabled the estimation of the in-situ strength gains due to matric suctions as the gathered field data was used as inputs for the unsaturated shear strength model. This resulted in plots of gains in shear strength over time which showed how matric suctions contributes to strength in the unsaturated region of tailings dams.

Limit equilibrium slope stability analyses on tailings dams do not typically include matric suctions in their calculations. However, the studied behaviour and effect of matric suctions on strength in active tailings dams allowed for the inclusion of matric suctions in the analyses. This was done by replacing the typical strength models, originally only considering saturated soil mechanics, with an unsaturated shear strength model to show how safety factors would change with the inclusion of matric suctions.

5 CONCLUSIONS AND RECOMMENDATIONS

5.1 CONCLUSION SUMMARY

The conclusions from this study are discussed in this chapter by addressing each of the objectives as listed in section 1.2.

The main objective was to find the contribution of matric suction to the slope stability of tailings dams. Figure 4.54 and Figure 4.55 show the increase in safety factor for failure surfaces extended from the toe to each berm of the platinum and gold tailings dams respectively when considering matric suctions. Matric suctions were considered in the analyses using two methods, i.e., by replacing the Mohr-Coulomb strength model with the unsaturated shear strength model by Vanapalli et al. (1996) (Equation 4.1) and by assuming a cohesion value in the Mohr-Coulomb model. Matric suction related safety factor increases were found to range between 1.6% and 3.8% for the platinum tailings dam for both of the methods used to model matric suctions. The effect of matric suction on the slope stability of the gold tailings dam ranged between 5.6% and 13%. The results of this study therefore show that the contribution of matric suction to the slope stability of platinum and gold tailings dams is small and can probably be ignored by the tailings industry in most practical applications considering upstream facilities impounding non-plastic tailings materials.

In the case of platinum, deposition resulted in an increase in the FoS, while in the case of the gold tailings dam, a decrease in FoS was found with deposition. The response depends on the ambient moisture state in the dam relative to the SWRC. This relationship controls the suction-induced shear strength vs matric suction function. For the coarser grained platinum tailings, the ambient moisture state occurs to the right of the peak, so that a moisture increase (reduction in suction) results in an increase in shear strength. However, for the gold tailings, the ambient moisture state is to the left of the peak, so that in increase in moisture content (reduction in suction) results in a loss of shear strength. (Refer to Figure 4.46 and Figure 4.49).

Monotonic, constant stress, direct simple shear tests on unsaturated platinum tailings were carried out in an attempt to find a relationship between shear strength and matric suction. Figure 4.24 plots the gain in shear strength against matric suctions and shows the typical trend observed. Matric suctions were controlled by varying sample water contents. To observe the contribution of only matric suction to the shear strength of different samples it is important that the void ratios be kept constant. Loose samples

suffered different amounts of compaction during testing so that the identification of the suction induced contribution to shear strength was not possible. The samples therefore had to be tested at a relatively dense state.

The tests were carried out a low confining stresses so that the contribution of matric suctions would not be masked as it was expected to be relatively small. However, the combination of low void ratios and low confining stresses led to strong dilation, contributing to strength which masked the strengthening effect of matric suctions. To minimise this masking effect of dilation, the mobilised shear stress during phase transfer, i.e. a point where zero dilation occurred, was selected as the point where the effect of matric suction on strength between tests could be compared. The performance of different models to predict the contribution of suction to shear strength from the literature is summarized in Table 4.1. The unsaturated shear strength model by Vanapalli et al. (1996) showed the best results. The model by Öberg and Sällfors (1995) also provided good correlation with the measured datapoints.

Figure 4.25 plots the matric suction and water content data gathered over time from the platinum tailings dam. Deposition events always increased the water content of the tailings to the same value (approximately S_r = 45%) regardless of measurement depth. This contrasts observations made by Daliri et al. (2016) from a drying box experiment where water content measurements, after deposition, varied according to measurement depth. The fact that matric suctions never dissipated entirely due to deposition, combined with the increase in water content, led to the counterintuitive phenomenon that the estimated shear strength increased upon wetting rather than decreasing (Figure 4.45). This phenomenon can be explained with reference to the SWRC (Figure 3.7). The transition zone within the SWRC between the residual state and saturated state occurs over a narrow range of matric suctions, implying that a large change in water content will cause a smaller change in suctions. This is typical of coarser materials. Thus, if matric suctions are never dissipated entirely, and the degree of saturation increases, a larger proportion of the suctions can be converted to effective stress leading to higher strengths. Typical matric suctions ranged between 10 and 30 kPa and degrees of saturations ranged between 20% and 45%.

Figure 4.38 plots the matric suction and water content data gathered from the gold tailings dam. Matric suctions routinely dissipated entirely as opposed to the case of the platinum tailings dam due to the change in deposition method. Once again, this phenomenon can be explained by the shape of the SWRC. The SWRC of the gold tailings samples shows a larger change in matric suction with the same change in water

content compared to platinum tailings. Matric suctions in the gold tailings dam ranged between 0 kPa upon deposition and 50 kPa in between depositions for the shallowest measurement. This result in a consequence of the finer grading of the gold tailings compared to the platinum tailings.

Matric suction versus depth profiles for both tailings dams, plotted in Figure 4.28 to Figure 4.30 and Figure 4.33, did not show clear relationships between matric suction and depth for either of the tailings dams. However, matric suction measurements tended to converge to an average suction of 20 kPa and 13 kPa for the platinum and gold tailings dam respectively. The lower suction in the case of the finer grained gold tailings is a consequence of the daywall deposition method, which more effectively floods an area compared to spigotting as used on the platinum dam. The variability in matric suction data in both dams tended to reduce with depth as plotted in Figure 4.44.

Rainfall events of up to 30 mm per day only caused only small reductions in matric suctions of about 4 kPa to 5kPa at the shallowest installations on both the platinum and gold tailings dams, with little or no effect at greater depths.

5.2 RECOMMENDATIONS

5.2.1 Consideration of additional materials

This study only included gold and platinum tailings which are non-plastic, silty sands. Consideration of other tailings materials should be included such as iron tailings and kimberlite tailings which can exhibit some plasticity and potentially different behaviour.

5.2.2 Practical considerations regarding logger installations

The logger placement on tailings dams is often challenging due to the nature of the structure. Tailings dams grow continuously throughout their lifetime and it is thus advised against placement on the beach as this would require periodical lifting of the logger to prevent it from being buried. Installations should be such that the logger can be placed on an outer slope with cables long enough to reach the locations of interest.

The availability of Internet of Things (IoT) services should be considered when relying on IoT technology for data transmission. Tailings dams are often located in remote areas where GSM coverage, used by cell phones, is the only available network. Consideration of a logging device capable of transmitting data via cell phone networks might thus be the better solution.

The long-term stability of logging devices consisting of hobby-related components should be further investigated. Especially when the components directly measure outputs from sensors as in the case of the tensiometer where the performance of the differential voltage measurement can be affected by long term usage. The Teros 12 probes provide digital outputs containing the measured data, the reliability of the measured data does thus not lie on the datalogger anymore but on the sensor which is likely more robust.

5.2.3 Measurement of unsaturated shear strength with a DSS apparatus

The measurement of unsaturated shear strengths is challenging without active control over pore pressures. It is advised to modify the end caps in such a manner that pore pressures can be monitored during testing of unsaturated soils in a DSS device without pore pressure control. Installation of a tensiometer in the top cap would likely be the preferred method as the small sample size does not provide enough space for the installation of a tensiometer in the sample itself without creating uncertainties in its effect on strength.

Another challenge related to the matter is control over void ratio. Testing without pore pressure control requires the formation of samples under varying water contents. Materials with peaky compaction curves will complicate sample formation as a change in water content will relate to a significant change in density. It is thus advised that testing should be done on samples slurried into the assembled membrane and confining rings as this produces relatively dense samples, likely to be more representative of conditions on actual tailings dams. Matric suctions should then be monitored whilst the samples dry or, a water content should be targeted which relates to the desired suction value by means of a SWRC. This, however, implies that testing can only be done on dense samples as slurry deposition often tends to create low void ratios. Low void ratios complicate the matter further, as testing of unsaturated materials to observe the effect of matric suctions requires low confining stresses, and combination of low void ratios with low confining stresses will cause significant dilation, obscuring the effect of matric suctions on strength.

Shear strength testing of unsaturated soils is challenging as various components contribute to strength such as interparticle friction, particle interlock, density, dilation, fabric and matric suction. It is thus important to isolate the effect of matric suction by keeping the remaining contributions constant. This is challenging. Pore pressure control during testing will thus greatly simplify unsaturated strength tests.

If the purpose of unsaturated testing is to measure the contribution of matric suctions to strength and the pore pressure control is a possibility, then the following would be advised:

- Prepare all samples to equal densities at equal water contents.
- Consolidate all the samples unsaturated as saturation will cause collapse.
- Pore pressure control should be executed after consolidation as this would most likely have the smallest effect on density.

5.2.4 Confirmation of the pore pressure profile above the phreatic surface

The evaluation of in-situ infiltration behaviour was not included in the scope of this thesis. Lessons learnt from this study suggest that further work should consider the installation of tensiometers and water content probes along certain cross sections at equal intervals down to the phreatic surface in slopes. Wetting events such as tailings deposition or rainfall can then be evaluated in more detail and compared to hydraulic infiltration models.

More research into the behaviour of the unsaturated pore pressure regime above the phreatic surface in tailings dams will shed more light on the temporal behaviour of matric suctions in tailings slopes and its role in the slope stability of these important structures.

6 REFERENCES

ABRAMENTO, M. & CARVALHO, C. Geotechnical parameters for the study of natural slopes instabilization at'Serra do Mar', Brazil. Congrès intrnational de mécanique des sols et des travaux de fondations. 12, 1989. 1599-1602.

AL TARHOUNI, M. A. & HAWLADER, B. 2021. Monotonic and cyclic behaviour of sand in direct simple shear test conditions considering low stresses. *Soil Dynamics and Earthquake Engineering,* 150**,** 106931.

ASADZADEH, M. & SOROUSH, A. 2016. Fundamental investigation of constant stress simple shear test using DEM. *Powder Technology,* 292**,** 129-139.

AUBENY, C. & LYTTON, R. 2003. Estimating strength versus location and time in high-plasticity clays.

AZAM, S. & LI, Q. 2010. Tailings dam failures: a review of the last one hundred years. *Geotechnical news,* 28**,** 50-54.

BAO, C. G., GONG, B.-W. & ZHAN, L.-T. Properties of unsaturated soils and slope stability of expansive soils. Keynote Lecture, Proceedings of the 2nd International Conference on Unsaturated Soils (UNSAT 98). Beijing, China, 1998. 71-98.

BASSON, J. A., BROEKMAN, A. & JACOBSZ, S. W. 2021. TD-DAQ: A low-cost data acquisition system monitoring the unsaturated pore pressure regime in tailings dams. *HardwareX,* 10**,** e00221.

BISHOP, A. W. 1966. The strength of soils as engineering materials. *Geotechnique,* 16**,** 91-130.

BISHOP, A. W., ALPAN, I., BLIGHT, G. & DONALD, I. 1960. Factors controlling the strength of partly saturated cohesive soils.

BLIGHT, G. 1981. Assessment for environmentally acceptable disposal of mine wastes. *Civil Engineer in South Africa,* 23**,** 489-499.

BOLTON, M. 1986. Discussion: The strength and dilatancy of sands. *Géotechnique,* 37**,** 219-226.

CROUS, P. A. 2021. *Centrifuge and numerical modelling of liquefied flow and non-liquefied slide failures.* Master of Philosphy in Civil and Environmental Engineering, HKUST.

D-17, A. 2017. Standard test method for consolidated undrained direct simple shear testing of fine grain soils. *ASTM International: West Conshohocken, PA, USA*.

DALIRI, F., KIM, H., SIMMS, P. & SIVATHAYALAN, S. 2014. Impact of desiccation on monotonic and cyclic shear strength of thickened gold tailings. *Journal of Geotechnical and Geoenvironmental Engineering,* 140**,** 04014048.

DALIRI, F., SIMMS, P. & SIVATHAYALAN, S. 2016. Shear and dewatering behaviour of densified gold tailings in a laboratory simulation of multi-layer deposition. *Canadian Geotechnical Journal,* 53**,** 1246-1257.

DE JOSSELIN DE JONG, G. 1971. The double sliding, free rotating model for granular assemblies. *Geotechnique,* 21**,** 155-163.

DONALD, I. 1957. Effective stresses in unsaturated non-cohesive soils with controlled negative pore pressure. *M. Eng. Sc. Thesis, University of Melbourne, Melbourne, Australia*.

DUNLOP, P. & DUNCAN, J. 1966. Behaviour of soils in simple shear tests. *7th International Conference on Soil Mechanics and Foundation Engineering (Mexico).* Mexico.

DYVIK, R., BERRE, T., LACASSE, S. & RAADIM, B. 1987. Comparison of truly undrained and constant volume direct simple shear tests. *Geotechnique,* 37**,** 3-10.

FREDLUND, D., MORGENSTERN, N. R. & WIDGER, R. 1978. The shear strength of unsaturated soils. *Canadian geotechnical journal,* 15**,** 313-321.

FREDLUND, D. & ZHANG, F. Combination of shrinkage curve and soil-water characteristic curves for soils that undergo volume change as soil suction is increased. Proceedings of the 18th International Conference on Soil Mechanics and Geotechnical Engineering, Paris, September 2–6, 2013.

FREDLUND, D. G. & RAHARDJO, H. 1993. *Soil mechanics for unsaturated soils*, John Wiley & Sons.

FREDLUND, D. G. & XING, A. 1994. Equations for the soil-water characteristic curve. *Canadian geotechnical journal,* 31**,** 521-532.

FREDLUND, D. G., XING, A., FREDLUND, M. D. & BARBOUR, S. 1996. The relationship of the unsaturated soil shear strength to the soil-water characteristic curve. *Canadian geotechnical journal,* 33**,** 440-448.

FREDLUND, M., WILSON, G. & FREDLUND, D. Representation and estimation of the shrinkage curve. Unsaturated Soils: Proceedings of the Third International Conference, UNSAT2002, Recife, Brazil, 10-13 March 2002, 2002. Taylor & Francis US, 145.

FUKUSHIMA, S. & TATSUOKA, F. 1984. Strength and deformation characteristics of saturated sand at extremely low pressures. *Soils and Foundations,* 24**,** 30-48.

GARVEN, E. A. 2009. *Review of the empirical equations for predicting the shear strength of unsaturated soils.* University of Ottawa (Canada).

GEOCOMP. 2022. *Products* [Online]. [Accessed 27 September 2022].

JACOBSZ, S. 2018. Low cost tensiometers for geotechnical applications. *Physical Modelling in Geotechnics.* CRC Press.

KHALILI, N. & KHABBAZ, M. 1998. A unique relationship for χ for the determination of the shear strength of unsaturated soils. *Geotechnique,* 48**,** 681-687.

LADD, C. C. & EDGERS, L. 1972. Consolidated-Undrained Direct-Simple Shear Tests on Saturated Clays. MASSACHUSETTS INST OF TECH CAMBRIDGE SOIL MECHANICS DIV.

LE ROUX, P. F. & JACOBSZ, S. W. 2021. Performance of the Tensiometer Method for the Determination of Soil-Water Retention Curves in Various Soils. *Geotechnical Testing Journal,* 44**,** 1079-1096.

LIKOS, W. J. & LU, N. 2004. Unsaturated soil mechanics. *Ed: John Wiley and Sons Inc., New Jersey*.

LINGS, M. & DIETZ, M. 2004. An improved direct shear apparatus for sand. *Geotechnique,* 54**,** 245-256.

LYTTON, R. Foundations and pavements on unsaturated soils. PROCEEDINGS OF THE FIRST INTERNATIONAL CONFERENCE ON UNSATURATED SOILS/UNSAT'95/PARIS/FRANCE/6-8 SEPTEMBER 1995. VOLUME 3, 1996.

MAREE, L. 1987. *Ontwerpparameters vir platinumslykdamme.* Universiteit van Pretoria.

MATTHEWS, M. 1988. The engineering application of direct and simple shear testing. *Ground engineering,* 21**,** 613-621.

METER GROUP, I. 2019. *5TM User's Manual* [Online]. [Accessed 16 February 2022].

NAM, S., GUTIERREZ, M., DIPLAS, P. & PETRIE, J. 2011. Determination of the shear strength of unsaturated soils using the multistage direct shear test. *Engineering Geology,* 122**,** 272-280.

NG, C. W. W. & MENZIES, B. 2014. *Advanced unsaturated soil mechanics and engineering*, CRC Press.

ÖBERG, A. 1995. Stability of sand and silt slopes. *Internal Rep., Dept. of Geotechnical Engineering, Chalmers Univ. of Technology, Gothenburg, Sweden*.

ÖBERG, A. & SÄLLFORS, G. A rational approach to the determination of the shear strength parameters of unsaturated soils. PROCEEDINGS OF THE FIRST INTERNATIONAL CONFERENCE ON UNSATURATED SOILS/UNSAT'95/PARIS/FRANCE/6-8 SEPTEMBER 1995. VOLUME 1, 1995.

ROTTA, L. H. S., ALCANTARA, E., PARK, E., NEGRI, R. G., LIN, Y. N., BERNARDO, N., MENDES, T. S. G. & SOUZA FILHO, C. R. 2020. The 2019 Brumadinho tailings dam collapse: Possible cause and impacts of the worst human and environmental disaster in Brazil. *International Journal of Applied Earth Observation and Geoinformation,* 90**,** 102119.

ROUSÉ, P. C. 2018. Relation between the critical state friction angle of sands and low vertical stresses in the direct shear test. *Soils and foundations,* 58**,** 1282-1287.

SADREKARIMI, A. 2014. Effect of the mode of shear on static liquefaction analysis. *Journal of Geotechnical and Geoenvironmental Engineering,* 140**,** 04014069.

SANTAMARINA, J. C., TORRES-CRUZ, L. A. & BACHUS, R. C. 2019. Why coal ash and tailings dam disasters occur. *Science,* 364**,** 526-528.

SILLERS, W. S. & FREDLUND, D. G. 2001. Statistical assessment of soil-water characteristic curve models for geotechnical engineering. *Canadian Geotechnical Journal,* 38**,** 1297-1313.

TEKINSOY, M., KAYADELEN, C., KESKIN, M. & SÖYLEMEZ, M. 2004. An equation for predicting shear strength envelope with respect to matric suction. *Computers and Geotechnics,* 31**,** 589-593.

VANAPALLI, S., FREDLUND, D., PUFAHL, D. & CLIFTON, A. 1996. Model for the prediction of shear strength with respect to soil suction. *Canadian geotechnical journal,* 33**,** 379-392.

VILAR, O. M. 2006. A simplified procedure to estimate the shear strength envelope of unsaturated soils. *Canadian Geotechnical Journal,* 43**,** 1088-1095.

YOSHIMINE, M., ISHIHARA, K. & VARGAS, W. 1998. Effects of principal stress direction and intermediate principal stress on undrained shear behavior of sand. *Soils and Foundations,* 38**,** 179-188.

ZHANG, L., FREDLUND, D. G., FREDLUND, M. D. & WILSON, G. W. 2014. Modeling the unsaturated soil zone in slope stability analysis. *Canadian Geotechnical Journal,* 51**,** 1384-1398.